2016

Glutamate Transport Affects Mitochondria And Calcium Signaling In Astrocytic Processes Under Normal And Pathological Conditions

John Charles O'donnell
University of Pennsylvania, john.charles.odonnell@gmail.com

Glutamate Transport Affects Mitochondria And Calcium Signaling In Astrocytic Processes Under Normal And Pathological Conditions

Abstract
ABSTRACT

GLUTAMATE TRANSPORT AFFECTS MITOCHONDRIA AND CALCIUM SIGNALING IN ASTROCYTIC PROCESSES UNDER NORMAL AND PATHOLOGICAL CONDITIONS

John Charles O'Donnell

Michael B. Robinson

Mitochondria are responsible for synthesis and metabolism of the primary excitatory neurotransmitter, glutamate, which is cleared from synapses via Na+-dependent transporters on astrocytes. Astrocytic clearance of glutamate is required to prevent excitotoxic neuronal death. Mitochondria also participate in calcium signaling in various cell types. Astrocytic calcium signaling is implicated in neurovascular coupling. Glutamate transport and calcium signaling are central to the function of astrocytic processes that are in turn vital for normal brain function. We recently confirmed that mitochondria are present throughout astrocytic processes. Using confocal microscopy and hippocampal slice cultures along with a variety of biochemical assays, we sought to elucidate the physiological and pathological interactions between mitochondria, glutamate transport, and calcium signaling in astrocytic processes. We found that glutamate uptake is reduced after displacing hexokinase from the voltage-dependent anion channel on the outer mitochondrial membrane, but coimmunoprecipitations between transporter and mitochondrial proteins are not changed. As in neurons, we found that some astrocytic mitochondria are mobile. We provide evidence that neuronal activity, activation of astrocytic glutamate transporters, and subsequent reversal of the Na+/Ca2+ exchanger leads to immobilization of mitochondria near transporters and synapses, where they can oxidize glutamate, buffer ions, and provide ATP. Finally, I found that following transient oxygen/glucose deprivation (a model of ischemia/reperfusion injury), mitochondria in astrocytic processes undergo fragmentation and autophagic degradation, culminating 24 h after insult with an ~50% reduction in mitochondrial size and the percentage of process length occupied by mitochondria. This loss of mitochondria is independent of the accompanying excitotoxic neuropathology, and seems to instead be driven by an extended period of high glutamate uptake. I also identified a previously overlooked distinction between Ca2+ signals in astrocytic processes, showing two populations with different properties based on their anatomical relationship to mitochondria. These Ca2+ signals were greatly increased after mitochondrial loss and were no longer spatially restricted by the remaining mitochondria. In summary, we found that glutamate transport positions mitochondria at sites of activity in astrocytic processes where they shape calcium signals; but glutamate uptake under excitoxic conditions leads to mitochondrial loss and dramatically altered calcium signaling, potentially impacting neuronal injury and recovery.

Degree Type
Dissertation

Degree Name
Doctor of Philosophy (PhD)

GLUTAMATE TRANSPORT AFFECTS MITOCHONDRIA AND CALCIUM SIGNALING IN ASTROCYTIC PROCESSES UNDER NORMAL AND PATHOLOGICAL CONDITIONS

John Charles O'Donnell

A DISSERTATION

in

Pharmacology

Presented to the Faculties of the University of Pennsylvania

in

Partial Fulfillment of the Requirements for the

Degree of Doctor of Philosophy

2016

Supervisor of Dissertation

_____

Michael B. Robinson, Ph.D.

Professor of Pediatrics

Graduate Group Chairperson

_____

Julie A. Blendy, Ph.D.

Professor of Pharmacology

Dissertation Committee

William M. Armstead, Ph.D., Research Professor of Anesthesiology and Critical Care

Erika L.F. Holzbaur, Ph.D., William Maul Measey Professor in Physiology

Harry Ischiropoulos, Ph.D., Research Professor of Pediatrics

David R. Lynch, MD, Ph.D., Professor of Neurology

GLUTAMATE TRANSPORT AFFECTS MITOCHONDRIA AND CALCIUM SIGNALING IN ASTROCYTIC PROCESSES UNDER NORMAL AND PATHOLOGICAL CONDITIONS

ABSTRACT

GLUTAMATE TRANSPORT AFFECTS MITOCHONDRIA AND CALCIUM SIGNALING IN ASTROCYTIC PROCESSES UNDER NORMAL AND PATHOLOGICAL CONDITIONS

John Charles O'Donnell

Michael B. Robinson

Mitochondria are responsible for synthesis and metabolism of the primary excitatory neurotransmitter, glutamate, which is cleared from synapses via Na^+-dependent transporters on astrocytes. Astrocytic clearance of glutamate is required to prevent excitotoxic neuronal death. Mitochondria also participate in calcium signaling in various cell types. Astrocytic calcium signaling is implicated in neurovascular coupling. Glutamate transport and calcium signaling are central to the function of astrocytic processes that are in turn vital for normal brain function. We recently confirmed that mitochondria are present throughout astrocytic processes. Using confocal microscopy and hippocampal slice cultures along with a variety of biochemical assays, we sought to elucidate the physiological and pathological interactions between mitochondria, glutamate transport, and calcium signaling in astrocytic processes. We found that glutamate uptake is reduced after displacing hexokinase from the voltage-dependent anion channel on the outer mitochondrial membrane, but coimmunoprecipitations between transporter and mitochondrial proteins are not changed. As in neurons, we found that some astrocytic mitochondria are mobile. We provide evidence that neuronal activity, activation of astrocytic glutamate transporters, and subsequent reversal of the Na^+/Ca^{2+} exchanger leads to immobilization of mitochondria near transporters and synapses, where they can oxidize glutamate, buffer ions, and provide ATP. Finally, I found that following transient oxygen/glucose deprivation (a model of ischemia/reperfusion injury), mitochondria in astrocytic processes undergo fragmentation and autophagic degradation, culminating 24 h after insult with an ~50% reduction in

mitochondrial size and the percentage of process length occupied by mitochondria. This loss of mitochondria is independent of the accompanying excitotoxic neuropathology, and seems to instead be driven by an extended period of high glutamate uptake. I also identified a previously overlooked distinction between Ca^{2+} signals in astrocytic processes, showing two populations with different properties based on their anatomical relationship to mitochondria. These Ca^{2+} signals were greatly increased after mitochondrial loss and were no longer spatially restricted by the remaining mitochondria. In summary, we found that glutamate transport positions mitochondria at sites of activity in astrocytic processes where they shape calcium signals; but glutamate uptake under excitoxic conditions leads to mitochondrial loss and dramatically altered calcium signaling, potentially impacting neuronal injury and recovery.

TABLE OF CONTENTS

LIST OF ILLUSTRATIONS

CHAPTER 1

Background

1.1 Introduction

Through its dual role as neurotransmitter and oxidative fuel, glutamate couples the transfer of information with the energy needed to process it (for reviews, see McKenna, 2013; Robinson and Jackson, 2016). Similar to the joint role of glutamate as molecular substrate for information/energy, astrocytes couple information and energy at the macroscopic level by coordinating changes in brain activity with blood flow, referred to as neurovascular coupling (for review, see Bazargani and Attwell, 2016). Previously overlooked electron micrographs (Mugnaini, 1964; Fernandez et al., 1983; Aoki et al., 1987; Xu et al., 2003; Lovatt et al., 2007; Ito et al., 2009; Oberheim et al., 2009; Lavialle et al., 2011; Pardo et al., 2011), along with more recent confocal images (Genda et al., 2011a; Motori et al., 2013; Jackson et al., 2014; Derouiche et al., 2015; Jackson and Robinson, 2015; Stephen et al., 2015; O'Donnell et al., 2016; for review, see Benjamin Kacerovsky and Murai, 2016) have revealed the presence of mitochondria throughout fine astrocytic

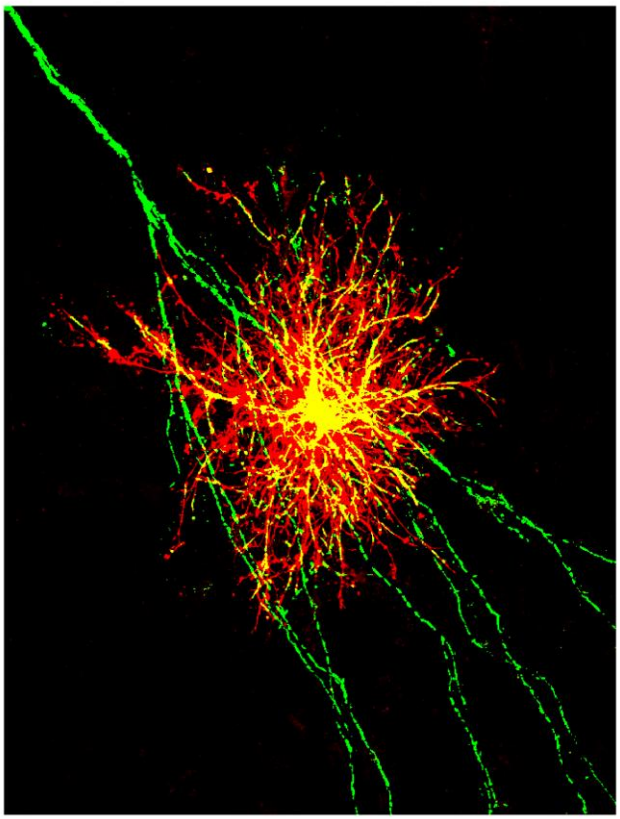

Figure 1.1. Mitochondria are found throughout astrocytic processes. This image shows an astrocyte (Green: mitochondrially-targeted GFP; Red: plasma-membrane-targeted mcherry driven by gfap promoter) intercalated throughout the apical dendrites of a CA1 pyramidal neuron (Green: mitochondrially-targeted GFP) at its branch point in stratum radiatum of a rat hippocampal slice. This image was published on the cover of The Journal of Neuroscience, July 6, 2016, Volume 36, Issue 27 in association with O'Donnell et al., 2016 found in Chapter 4 of this dissertation.

processes (Fig. 1.1). Mitochondria in astrocytic processes are vital for information/energy coupling at the level of glutamate, through interactions with transporters and glutamate oxidation (Genda et al., 2011a; Bauer et al., 2012; Jackson et al., 2014, 2015; Ugbode et al., 2014; for review, see Robinson and Jackson, 2016), and at the level of astrocytes, through their regulation of calcium signaling involved in the neurovascular response (Jackson and Robinson, 2015; Stephen et al., 2015; O'Donnell et al., 2016). The following chapters present early, though hopefully insightful, investigations of mitochondria in astrocytic processes, and suggest many exciting discoveries to come.

1.2 Receptor-mediated signaling emergent from the intercellular metabolic flux of glutamate

Glutamate is an acidic, negatively charged amino acid vital for several biological functions that are mechanistically distinct, but intricately linked. It is an essential building block of life as one of the twenty proteinogenic amino acids encoded in our DNA. It is necessary for ammonia fixation and nitrogen biosynthesis through the activity of the enzymes glutamate dehydrogenase and glutamine synthetase (for review, see Adeva et al., 2012). It serves as fuel for oxidative metabolism through conversion to α-ketoglutarate and entry into the tricarboxylic acid cycle (for review, see McKenna, 2013). And it is an intercellular signaling molecule in various tissues, including the central nervous system where it functions as the primary excitatory neurotransmitter and as the precursor for GABA, the primary inhibitory neurotransmitter.

The myriad of vital functions relying on glutamate was actually part of the argument against its proposed role as the primary excitatory neurotransmitter. During a

pivotal period of neurotransmitter discovery beginning in the 1950s, many believed that the excitatory signaling molecule they were searching for would be highly specialized for receptor-mediated signaling, like the previously discovered acetylcholine (for reviews, see Bennett and Balcar, 1999; Watkins and Jane, 2006; Krnjević, 2010). However, it has since been postulated that glutamate's ubiquitous role as intercellular metabolic currency may have actually led to its role as a receptor-mediated signaling molecule (for reviews, see Mangia et al., 2012; DiNuzzo, 2016). This process in which a previously established trait is co-opted by evolution for a new purpose is commonly referred to as exaptation (Gould and Vrba, 1982). Biofilm communities of single-celled bacteria regulate expansion and prevent starvation by communicating through glutamate metabolic flux and associated electrochemical K^+ signaling; functions that predate the emergence of receptor-mediated intercellular glutamate signaling (Liu et al., 2015; Prindle et al., 2015). Mammalian glutamate receptors share a common lineage with those found in plants (Chiu et al., 1999), nematodes (Brockie and Maricq, 2003; Kano et al., 2008), and even with chemosensory receptors that some bacteria rely on for finding food (Van Houten et al., 2000; Janovjak et al., 2011; Ramoino et al., 2014). It appears likely that intercellular metabolic flux of glutamate, and the existence of primitive chemosensory receptors, converged over millions of years to give us the sophisticated systems of receptor-mediated intercellular glutamate signaling observed in complex multicellular organisms. It should come as little surprise that the intercellular metabolic flux of neurotransmitter glutamate remains every bit as important as its more modern excitatory signaling role for shaping brain function.

1.3 Metabolic flux of neurotransmitter glutamate is facilitated by astrocytic mitochondria and glutamate transporters

Neuroactive amino acids (i.e. glutamate, GABA, aspartate, glutamine) are predominantly restricted from crossing the blood brain barrier into the brain (for reviews, see Smith, 2000; Hawkins et al., 2006). Therefore, these vital molecules must be derived from glucose in the brain through the TCA cycle, predominantly in astrocytic mitochondria (Fig. 1.2). Astrocytic glucose is either converted to glycogen for storage or to pyruvate via glycolysis. Pyruvate dehydrogenase can then convert pyruvate to acetyl CoA for entry into the TCA cycle through combination with recycled oxaloacetate and synthesis of citrate. The enzyme pyruvate carboxylase provides a source of four-carbon backbone for the TCA cycle through synthesis of new oxaloacetate from pyruvate; this influx of four-carbon molecules shifts the TCA cycle from a catalytic to a biosynthetic process, facilitating de novo synthesis of glutamate (for reviews, see McKenna, 2007; Schousboe et al., 2014). Pyruvate carboxylase is an astrocyte-specific enzyme in brain, thus *de novo* synthesis of glutamate in the brain takes place almost exclusively in astrocytic mitochondria (for review, see Schousboe et al., 2013). Astrocytes are responsible for ~30% of cerebral oxidative metabolism (for review, see Hertz et al., 2007), and of the glucose oxidized in astrocytes, ~80% is used to synthesize glutamate (for review, see Hertz, 2011). Oxidative glutamate synthesis has the benefit of generating ATP (one glucose molecule nets 11 ATP and one glutamate), though not as much as would be generated if that carbon backbone was to complete the TCA cycle (one glucose molecule nets 32 ATP) (for review, see Hertz et al., 2007). At the cost of one ATP, glutamate can then be converted to glutamine by the astrocyte-specific enzyme glutamine synthetase (Norenberg and Martinez-Hernandez, 1979), and transferred to presynaptic nerve terminals where mitochondrial glutaminase can convert

it back to glutamate for packaging in vesicles and entry into the neurotransmitter pool (for reviews, see Kvamme et al., 2000; McKenna, 2007).

Neurotransmitter glutamate is released into the synaptic cleft, where it can activate glutamate receptors on the postsynaptic neuron as well as those on surrounding astrocytic processes. Unlike acetylcholine, there is no known mechanism for extracellular glutamate deactivation. Glutamatergic signaling events are terminated by diffusion away from the cleft and uptake into astrocytes via Na^+-dependent glutamate transporters, GLT-1 and GLAST (for reviews, see Danbolt, 2001; Sheldon and Robinson, 2007). The clearance of extracellular glutamate predominantly into astrocytes is unique among neurotransmitters, which are typically taken back up into neurons or enzymatically deactivated in the extracellular space. The primary excitatory neurotransmitter is also unique in that it is, somewhat paradoxically, a potent neurotoxin. Astrocytic glutamate uptake is therefore vital for preventing overactivation of neuronal glutamate receptors that could lead to the death of neurons through a process called excitotoxicity (for reviews, see Choi and Rothman, 1990; Schousboe and Waagepetersen, 2005). Once inside the astrocyte, the majority of neurotransmitter glutamate is converted to glutamine, presumably for safe transport back to neurons where it can be converted back to glutamate for partial replenishment of the neurotransmitter pool (for review, see McKenna, 2007). However, since a portion of this glutamate is oxidized, the glutamate/glutamine cycle is not sufficient to maintain the neurotransmitter pool, which therefore relies on *de novo* synthesis of glutamate in astrocytic mitochondria (for review, see McKenna, 2007). A significant portion of neurotransmitter glutamate is oxidized in astrocytic mitochondria through conversion to α-ketoglutarate and entry into the TCA cycle (Yu et al., 1982; McKenna et al., 2002; for

reviews, see McKenna, 2013; Dienel and McKenna, 2014; Sonnewald, 2014). This oxidative metabolic route represents a vital, though previously controversial component of the metabolic flux of neurotransmitter glutamate.

The controversy surrounding the oxidation of transported glutamate seems to have stemmed from two assumptions: one, based mainly on extrapolation from observations in primary astrocytic cultures, that astrocytes are almost exclusively glycolytic (Pellerin and Magistretti, 1994); and two, based on the narrow diameter of astrocytic processes, that mitochondria necessary for this oxidation could not be present near transporters and synapses (Hertz et al., 2007). We now know both of these assumptions were untrue. Studies utilizing *in vivo* nuclear magnetic resonance spectroscopy and autoradiography found that oxidative metabolism in astrocytes was equivalent to that of neurons, though it was still believed that fine processes were too small to contain mitochondria, and therefore must be glycolytic compartments (for review, see Hertz et al., 2007). Electron micrographs displaying mitochondria in astrocytic processes surrounding synapses (Lovatt et al., 2007; Ito et al., 2009; Oberheim et al., 2009; Lavialle et al., 2011; Pardo et al., 2011) were, until recently, largely overlooked in favor of a model in which these compartments simply converted glutamate to glutamine and were dependent on glycolysis for ATP. However, the accumulation of these images along with growing evidence for oxidation of neurotransmitter glutamate has forced the field to acknowledge that the presence of mitochondria within astrocytic processes is likely central to determining the metabolic fate of glutamate and the astrocytic energy economy.

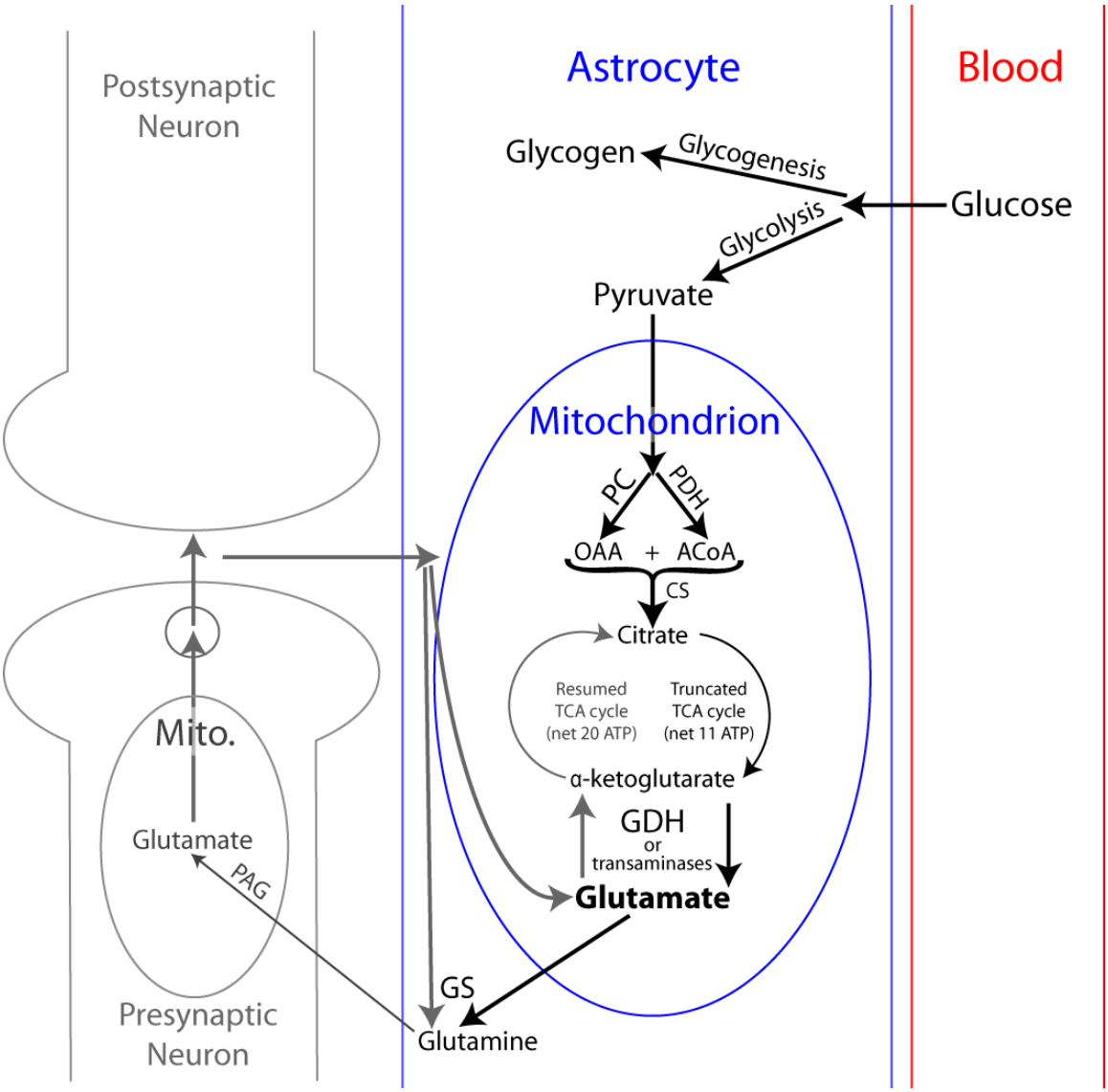

Figure 1.2. Astrocytic mitochondria are required for de novo synthesis of brain glutamate and oxidation of neurotransmitter glutamate. In this simplified schematic, astrocytic glucose transporters take up glucose from the blood into the cytoplasm, where it can be stored as glycogen or converted to pyruvate via glycolysis. Pyruvate can enter the TCA cycle in mitochondria via conversion to acetyl CoA (ACoA) by pyruvate dehydrogenase (PDH), or to oxaloacetate (OAA) via the astrocyte-specific enzyme pyruvate carboxylase (PC). PC activity shifts the TCA cycle in favor of biosynthesis. Citrate synthase uses OAA and ACoA to form citrate, which proceeds through the TCA cycle until formation α-ketoglutarate, generating 11 molecules of ATP in the process. α-ketoglutarate is then converted to glutamate by glutamate dehydrogenase (GDH) or one of several transaminases. Glutamate is then transported out of mitochondria and converted to glutamine in the cytoplasm by the astrocyte-specific enzyme glutamine synthetase (GS). Glutamine can then be transported to mitochondria within presynaptic nerve terminals for conversion back to glutamate by phosphate-activated glutaminase (PAG). Glutamate is then packaged in vesicles, released into the synapse and taken back up by astrocytes via Na+-dependent glutamate transporters; after which some glutamate is converted back to glutamine by GS, and some enters mitochondria to be converted back to α-ketoglutarate and complete the TCA cycle. By completing the TCA cycle, glutamate can generate an additional 20 molecules of ATP.

A variable percentage of transported glutamate is converted to α-ketoglutarate via the mitochondrial enzyme glutamate dehydrogenase, and oxidized via the TCA cycle in mitochondria, producing ATP (Yu et al., 1982; McKenna et al., 2002; for reviews, see McKenna, 2013; Dienel and McKenna, 2014; Sonnewald, 2014). In fact, astrocytic glutamate oxidation outpaces glucose oxidation in primary cultures from rat brain (McKenna, 2012). Inhibiting glutamate dehydrogenase reduces Na^+-dependent glutamate uptake in crude synaptosomes (Whitelaw and Robinson, 2013). Furthermore, CNS-specific deletion of glutamate dehydrogenase increases glucose deployment from the periphery to the brain to compensate for the loss glutamate as a fuel source (Karaca et al., 2015). Oxidation of neurotransmitter glutamate allows astrocytes to recoup most of the ATP lost to the incomplete TCA cycle during *de novo* glutamate synthesis; 2 glutamate molecules generate a net 20 molecules of ATP, so synthesis and oxidation of 2 molecules of neurotransmitter glutamate from 1 molecule of glucose nets 31 ATP, compared to the 32 ATP that would have been generated if those carbons had not taken a detour through neurotransmitter glutamate (Hertz et al., 2007).

1.4 Protein interactions between mitochondria and glutamate transporters

The astrocytic glutamate transporter GLT-1 is enriched in fine processes near synapses (Chaudhry et al., 1995; Lehre et al., 1995). In keeping with the oxidation of neurotransmitter glutamate, we recently demonstrated that glycolytic and mitochondrial proteins coimmunoprecipitate with astrocytic glutamate transporters, and vice versa. We also observed overlap of fluorescently labeled mitochondria and transporters in astrocytic processes that was statistically greater than would be observed by chance,

suggesting physical and/or functional interactions between mitochondria and glutamate transporters in astrocytic processes (Genda et al., 2011; Bauer et al., 2012).

Multiprotein complexes increase the efficiency of biological pathways by increasing availability and decreasing diffusion distance of substrates exchanged within the pathway. Multiprotein assemblies between transporters, receptors, ion channels, and cytosolic proteins have been identified in brain, positioning receptors at synapses, limiting nonspecific protein modification by tethering kinases and phosphatases, and increasing substrate transfer efficiency between associated enzymes (Levitan, 2006; Mandela and Ordway, 2006; Torres, 2006; Chen and Olsen, 2007; Müller et al., 2010). A multiprotein complex between the voltage-dependent anion channel (VDAC) on mitochondria and the IP_3 receptor on endoplasmic reticulum facilitates calcium transfer between the organelles, important for energy regulation and cell death signaling (Rizzuto et al., 1998; Szabadkai et al., 2006; Csordás et al., 2010).

The michondria-ER interaction provides an example of a multi-membrane complex involving mitochondria, and includes the cytoplasmic scaffolding protein Grp75 (Szabadkai et al., 2006). We hypothesized that similar scaffold architecture may exist between the plasma membrane glutamate transporter and mitochondria. Identifying this scaffold could allow us to stabilize or disrupt assembly of the complex, providing a means by which to study the physiological relevance of the transporter-mitochondria interaction. Hexokinase 1 (HK1), the enzyme that carries out the first and rate-limitimg step of glycolysis, was identified from our GLT-1 proteome as a potential scaffold. The HK isoform HK2 binds the plasma membrane glucose transporter GLUT4 (Zaid et al., 2009), and the localization of both HK1 and 2 to mitochondria via their binding to VDAC has been studied extensively (Lindén et al., 1982; Nakashima et al., 1986; BeltrandelRio

and Wilson, 1991; Sui and Wilson, 1997; Rodrigues-Ferreira et al., 2012). We therefore hypothesized that displacing HK1 from VDAC would disrupt the transporter-mitochondria complex. As you will read in Chapter 2, displacing HK1 from VDAC impairs glutamate transport, but does not interfere with coimmunoprecipitation of the transporter and other mitochondrial proteins (Jackson et al., 2015).

1.5 Mitochondrial mobility and distribution

In neurons, mitochondria are distributed at sites with high demand for ATP or calcium buffering, including growth cones, axon branch points, synapses, and nodes of Ranvier, (Morris and Hollenbeck, 1993; Ruthel and Hollenbeck, 2003; Zhang et al., 2010). This distribution is established by cytoskeletal motors attached to mitochondria (Morris and Hollenbeck, 1995; Ligon and Steward, 2000). Immobilization of mitochondria in areas of low ATP and high calcium is primarily attributed to calcium binding to the motor adaptor protein Miro, resulting in motor deactivation (Schwarz, 2013). Mitochondrial mobility is required not only for establishing a distribution that can support cellular functions and respond to changes in activity, but also has significant overlap with fission and fusion events that are necessary for maintaining the health of the mitochondrial population (for review, see Youle and Bliek, 2012). Disruption of mitochondrial mobility and dynamics in neurons is implicated in the progression of several neurodegenerative diseases (Baloh et al., 2007; Waterham et al., 2007; for review, see Sheng and Cai, 2012).

Given the reluctance in the field to accept that mitochondria were present in astrocytic processes, relatively little was known about the mechanisms regulating

transport of mitochondria in astrocytes. As described above, much of the evidence for the presence of mitochondria out in processes relied on two-dimensional electron micrographs from small brain areas. Block scan electron microscopy with three-dimensional reconstruction is arduous and expensive, but without evidence of mitochondrial distribution throughout the entire astrocyte, many were unwilling to reject the longstanding belief that processes were too small to contain mitochondria. Unlike in primary cultures, the complex morphology of astrocytes is maintained in organotypic hippocampal slice cultures, along with neuronal circuitry (Stoppini et al., 1991; Benediktsson et al., 2005). Biolistic transfection of these cultures provides sparse flourescent labeling of individual cells within the context of a greater cellular matrix. By targeting fluorophores to mitochondria and plasma membrane within individual astrocytes in a slice culture, we observed three-dimensional distribution of mitochondria throughout the processes of astrocytes. We also found that we could record mitochondrial mobility in processes and manipulate activity within the slice to evaluate mechanisms regulating that mobility.

Chapter 3 describes the first study examining the mobility of mitochondria in astrocytic processes. We found that they move more slowly compared to their neuronal counterparts, and that mitochondrial mobility in astrocytic processes is regulated by neuronal activity and astrocytic glutamate uptake, positioning mitochondria near transporters and synapses (Jackson et al., 2014). Similar findings have since been reported by other groups using primary cultures (Ugbode et al., 2014) and a similar hippocampal slice culture model (Stephen et al., 2015), and mitochondria have been found even in ultra-fine peripheral astrocytic processes (Derouiche et al., 2015; for review, see Benjamin Kacerovsky and Murai, 2016). It is now apparent that

mitochondria occupy most of the volume of astrocytic processes, and we are just beginning to understand the implications for astrocyte biology and brain function.

1.6 Ca^{2+} signaling in astrocytic processes is shaped by mitochondria and glutamate transporters

Just as glutamate couples information and energy at the molecular level, astrocytes provide more macroscopic information/energy coupling by coordinating neuronal activity with changes in blood flow and regulation of breathing. Synapses are the greatest consumers of energy in the brain (Harris et al., 2012), but they have little or no contact with the vasculature from which energy is supplied. Instead, astrocytes ensheathe the vasculature and thousands of synapses, positioning them as gatekeepers between systemic circulation and the brain. Unlike neurons, astrocytes are not considered electrochemically excitable since they are not myelinated and do not express voltage-gated Na^{+} channels; instead they rely mainly on Ca^{2+} signaling to propagate information through processes and between cells via gap junctions (for review, see Bazargani and Attwell, 2016). Neuronally evoked elevations in astrocytic Ca^{2+} can cause release of arachidonic acid derivatives that regulate the tone of vascular smooth muscle (Zonta et al., 2003; Mulligan and MacVicar, 2004; Gordon et al., 2008). Additionally, Ca2+-activated calmodulin binds and activates several isoforms of nitric oxide synthase, leading to increases in nitric oxide synthesis and diffusion to neighboring cells, where it can cause relaxation of vascular smooth muscle (Chen and Wu, 2000; Garcin et al., 2004; Spratt et al., 2007).

Previously, the role of astrocytes in neurovascular coupling was brought into question due to slow Ca^{2+} responses measured from the soma, and the lack of an effect on vascular responsiveness when blocking IP_3R-mediated Ca^{2+} signals in astrocytes (Schulz et al., 2012; Nizar et al., 2013). This controversy was resolved by the discovery of Ca^{2+} signals out in astrocytic processes that are more rapid and frequent than their somatic counterparts, precede the vascular response, and occur independent of IP_3R activity (Lind et al., 2013; Otsu et al., 2015; Srinivasan et al., 2015; Tang et al., 2015; for review see Bazargani and Attwell, 2016). In addition to mediating neurovascular coupling, astrocytes in brainstem sense changes in partial pressure of oxygen via mitochondrial respiration, triggering Ca^{2+} signals that stimulate vesicular release of ATP to increase breathing activity in response to changes in brain oxygenation (Gourine et al., 2010; Kasymov et al., 2013; Angelova et al., 2015).

Investigations into the sources of IP_3R-independent Ca^{2+} signaling in astrocytic processes have focused on transmembrane routes of entry as an alternative to the IP_3R-mediated release from internal endoplasmic reticulum Ca^{2+} stores (Fig. 1.3). Transmembrane Ca^{2+} entry mechanisms identified thus far include TRPA1 channels (Shigetomi et al., 2012, 2013), G-protein coupled receptors associated with ion channels (Srinivasan et al., 2015), purinergic P2X1/5 receptors and NMDA receptors unique to cortical astrocytes (Hamilton et al., 2008; Palygin et al., 2010; for review, see Verkhratsky et al., 2012), and plasma membrane transporters for glutamate and GABA associated with reversal of Na^+/Ca^{2+} exchangers (Schummers et al., 2008; Doengi et al., 2009; Magi et al., 2013a; Rojas et al., 2013; Jackson and Robinson, 2015). However, the endoplasmic reticulum is not the only source of internal Ca^{2+} release. Mitochondria also serve as internal Ca^{2+} stores, and participate in Ca^{2+} signaling in dissociated

astrocyte cultures (Parnis et al., 2013) and other cell types (for review, see Rizzuto et al., 2012). Our lab and another recently found that Ca^{2+} signaling influences the mobility of mitochondria in astrocytic processes by binding to MIRO motor adaptor proteins, and that these mitochondria in turn shape Ca^{2+} signaling in processes (Jackson and Robinson, 2015; Stephen et al., 2015).

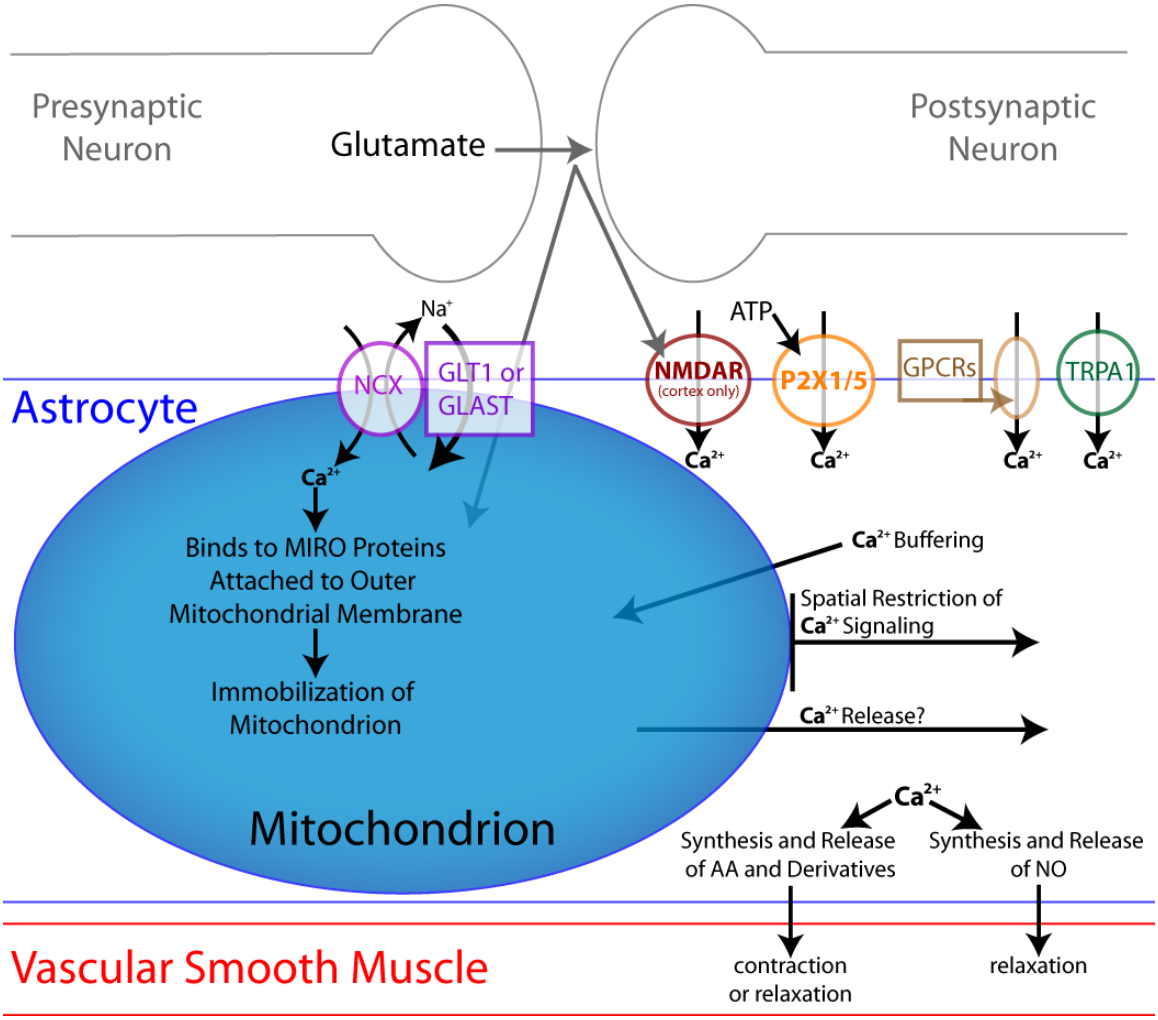

Figure 1.3. IP3R-independent Ca2+ signaling in astrocytic processes is shaped by mitochondria, and mediates neurovascular coupling and mitochondrial mobility. This simplified illustration depicts the various routes by which extracellular Ca2+ can enter astrocytic processes. Ca2+-mediated immobilization of mitochondria is highlighted, as well as the roles of mitochondria in Ca2+ signaling, to include buffering, spatial restriction, and possibly release. Ca2+-mediated mechanisms of vascular signaling are displayed, and include arachidonic acid (AA) derivatives and nitric oxide (NO).

While performing live Ca^{2+} imaging experiments in transfected hippocampal slice cultures using a highly sensitive genetic Ca^{2+} sensor in tandem with a mitochondrially-targeted fluorescent marker, I discovered two anatomically distinct types of spontaneous cytosolic Ca^{2+} signals in astrocytic processes (O'Donnell et al., 2016). As detailed in Chapter 4, I observed extra-mitochondrial spikes with high spatial spread, as well as persistent mitochondrially-centered signals that fluctuated with high frequency and duration, appearing as Ca^{2+} clouds surrounding mitochondria. While that paper was under review, Baljit Khakh's group published a paper in which they also described two distinct types of Ca^{2+} signals in astrocytic processes with similar properties to those we had observed, but did not image mitochondria (Jiang et al., 2016). Though additional investigations will provide more detail, there is compelling evidence that mitochondria shape Ca^{2+} signals in astrocytic processes, and may even serve as an intracellular source for IP_3R-independent Ca^{2+} signaling. Furthermore, by regulating the distribution of mitochondria in processes and serving as an extracellular source of Ca^{2+} linked to neuronal activity, glutamate transporters may play an important role in neurovascular coupling.

1.7 Mitochondria in astrocytic processes under pathological conditions

In the brain, astrocytes are primarily responsible for ion homeostasis, facilitating anabolic and catabolic metabolism, providing antioxidant protection, fixing NH_4, incorporating nitrogen into biological molecules, preventing edema, removing glutamate from the extracellular space, coupling neuronal activity to changes in blood flow and glucose uptake, regulating breathing in response to changes in brain oxygenation, directly participating in signaling and plasticity, and many other vital functions. Not

surprisingly, disruptions of each of these functions, often in combination, have been implicated in acute trauma and neurodegenerative disease, and many of them directly involve astrocytic mitochondria (for reviews, see Chen and Swanson, 2003; Rossi et al., 2007; Barreto et al., 2011; Lange et al., 2012; Brambilla et al., 2013; Stary and Giffard, 2015).

Since mitochondria in astrocytic processes were largely overlooked until recently, there have only been a few investigations into their pathological relevance. Using a focal ischemia model in gerbils, Ito et al. observed neuronal death in and around the cortical infarct with no increase in astrocyte death. Electron micrographs showed a reduced number of “normal-appearing” peripheral processes and reduced mitochondrial size with greater effects in areas of high neuronal death (Ito et al., 2009). Cortical stab wound in transgenic mice caused inflammation-dependent, DRP1-mediated fragmentation of mitochondria in the lesion core, while astrocytes in the penumbra exhibited elongated mitochondria. The fragmentation of mitochondria was transient, and reestablishing normal mitochondrial distribution and dynamics was prevented by blocking autophagy (Motori et al., 2013). The specialized form of autophagy responsible for degradation of damaged mitochondria is termed mitophagy (Lemasters, 2005). In neurons, mitochondria are targeted for mitophagy via ubiquitination of surface proteins by the E3 ubiquitin ligase Parkin (Matsuda et al., 2010 p.1; Chan et al., 2011; Wang et al., 2011; Yoshii et al., 2011; Wong and Holzbaur, 2014, 2015). Autophagosomes engulf mitochondria in distal neurites, and degradation proceeds during retrograde transport back to the cell body (Maday et al., 2012). Very little is known regarding the mechanisms and relevance of mitophagy in astrocytic processes.

Studies examining astrocytic mitochondria in primary culture have revealed depolarization and dysfunction in response to various pathological conditions and a few techniques to prevent that dysfunction (for review, see Stary and Giffard, 2015). Heat shock proteins involved in mitochondrial Ca^{2+} handling have been implicated in mitochondrial dysfunction in primary astrocytes, and pharmacological or genetic induction is neuroprotective in *in vitro* and *in vivo* models of ischemia (Ouyang et al., 2005, 2006; Sun et al., 2006; Xu et al., 2010). Astrocyte-targeted reduction of microRNAs that have been implicated in mitochondrial homeostatic mechanisms are neuroprotective in an *in vivo* model of ischemic stroke (Ouyang et al., 2011, 2012a, 2012b, 2013; Xu et al., 2015). Purinergic signaling plays a prominent role in astrocytic communication during health and disease (for review, see Franke et al., 2012). Calcium-mediated stimulation of mitochondrial metabolism in astrocytes via activation of purinergic P2Y1 receptors provides neuroprotection against oxidative stress in primary co-cultures (Wu et al., 2007), and reduces edema and infarct size in an in vivo photothrombotic stroke model in mice (Zheng et al., 2010, 2013). While these studies demonstrate the promise of targeting astrocytic mitochondria to provide neuroprotection *in vivo*, data regarding the astrocytic mitochondria themselves were almost entirely acquired using primary astrocyte cultures.

Astrocytes in primary culture provide a valuable, but limited, research platform (for review, see Lange et al., 2012). They lack the complex morphology found *in vivo*, and thus, cannot be used to study the unique cellular compartment of astrocytic processes in which many vital functions transpire. Organotypic hippocampal slice cultures maintain circuits and morphologies very similar to what is found *in vivo* (Stoppini et al., 1991), while allowing for high experimental control and easy access to various

output measures, including high resolution confocal microscopy. Sparse flourescent labeling of individual cells within slice cultures via biolistic transfection provides an optimal model for single cell analyses in the context of a greater cellular matrix. This slice culture model also exhibits delayed, progressive, excitotoxic neuropathology in area CA1 following transient oxygen/glucose deprivation (OGD), modeling the secondary pathology that emerges after cerebral ischemia/reperfusion injury *in vivo* (Bonde et al., 2005; for review, see Noraberg et al., 2005). After dissecting slices from rat pups 6-8 days postnatal, culturing slices for 14-18 days allows for synapse formation and expression of NMDAR subunits that sensitize the slice to excitotoxic injury (Ahlgren et al., 2011). At 14-18 days *in vitro,* there are still several weeks before spontaneous epileptiform activity emerges in the cultures (Albus et al., 2013). Utilizing a 30 min oxygen/glucose deprivation insult in biolistically transfected hippocampal slice cultures, I was able to conduct the first study of mitochondria, mitophagy, and calcium signaling in astrocytic processes during the development of secondary neuronal pathology, as detailed in Chapter 4 (O'Donnell et al., 2016).

I found that mitochondrial occupancy was reduced from ~60% of the length of astrocytic processes to ~30% due to fragmentation and, at least in part, autophagic degradation over the 24 h following the insult. Surprisingly, we found that while blocking astrocytic glutamate uptake with TFB-TBOA increased neuronal pathology in stratum pyramidale, it completely blocked the loss of astrocytic mitochondria. Additional experiments utilizing extended exposure to high exogenous glutamate concentrations in the presence of iGluR antagonists resulted in loss of astrocytic mitochondria in the absence of neuropathology. Taken together these results suggest that astrocytic mitochondrial loss is driven by an extended period of high glutamate transporter activity, and not by the concomitant neuronal damage. At 24 h after OGD, spontaneous

cytosolic calcium spikes in astrocytic processes were more intense and spread farther, no longer spatially restricted by mitochondria. The mitochondrially-centered signals were also more intense, but spatially smaller, tracking with a reduction in mitochondrial size in a manner that suggests that mitochondria may be the source of the Ca^{2+} signal.

As mentioned above, astrocytic Ca^{2+} signals are involved in mediating neurovascular coupling (Takano et al., 2006; Lind et al., 2013; Otsu et al., 2015; Srinivasan et al., 2015; Tang et al., 2015; Bazargani and Attwell, 2016), which is depressed after ischemia/reperfusion injury (Salinet et al., 2015). Astrocytic calcium signals can also trigger vesicular release of glutamate from astrocytes, which is increased after seizure or stroke and contributes to excitotoxic neuronal pathology (Ding et al., 2007; Hines and Haydon, 2013; Takemiya and Yamagata, 2013). Altered Ca^{2+} signaling is unlikely to be the only consequence of mitochondrial loss in astrocytic processes, and we are currently investigating the effects on glutamate transport and metabolism.

Astrocytes are vital for brain metabolism, a myriad of essential homeostatic functions, stemming the perpetual threat of excitotoxicity, and communicating between brain and body. All of these functions in some way rely on mitochondria in fine astrocytic processes, which appear to be uniquely susceptible to pathological conditions. Compared to the cell death among neurons, mitochondrial dysfunction is far less severe and very rarely fatal for astrocytes. Since astrocytes are capable of rescuing neurons from a multitude of angles all at once, a therapeutic approach that targets the less-severe dysfunction in astrocytes offers greater chances of success compared to therapies focused on a single neuronal target.

1.8 Summary

Mitochondria in astrocytic processes are central to the synthesis and metabolic flux of neurotransmitter glutamate, as well as the Ca^{2+} signaling that mediates neurovascular coupling and other functions. They are also central to pathology from acute brain trauma and neurodegenerative disease, offering unique opportunities for therapeutic intervention. In the following chapters, you will read about the effects of glutamate transporter activity on mitochondria and Ca^{2+} signaling in astrocytic processes. In healthy cells, glutamate transport positions mitochondria near transporters and synapses. This facilitates oxidation of neurotransmitter glutamate and shapes Ca^{2+} signaling. Under pathological conditions, excessive, extended periods of glutamate transport can cause mitochondrial fragmentation and autophagic degradation, leading to drastically altered Ca^{2+} signaling in processes. The following results prompted far more questions than they answered, indicating that science is working as it should, and the field is ripe for discovery.

1.9 References

Adeva MM, Souto G, Blanco N, Donapetry C (2012) Ammonium metabolism in humans. Metabolism 61:1495–1511.

Ahlgren H, Henjum K, Ottersen OP, Rundén-Pran E (2011) Validation of organotypical hippocampal slice cultures as an ex vivo model of brain ischemia: different roles of NMDA receptors in cell death signalling after exposure to NMDA or oxygen and glucose deprivation. Cell Tissue Res 345:329–341.

Albus K, Heinemann U, Kovács R (2013) Network activity in hippocampal slice cultures revealed by long-term in vitro recordings. J Neurosci Methods 217:1–8.

Angelova PR, Kasymov V, Christie I, Sheikhbahaei S, Turovsky E, Marina N, Korsak A, Zwicker J, Teschemacher AG, Ackland GL, Funk GD, Kasparov S, Abramov AY, Gourine AV (2015) Functional Oxygen Sensitivity of Astrocytes. J Neurosci 35:10460–10473.

Aoki C, Milner TA, Berger SB, Sheu KF, Blass JP, Pickel VM (1987) Glial glutamate dehydrogenase: ultrastructural localization and regional distribution in relation to the mitochondrial enzyme, cytochrome oxidase. J Neurosci Res 18:305–318.

Baloh RH, Schmidt RE, Pestronk A, Milbrandt J (2007) Altered axonal mitochondrial transport in the pathogenesis of Charcot-Marie-Tooth disease from mitofusin 2 mutations. J Neurosci 27:422–430.

Barreto G, White RE, Ouyang Y, Xu L, Giffard RG (2011) Astrocytes: targets for neuroprotection in stroke. Cent Nerv Syst Agents Med Chem 11:164–173.

Bauer DE, Jackson JG, Genda EN, Montoya MM, Yudkoff M, Robinson MB (2012) The glutamate transporter, GLAST, participates in a macromolecular complex that supports glutamate metabolism. Neurochem Int 61:566–574.

Bazargani N, Attwell D (2016) Astrocyte calcium signaling: the third wave. Nat Neurosci 19:182–189.

BeltrandelRio H, Wilson JE (1991) Hexokinase of rat brain mitochondria: Relative importance of adenylate kinase and oxidative phosphorylation as sources of substrate ATP, and interaction with intramitochondrial compartments of ATP and ADP. Arch Biochem Biophys 286:183–194.

Benediktsson AM, Schachtele SJ, Green SH, Dailey ME (2005) Ballistic labeling and dynamic imaging of astrocytes in organotypic hippocampal slice cultures. J Neurosci Methods 141:41–53.

Benjamin Kacerovsky J, Murai KK (2016) Stargazing: Monitoring subcellular dynamics of brain astrocytes. Neuroscience 323:84–95.

Bennett MR, Balcar VJ (1999) Forty years of amino acid transmission in the brain. Neurochem Int 35:269–280.

Bonde C, Noraberg J, Noer H, Zimmer J (2005) Ionotropic glutamate receptors and glutamate transporters are involved in necrotic neuronal cell death induced by oxygen-glucose deprivation of hippocampal slice cultures. Neuroscience 136:779–794.

Brambilla L, Martorana F, Rossi D (2013) Astrocyte signaling and neurodegeneration: new insights into CNS disorders. Prion 7:28–36.

Brockie PJ, Maricq AV (2003) Ionotropic glutamate receptors in Caenorhabditis elegans. Neurosignals 12:108–125.

Chan NC, Salazar AM, Pham AH, Sweredoski MJ, Kolawa NJ, Graham RLJ, Hess S, Chan DC (2011) Broad activation of the ubiquitin-proteasome system by Parkin is critical for mitophagy. Hum Mol Genet 20:1726–1737.

Chaudhry FA, Lehre KP, van Lookeren Campagne M, Ottersen OP, Danbolt NC, Storm-Mathisen J (1995) Glutamate transporters in glial plasma membranes: highly differentiated localizations revealed by quantitative ultrastructural immunocytochemistry. Neuron 15:711–720.

Chen PF, Wu KK (2000) Characterization of the roles of the 594-645 region in human endothelial nitric-oxide synthase in regulating calmodulin binding and electron transfer. J Biol Chem 275:13155–13163.

Chen Y, Swanson RA (2003) Astrocytes and Brain Injury. J Cereb Blood Flow Metab 23:137–149.

Chen Z-W, Olsen RW (2007) GABAA receptor associated proteins: a key factor regulating GABAA receptor function. J Neurochem 100:279–294.

Chiu J, DeSalle R, Lam HM, Meisel L, Coruzzi G (1999) Molecular evolution of glutamate receptors: a primitive signaling mechanism that existed before plants and animals diverged. Mol Biol Evol 16:826–838.

Choi DW, Rothman SM (1990) The role of glutamate neurotoxicity in hypoxic-ischemic neuronal death. Annu Rev Neurosci 13:171–182.

Csordás G, Várnai P, Golenár T, Roy S, Purkins G, Schneider TG, Balla T, Hajnóczky G (2010) Imaging interorganelle contacts and local calcium dynamics at the ER-mitochondrial interface. Mol Cell 39:121–132.

Danbolt NC (2001) Glutamate uptake. Prog Neurobiol 65:1–105.

Derouiche A, Haseleu J, Korf H-W (2015) Fine Astrocyte Processes Contain Very Small Mitochondria: Glial Oxidative Capability May Fuel Transmitter Metabolism. Neurochem Res 40:2402–2413.

Dienel GA, McKenna MC (2014) A dogma-breaking concept: glutamate oxidation in astrocytes is the source of lactate during aerobic glycolysis in resting subjects. J Neurochem 131:395–398.

Ding S, Fellin T, Zhu Y, Lee S-Y, Auberson YP, Meaney DF, Coulter DA, Carmignoto G, Haydon PG (2007) Enhanced Astrocytic Ca2+ Signals Contribute to Neuronal Excitotoxicity after Status Epilepticus. J Neurosci 27:10674–10684.

DiNuzzo M (2016) Astrocyte-Neuron Interactions during Learning May Occur by Lactate Signaling Rather than Metabolism. Front Integr Neurosci 10:2.

Doengi M, Hirnet D, Coulon P, Pape H-C, Deitmer JW, Lohr C (2009) GABA uptake-dependent Ca(2+) signaling in developing olfactory bulb astrocytes. Proc Natl Acad Sci U S A 106:17570–17575.

Fernandez B, Suarez I, Gianonatti C (1983) Fine structure of astrocytic mitochondria in the hypothalamus of the hamster. J Anat 137 (Pt 3):483–488.

Franke H, Verkhratsky A, Burnstock G, Illes P (2012) Pathophysiology of astroglial purinergic signalling. Purinergic Signal 8:629–657.

Garcin ED, Bruns CM, Lloyd SJ, Hosfield DJ, Tiso M, Gachhui R, Stuehr DJ, Tainer JA, Getzoff ED (2004) Structural basis for isozyme-specific regulation of electron transfer in nitric-oxide synthase. J Biol Chem 279:37918–37927.

Genda EN, Jackson JG, Sheldon AL, Locke SF, Greco TM, O'Donnell JC, Spruce LA, Xiao R, Guo W, Putt M, Seeholzer S, Ischiropoulos H, Robinson MB (2011) Co-compartmentalization of the astroglial glutamate transporter, GLT-1, with glycolytic enzymes and mitochondria. J Neurosci 31:18275–18288.

Gordon GRJ, Choi HB, Rungta RL, Ellis-Davies GCR, MacVicar BA (2008) Brain metabolism dictates the polarity of astrocyte control over arterioles. Nature 456:745–749.

Gould SJ, Vrba ES (1982) Exaptation-A Missing Term in the Science of Form. Paleobiology 8:4–15.

Gourine AV, Kasymov V, Marina N, Tang F, Figueiredo MF, Lane S, Teschemacher AG, Spyer KM, Deisseroth K, Kasparov S (2010) Astrocytes control breathing through pH-dependent release of ATP. Science 329:571–575.

Hamilton N, Vayro S, Kirchhoff F, Verkhratsky A, Robbins J, Gorecki DC, Butt AM (2008) Mechanisms of ATP- and glutamate-mediated calcium signaling in white matter astrocytes. Glia 56:734–749.

Harris JJ, Jolivet R, Attwell D (2012) Synaptic Energy Use and Supply. Neuron 75:762–777.

Hawkins RA, O'Kane RL, Simpson IA, Viña JR (2006) Structure of the blood-brain barrier and its role in the transport of amino acids. J Nutr 136:218S–26S.

Hertz L (2011) Astrocytic energy metabolism and glutamate formation--relevance for 13C-NMR spectroscopy and importance of cytosolic/mitochondrial trafficking. Magn Reson Imaging 29:1319–1329.

Hertz L, Peng L, Dienel GA (2007) Energy metabolism in astrocytes: high rate of oxidative metabolism and spatiotemporal dependence on glycolysis/glycogenolysis. J Cereb Blood Flow Metab Off J Int Soc Cereb Blood Flow Metab 27:219–249.

Hines DJ, Haydon PG (2013) Inhibition of a SNARE-Sensitive Pathway in Astrocytes Attenuates Damage following Stroke. J Neurosci 33:4234–4240.

Ito U, Hakamata Y, Kawakami E, Oyanagi K (2009) Degeneration of Astrocytic Processes and Their Mitochondria in Cerebral Cortical Regions Peripheral to the Cortical Infarction:

Heterogeneity of Their Disintegration Is Closely Associated With Disseminated Selective Neuronal Necrosis and Maturation of Injury. Stroke 40:2173–2181.

Jackson JG, O'Donnell JC, Krizman E, Robinson MB (2015) Displacing hexokinase from mitochondrial voltage-dependent anion channel impairs GLT-1-mediated glutamate uptake but does not disrupt interactions between GLT-1 and mitochondrial proteins: HK1 Supports GLT-1 Function. J Neurosci Res 93:999–1008.

Jackson JG, O'Donnell JC, Takano H, Coulter DA, Robinson MB (2014) Neuronal Activity and Glutamate Uptake Decrease Mitochondrial Mobility in Astrocytes and Position Mitochondria Near Glutamate Transporters. J Neurosci 34:1613–1624.

Jackson JG, Robinson MB (2015) Reciprocal Regulation of Mitochondrial Dynamics and Calcium Signaling in Astrocyte Processes. J Neurosci 35:15199–15213.

Janovjak H, Sandoz G, Isacoff EY (2011) A modern ionotropic glutamate receptor with a K+ selectivity signature sequence. Nat Commun 2:232.

Jiang R, Diaz-Castro B, Looger LL, Khakh BS (2016) Dysfunctional Calcium and Glutamate Signaling in Striatal Astrocytes from Huntington's Disease Model Mice. J Neurosci 36:3453–3470.

Kano T, Brockie PJ, Sassa T, Fujimoto H, Kawahara Y, Iino Y, Mellem JE, Madsen DM, Hosono R, Maricq AV (2008) Memory in Caenorhabditis elegans is mediated by NMDA-type ionotropic glutamate receptors. Curr Biol CB 18:1010–1015.

Karaca M, Frigerio F, Migrenne S, Martin-Levilain J, Skytt DM, Pajecka K, Martin-del-Rio R, Gruetter R, Tamarit-Rodriguez J, Waagepetersen HS, Magnan C, Maechler P (2015) GDH-Dependent Glutamate Oxidation in the Brain Dictates Peripheral Energy Substrate Distribution. Cell Rep 13:365–375.

Kasymov V, Larina O, Castaldo C, Marina N, Patrushev M, Kasparov S, Gourine AV (2013) Differential sensitivity of brainstem versus cortical astrocytes to changes in pH reveals functional regional specialization of astroglia. J Neurosci 33:435–441.

Krnjević K (2010) When and why amino acids? J Physiol 588:33–44.

Kvamme E, Roberg B, Torgner IA (2000) Phosphate-activated glutaminase and mitochondrial glutamine transport in the brain. Neurochem Res 25:1407–1419.

Lange SC, Bak LK, Waagepetersen HS, Schousboe A, Norenberg MD (2012) Primary Cultures of Astrocytes: Their Value in Understanding Astrocytes in Health and Disease. Neurochem Res 37:2569–2588.

Lavialle M, Aumann G, Anlauf E, Prols F, Arpin M, Derouiche A (2011) Structural plasticity of perisynaptic astrocyte processes involves ezrin and metabotropic glutamate receptors. Proc Natl Acad Sci 108:12915–12919.

Lehre KP, Levy LM, Ottersen OP, Storm-Mathisen J, Danbolt NC (1995) Differential expression of two glial glutamate transporters in the rat brain: quantitative and immunocytochemical observations. J Neurosci 15:1835–1853.

Lemasters JJ (2005) Selective Mitochondrial Autophagy, or Mitophagy, as a Targeted Defense Against Oxidative Stress, Mitochondrial Dysfunction, and Aging. Rejuvenation Res 8:3–5.

Levitan IB (2006) Signaling protein complexes associated with neuronal ion channels. Nat Neurosci 9:305–310.

Ligon LA, Steward O (2000) Role of microtubules and actin filaments in the movement of mitochondria in the axons and dendrites of cultured hippocampal neurons. J Comp Neurol 427:351–361.

Lind BL, Brazhe AR, Jessen SB, Tan FCC, Lauritzen MJ (2013) Rapid stimulus-evoked astrocyte Ca2+ elevations and hemodynamic responses in mouse somatosensory cortex in vivo. Proc Natl Acad Sci U S A 110:E4678-4687.

Lindén M, Gellerfors P, Nelson BD (1982) Pore protein and the hexokinase-binding protein from the outer membrane of rat liver mitochondria are identical. FEBS Lett 141:189–192.

Liu J, Prindle A, Humphries J, Gabalda-Sagarra M, Asally M, Lee DD, Ly S, Garcia-Ojalvo J, Süel GM (2015) Metabolic codependence gives rise to collective oscillations within biofilms. Nature 523:550–554.

Lovatt D, Sonnewald U, Waagepetersen HS, Schousboe A, He W, Lin JH-C, Han X, Takano T, Wang S, Sim FJ, Goldman SA, Nedergaard M (2007) The Transcriptome and Metabolic Gene Signature of Protoplasmic Astrocytes in the Adult Murine Cortex. J Neurosci 27:12255–12266.

Maday S, Wallace KE, Holzbaur ELF (2012) Autophagosomes initiate distally and mature during transport toward the cell soma in primary neurons. J Cell Biol 196:407–417.

Magi S, Arcangeli S, Castaldo P, Nasti AA, Berrino L, Piegari E, Bernardini R, Amoroso S, Lariccia V (2013) Glutamate-induced ATP synthesis: relationship between plasma membrane Na+/Ca2+ exchanger and excitatory amino acid transporters in brain and heart cell models. Mol Pharmacol 84:603–614.

Mandela P, Ordway GA (2006) The norepinephrine transporter and its regulation. J Neurochem 97:310–333.

Mangia S, Giove F, DiNuzzo M (2012) Metabolic Pathways and Activity-Dependent Modulation of Glutamate Concentration in the Human Brain. Neurochem Res 37:2554–2561.

Matsuda N, Sato S, Shiba K, Okatsu K, Saisho K, Gautier CA, Sou Y-S, Saiki S, Kawajiri S, Sato F, Kimura M, Komatsu M, Hattori N, Tanaka K (2010) PINK1 stabilized by mitochondrial

depolarization recruits Parkin to damaged mitochondria and activates latent Parkin for mitophagy. J Cell Biol 189:211–221.

McKenna MC (2007) The glutamate-glutamine cycle is not stoichiometric: fates of glutamate in brain. J Neurosci Res 85:3347–3358.

McKenna MC (2012) Substrate Competition Studies Demonstrate Oxidative Metabolism of Glucose, Glutamate, Glutamine, Lactate and 3-Hydroxybutyrate in Cortical Astrocytes from Rat Brain. Neurochem Res 37:2613–2626.

McKenna MC (2013) Glutamate pays its own way in astrocytes. Front Endocrinol 4:191.

McKenna MC, Sonnewald U, Huang X, Stevenson J, Zielke HR (2002) Exogenous Glutamate Concentration Regulates the Metabolic Fate of Glutamate in Astrocytes. J Neurochem 66:386–393.

Morris RL, Hollenbeck PJ (1993) The regulation of bidirectional mitochondrial transport is coordinated with axonal outgrowth. J Cell Sci 104 (Pt 3):917–927.

Morris RL, Hollenbeck PJ (1995) Axonal transport of mitochondria along microtubules and F-actin in living vertebrate neurons. J Cell Biol 131:1315–1326.

Motori E, Puyal J, Toni N, Ghanem A, Angeloni C, Malaguti M, Cantelli-Forti G, Berninger B, Conzelmann K-K, Götz M, Winklhofer KF, Hrelia S, Bergami M (2013) Inflammation-induced alteration of astrocyte mitochondrial dynamics requires autophagy for mitochondrial network maintenance. Cell Metab 18:844–859.

Mugnaini E (1964) HELICAL FILAMENTS IN ASTROCYTIC MITOCHONDRIA OF THE CORPUS STRIATUM IN THE RAT. J Cell Biol 23:173–182.

Müller CS, Haupt A, Bildl W, Schindler J, Knaus H-G, Meissner M, Rammner B, Striessnig J, Flockerzi V, Fakler B, Schulte U (2010) Quantitative proteomics of the Cav2 channel nano-environments in the mammalian brain. Proc Natl Acad Sci U S A 107:14950–14957.

Mulligan SJ, MacVicar BA (2004) Calcium transients in astrocyte endfeet cause cerebrovascular constrictions. Nature 431:195–199.

Nakashima RA, Mangan PS, Colombini M, Pedersen PL (1986) Hexokinase receptor complex in hepatoma mitochondria: evidence from N,N'-dicyclohexylcarbodiimide-labeling studies for the involvement of the pore-forming protein VDAC. Biochemistry (Mosc) 25:1015–1021.

Nizar K et al. (2013) In vivo stimulus-induced vasodilation occurs without IP3 receptor activation and may precede astrocytic calcium increase. J Neurosci 33:8411–8422.

Noraberg J, Poulsen FR, Blaabjerg M, Kristensen BW, Bonde C, Montero M, Meyer M, Gramsbergen JB, Zimmer J (2005) Organotypic hippocampal slice cultures for studies of

brain damage, neuroprotection and neurorepair. Curr Drug Targets CNS Neurol Disord 4:435–452.

Norenberg MD, Martinez-Hernandez A (1979) Fine structural localization of glutamine synthetase in astrocytes of rat brain. Brain Res 161:303–310.

Oberheim NA, Takano T, Han X, He W, Lin JHC, Wang F, Xu Q, Wyatt JD, Pilcher W, Ojemann JG, Ransom BR, Goldman SA, Nedergaard M (2009) Uniquely Hominid Features of Adult Human Astrocytes. J Neurosci 29:3276–3287.

O'Donnell JC, Jackson JG, Robinson MB (2016) Transient Oxygen/Glucose Deprivation Causes a Delayed Loss of Mitochondria and Increases Spontaneous Calcium Signaling in Astrocytic Processes. J Neurosci 36:7109–7127.

Otsu Y, Couchman K, Lyons DG, Collot M, Agarwal A, Mallet J-M, Pfrieger FW, Bergles DE, Charpak S (2015) Calcium dynamics in astrocyte processes during neurovascular coupling. Nat Neurosci 18:210–218.

Ouyang Y-B, Lu Y, Yue S, Giffard RG (2012a) miR-181 targets multiple Bcl-2 family members and influences apoptosis and mitochondrial function in astrocytes. Mitochondrion 12:213–219.

Ouyang Y-B, Lu Y, Yue S, Xu L-J, Xiong X-X, White RE, Sun X, Giffard RG (2012b) miR-181 regulates GRP78 and influences outcome from cerebral ischemia in vitro and in vivo. Neurobiol Dis 45:555–563.

Ouyang Y-B, Xu L, Giffard RG (2005) Geldanamycin treatment reduces delayed CA1 damage in mouse hippocampal organotypic cultures subjected to oxygen glucose deprivation. Neurosci Lett 380:229–233.

Ouyang Y-B, Xu L, Lu Y, Sun X, Yue S, Xiong X-X, Giffard RG (2013) Astrocyte-enriched miR-29a targets PUMA and reduces neuronal vulnerability to forebrain ischemia. Glia 61:1784–1794.

Ouyang Y-B, Xu L-J, Emery JF, Lee AS, Giffard RG (2011) Overexpressing GRP78 influences Ca2+ handling and function of mitochondria in astrocytes after ischemia-like stress. Mitochondrion 11:279–286.

Ouyang Y-B, Xu L-J, Sun Y-J, Giffard RG (2006) Overexpression of inducible heat shock protein 70 and its mutants in astrocytes is associated with maintenance of mitochondrial physiology during glucose deprivation stress. Cell Stress Chaperones 11:180–186.

Palygin O, Lalo U, Verkhratsky A, Pankratov Y (2010) Ionotropic NMDA and P2X1/5 receptors mediate synaptically induced Ca2+ signalling in cortical astrocytes. Cell Calcium 48:225–231.

Pardo B, Rodrigues TB, Contreras L, Garzón M, Llorente-Folch I, Kobayashi K, Saheki T, Cerdan S, Satrústegui J (2011) Brain glutamine synthesis requires neuronal-born aspartate as amino donor for glial glutamate formation. J Cereb Blood Flow Metab 31:90–101.

Parnis J, Montana V, Delgado-Martinez I, Matyash V, Parpura V, Kettenmann H, Sekler I, Nolte C (2013) Mitochondrial exchanger NCLX plays a major role in the intracellular Ca2+ signaling, gliotransmission, and proliferation of astrocytes. J Neurosci 33:7206–7219.

Pellerin L, Magistretti PJ (1994) Glutamate uptake into astrocytes stimulates aerobic glycolysis: a mechanism coupling neuronal activity to glucose utilization. Proc Natl Acad Sci 91:10625–10629.

Prindle A, Liu J, Asally M, Ly S, Garcia-Ojalvo J, Süel GM (2015) Ion channels enable electrical communication in bacterial communities. Nature 527:59–63.

Ramoino P, Candiani S, Pittaluga AM, Usai C, Gallus L, Ferrando S, Milanese M, Faimali M, Bonanno G (2014) Pharmacological characterization of NMDA-like receptors in the single-celled organism Paramecium primaurelia. J Exp Biol 217:463–471.

Rizzuto R, De Stefani D, Raffaello A, Mammucari C (2012) Mitochondria as sensors and regulators of calcium signalling. Nat Rev Mol Cell Biol 13:566–578.

Rizzuto R, Pinton P, Carrington W, Fay FS, Fogarty KE, Lifshitz LM, Tuft RA, Pozzan T (1998) Close contacts with the endoplasmic reticulum as determinants of mitochondrial Ca2+ responses. Science 280:1763–1766.

Robinson MB, Jackson JG (2016) Astroglial Glutamate Transporters Coordinate Excitatory Signaling and Brain Energetics. Neurochem Int.

Rodrigues-Ferreira C, Silva APP, Galina A (2012) Effect of the antitumoral alkylating agent 3-bromopyruvate on mitochondrial respiration: role of mitochondrially bound hexokinase. J Bioenerg Biomembr 44:39–49.

Rojas H, Colina C, Ramos M, Benaim G, Jaffe E, Caputo C, Di Polo R (2013) Sodium-calcium exchanger modulates the L-glutamate Ca(i) (2+) signalling in type-1 cerebellar astrocytes. Adv Exp Med Biol 961:267–274.

Rossi DJ, Brady JD, Mohr C (2007) Astrocyte metabolism and signaling during brain ischemia. Nat Neurosci 10:1377–1386.

Ruthel G, Hollenbeck PJ (2003) Response of mitochondrial traffic to axon determination and differential branch growth. J Neurosci 23:8618–8624.

Salinet ASM, Robinson TG, Panerai RB (2015) Effects of cerebral ischemia on human neurovascular coupling, CO_2 reactivity, and dynamic cerebral autoregulation. J Appl Physiol 118:170–177.

Schousboe A, Bak LK, Waagepetersen HS (2013) Astrocytic Control of Biosynthesis and Turnover of the Neurotransmitters Glutamate and GABA. Front Endocrinol 4:102.

Schousboe A, Scafidi S, Bak LK, Waagepetersen HS, McKenna MC (2014) Glutamate metabolism in the brain focusing on astrocytes. Adv Neurobiol 11:13–30.

Schousboe A, Waagepetersen HS (2005) Role of astrocytes in glutamate homeostasis: implications for excitotoxicity. Neurotox Res 8:221–225.

Schulz K, Sydekum E, Krueppel R, Engelbrecht CJ, Schlegel F, Schröter A, Rudin M, Helmchen F (2012) Simultaneous BOLD fMRI and fiber-optic calcium recording in rat neocortex. Nat Methods 9:597–602.

Schummers J, Yu H, Sur M (2008) Tuned responses of astrocytes and their influence on hemodynamic signals in the visual cortex. Science 320:1638–1643.

Schwarz TL (2013) Mitochondrial trafficking in neurons. Cold Spring Harb Perspect Biol 5:a011304.

Sheldon AL, Robinson MB (2007) The role of glutamate transporters in neurodegenerative diseases and potential opportunities for intervention. Neurochem Int 51:333–355.

Sheng Z-H, Cai Q (2012) Mitochondrial transport in neurons: impact on synaptic homeostasis and neurodegeneration. Nat Rev Neurosci 13:77–93.

Shigetomi E, Jackson-Weaver O, Huckstepp RT, O'Dell TJ, Khakh BS (2013) TRPA1 channels are regulators of astrocyte basal calcium levels and long-term potentiation via constitutive D-serine release. J Neurosci 33:10143–10153.

Shigetomi E, Tong X, Kwan KY, Corey DP, Khakh BS (2012) TRPA1 channels regulate astrocyte resting calcium and inhibitory synapse efficacy through GAT-3. Nat Neurosci 15:70–80.

Smith QR (2000) Transport of glutamate and other amino acids at the blood-brain barrier. J Nutr 130:1016S–22S.

Sonnewald U (2014) Glutamate synthesis has to be matched by its degradation - where do all the carbons go? J Neurochem 131:399–406.

Spratt DE, Taiakina V, Palmer M, Guillemette JG (2007) Differential binding of calmodulin domains to constitutive and inducible nitric oxide synthase enzymes. Biochemistry (Mosc) 46:8288–8300.

Srinivasan R, Huang BS, Venugopal S, Johnston AD, Chai H, Zeng H, Golshani P, Khakh BS (2015) Ca(2+) signaling in astrocytes from Ip3r2(-/-) mice in brain slices and during startle responses in vivo. Nat Neurosci 18:708–717.

Stary CM, Giffard RG (2015) Advances in Astrocyte-targeted Approaches for Stroke Therapy: An Emerging Role for Mitochondria and microRNAS. Neurochem Res 40:301–307.

Stephen T-L, Higgs NF, Sheehan DF, Awabdh SA, López-Doménech G, Arancibia-Carcamo IL, Kittler JT (2015) Miro1 Regulates Activity-Driven Positioning of Mitochondria within Astrocytic Processes Apposed to Synapses to Regulate Intracellular Calcium Signaling. J Neurosci 35:15996–16011.

Stoppini L, Buchs P-A, Muller D (1991) A simple method for organotypic cultures of nervous tissue. J Neurosci Methods 37:173–182.

Sui D, Wilson JE (1997) Structural determinants for the intracellular localization of the isozymes of mammalian hexokinase: intracellular localization of fusion constructs incorporating structural elements from the hexokinase isozymes and the green fluorescent protein. Arch Biochem Biophys 345:111–125.

Sun Y, Ouyang Y-B, Xu L, Chow AM-Y, Anderson R, Hecker JG, Giffard RG (2006) The carboxyl-terminal domain of inducible Hsp70 protects from ischemic injury in vivo and in vitro. J Cereb Blood Flow Metab 26:937–950.

Szabadkai G, Bianchi K, Várnai P, De Stefani D, Wieckowski MR, Cavagna D, Nagy AI, Balla T, Rizzuto R (2006) Chaperone-mediated coupling of endoplasmic reticulum and mitochondrial Ca2+ channels. J Cell Biol 175:901–911.

Takano T, Tian G-F, Peng W, Lou N, Libionka W, Han X, Nedergaard M (2006) Astrocyte-mediated control of cerebral blood flow. Nat Neurosci 9:260–267.

Takemiya T, Yamagata K (2013) Intercellular Signaling Pathway among Endothelia, Astrocytes and Neurons in Excitatory Neuronal Damage. Int J Mol Sci 14:8345–8357.

Tang W, Szokol K, Jensen V, Enger R, Trivedi CA, Hvalby Ø, Helm PJ, Looger LL, Sprengel R, Nagelhus EA (2015) Stimulation-Evoked Ca2+ Signals in Astrocytic Processes at Hippocampal CA3–CA1 Synapses of Adult Mice Are Modulated by Glutamate and ATP. J Neurosci 35:3016–3021.

Torres GE (2006) The dopamine transporter proteome. J Neurochem 97 Suppl 1:3–10.

Ugbode CI, Hirst WD, Rattray M (2014) Neuronal influences are necessary to produce mitochondrial co-localization with glutamate transporters in astrocytes. J Neurochem 130:668–677.

Van Houten JL, Yang WQ, Bergeron A (2000) Chemosensory signal transduction in paramecium. J Nutr 130:946S–9S.

Verkhratsky A, Pankratov Y, Lalo U, Nedergaard M (2012) P2X receptors in neuroglia. Wiley Interdiscip Rev Membr Transp Signal 1.

Wang X, Winter D, Ashrafi G, Schlehe J, Wong YL, Selkoe D, Rice S, Steen J, LaVoie MJ, Schwarz TL (2011) PINK1 and Parkin Target Miro for Phosphorylation and Degradation to Arrest Mitochondrial Motility. Cell 147:893–906.

Waterham HR, Koster J, van Roermund CWT, Mooyer PAW, Wanders RJA, Leonard JV (2007) A lethal defect of mitochondrial and peroxisomal fission. N Engl J Med 356:1736–1741.

Watkins JC, Jane DE (2006) The glutamate story. Br J Pharmacol 147 Suppl 1:S100-108.

Whitelaw BS, Robinson MB (2013) Inhibitors of glutamate dehydrogenase block sodium-dependent glutamate uptake in rat brain membranes. Front Endocrinol 4:123.

Wong YC, Holzbaur ELF (2014) Optineurin is an autophagy receptor for damaged mitochondria in parkin-mediated mitophagy that is disrupted by an ALS-linked mutation. Proc Natl Acad Sci 111:E4439–E4448.

Wong YC, Holzbaur ELF (2015) Temporal dynamics of PARK2/parkin and OPTN/optineurin recruitment during the mitophagy of damaged mitochondria. Autophagy 11:422–424.

Wu J, Holstein JD, Upadhyay G, Lin D-T, Conway S, Muller E, Lechleiter JD (2007) Purinergic Receptor-Stimulated IP3-Mediated Ca2+ Release Enhances Neuroprotection by Increasing Astrocyte Mitochondrial Metabolism during Aging. J Neurosci 27:6510–6520.

Xu L, Emery JF, Ouyang Y-B, Voloboueva LA, Giffard RG (2010) Astrocyte targeted overexpression of Hsp72 or SOD2 reduces neuronal vulnerability to forebrain ischemia. Glia 58:1042–1049.

Xu L-J, Ouyang Y-B, Xiong X, Stary CM, Giffard RG (2015) Post-stroke treatment with miR-181 antagomir reduces injury and improves long-term behavioral recovery in mice after focal cerebral ischemia. Exp Neurol 264:1–7.

Xu N-J, Bao L, Fan H-P, Bao G-B, Pu L, Lu Y-J, Wu C-F, Zhang X, Pei G (2003) Morphine withdrawal increases glutamate uptake and surface expression of glutamate transporter GLT1 at hippocampal synapses. J Neurosci 23:4775–4784.

Yoshii SR, Kishi C, Ishihara N, Mizushima N (2011) Parkin Mediates Proteasome-dependent Protein Degradation and Rupture of the Outer Mitochondrial Membrane. J Biol Chem 286:19630–19640.

Youle RJ, Bliek AM van der (2012) Mitochondrial Fission, Fusion, and Stress. Science 337:1062–1065.

Yu AC, Schousboe A, Hertz L (1982) Metabolic fate of 14C-labeled glutamate in astrocytes in primary cultures. J Neurochem 39:954–960.

Zaid H, Talior-Volodarsky I, Antonescu C, Liu Z, Klip A (2009) GAPDH binds GLUT4 reciprocally to hexokinase-II and regulates glucose transport activity. Biochem J 419:475–484.

Zhang CL, Ho PL, Kintner DB, Sun D, Chiu SY (2010) Activity-dependent regulation of mitochondrial motility by calcium and Na/K-ATPase at nodes of Ranvier of myelinated nerves. J Neurosci 30:3555–3566.

Zheng W, Talley Watts L, Holstein DM, Wewer J, Lechleiter JD (2013) P2Y1R-initiated, IP3R-dependent stimulation of astrocyte mitochondrial metabolism reduces and partially reverses ischemic neuronal damage in mouse. J Cereb Blood Flow Metab 33:600–611.

Zheng W, Watts LT, Holstein DM, Prajapati SI, Keller C, Grass EH, Walter CA, Lechleiter JD (2010) Purinergic Receptor Stimulation Reduces Cytotoxic Edema and Brain Infarcts in Mouse Induced by Photothrombosis by Energizing Glial Mitochondria. PLoS ONE 5:e14401.

Zonta M, Angulo MC, Gobbo S, Rosengarten B, Hossmann K-A, Pozzan T, Carmignoto G (2003) Neuron-to-astrocyte signaling is central to the dynamic control of brain microcirculation. Nat Neurosci 6:43–50.

CHAPTER 2

Displacing hexokinase from mitochondrial voltage-dependent anion channel (VDAC) impairs GLT-1-mediated glutamate uptake but does not disrupt interactions between GLT-1 and mitochondrial proteins

Joshua G. Jackson[1,2*], John C. O'Donnell[1,3*], Elizabeth Krizman[1], and Michael B. Robinson[1,2,3].

*Authors contributed equally to the completion of this manuscript.

Children's Hospital of Philadelphia Research Institute[1], and Departments of Pediatrics[2], and Pharmacology[3], University of Pennsylvania, Philadelphia, PA 19104

Address Correspondence to: Michael B. Robinson
Department of Pediatrics, 502N
Abramson Pediatric Research Building
3615 Civic Center Boulevard
Philadelphia, PA 19104-3779
Tel. 215-590-2205; Fax. 215-590-3779
Email: Robinson@mail.med.upenn.edu

Author contributions: J.G.J., J.C.O., and M.B.R. designed research; J.G.J., J.C.O., and E.K. performed research; J.G.J., J.C.O., and E.K. analyzed data; J.G.J., J.C.O., and M.B.R. wrote the paper.

Grant Support: This work was supported by a grant (RO1 NS077773) to M.B.R. from the National Institute of Neurological Disorders and Stroke. J.C.O. was partially supported by National Research Service Awards, T32 GM008076 and F31 NS086255, from the National Institutes of Health. J.G.J was partially supported by National Research Service Award T32 NS007413. The Institutional Intellectual and Developmental Disabilities Research Center (P30 HD26979) also provided valuable support for these studies.

Published in The Journal of Neuroscience Research, July 2015. Volume 93, Issue 7, pages 999-1008.

Abstract

The glutamate transporter GLT-1 is the major route for the clearance of extracellular glutamate in the forebrain, and most GLT-1 protein is found in astrocytes. This protein is coupled to the Na^+-electrochemical gradient, supporting the active intracellular accumulation of glutamate. We recently used a proteomic approach to identify proteins that may interact with GLT-1 in rat cortex, including the Na^+/K^+-ATPase, most glycolytic enzymes, and several mitochondrial proteins. We also showed that most GLT-1 puncta (~70%) are overlapped by mitochondria in astroglial processes in organotypic slices. Based on this analysis, we proposed that the glycolytic enzyme hexokinase 1 (HK1) might physically form a scaffold to link GLT-1 and mitochondria because HK1 is known to interact with the outer mitochondrial membrane protein, voltage-dependent anion channel (VDAC). In the present study, we first validated the interactions between HK-1, VDAC and GLT-1 using forward and reverse immunoprecipitations. We also provided evidence that a subfraction of HK1 co-localizes with GLT-1 *in vivo*. We found that a peptide, known to disrupt the interaction between HK and VDAC, did not disrupt interactions between GLT-1 and several mitochondrial proteins. In parallel experiments, we found that displacement of HK from VDAC reduced GLT-1-mediated glutamate uptake. These results suggest that although HK1 forms co-immunoprecipitatable complexes with both VDAC and GLT-1, it does not physically link GLT-1 to mitochondrial proteins. However, the interaction of HK1 with VDAC supports GLT-1-mediated transport activity.

2.1 Introduction

Glutamate is the principal excitatory neurotransmitter in the CNS. Synaptic concentrations of glutamate are maintained at low levels (approximately 25 nM) against brain concentrations that approach 10 mmol/Kg in order to ensure proper signaling and prevent excitotoxicity (Herman and Jahr 2007; Schousboe 1981). Glutamate is cleared from the synapse by a family of Na^+-dependent glutamate transporters of which GLT-1 and GLAST, the astroglial glutamate transporters, predominate (for reviews, see Danbolt 2001; Robinson 1999). These transporters couple the uptake of one molecule of glutamate with the co-transport of 3 Na^+ ions and a H^+, followed by the counter-transport of a K^+ ion (Zerangue and Kavanaugh 1996).

Using mass spectrometry, we previously identified subunits of the Na^+/K^+-ATPase, most of the glycolytic enzymes, and several mitochondrial proteins in GLT-1 immunoprecipitates from rat cortical homogenates (Genda et al. 2011). In this same study, we also showed that GLT-1 and mitochondria overlap more than 70% of the time in astroglial processes in cultured organotypic hippocampal slices and that this overlap was greater than would be observed by chance, consistent with a physical interaction between GLT-1 and mitochondria. We proposed that this complex might provide metabolic support to facilitate glutamate uptake. We also proposed that the glycolytic enzyme HK1 might serve as a scaffolding protein linking plasma membrane GLT-1 with mitochondrial proteins. A known interaction between HK and the plasma membrane glucose transporter GLUT4 gave precedence to the possibility of direct HK interactions with GLT-1 (Zaid et al. 2009).

Hexokinase catalyzes the first and one of the rate limiting steps of glycolysis, the phosphorylation of glucose to form glucose-6-phosphate. Glucose phosphorylation also represents the first step in the synthesis of glycogen and the pentose phosphate shunt. In brain, most HK1 is bound to mitochondria by a hydrophobic N-terminal domain that interacts with the voltage dependent anion channel (VDAC) found in the outer mitochondrial membrane (Linden et al. 1982; Nakashima et al. 1986 Sui and Wilson 1997). VDAC interacts with the adenine nucleotide translocase (ANT) in the inner mitochondrial membrane (Beutner et al. 1998 Crompton et al. 1998) and many of the mitochondrial proteins form supercomplexes (Acin-Perez et al. 2008). Hexokinase/VDAC interactions link glycolysis and oxidative phosphorylation. HK1 binding of VDAC is thought to increase the catalytic efficiency of both processes by facilitating mitochondrial ATP release from VDAC for glucose phosphorylation and by channeling ADP into mitochondria for oxidative phosphorylation (BeltrandelRio and Wilson 1991; Rodrigues-Ferreira et al. 2012).

Given the importance of glutamate signaling and the metabolic costs associated with maintaining glutamate uptake, it is not surprising that glutamate uptake is intimately associated with metabolism. Glutamate uptake and Na^+/K^+-ATPase activity are fueled by glycolysis, glycogenolysis, and oxidative phosphorylation (Fernandez-Moncada and Barros 2014; Genda et al. 2011; Sickmann et al. 2009). Glutamate uptake stimulates glycolysis (Pellerin and Magistretti 1994), glucose uptake (Hamai et al. 1999; Loaiza et al. 2003), and glycogen formation (Hamai et al. 1999; Swanson et al. 1990). In addition, glutamate can itself be oxidized within the mitochondria, potentially fueling its own uptake (Sonnewald and McKenna 2002). In fact, inhibitors of glutamate dehydrogenase (GDH) block glutamate uptake (Whitelaw and Robinson 2013).

In the present study, we validated GLT-1 interactions with VDAC and HK1 using both forward and reverse immunoprecipitations. We then tested whether HK1 might provide a mechanism to link the plasma membrane protein, GLT-1, with mitochondrial proteins (e.g. VDAC, UQCRC2, ANT). In addition, we determined if the interaction between HK1 and VDAC contributes to supporting glutamate uptake.

2.2 Methods

All procedures involving the use of animals were reviewed and approved by the Institutional Animal Care and Use Committee of the Children's Hospital of Philadelphia (Philadelphia, PA USA).

Preparation of tissue/immunoprecipitation. Cortical tissue was harvested from adult male Sprague Dawley rats after euthanasia by decapitation to avoid potential effects of anesthetic agents (Huang and Zuo 2005). Total tissue lysates were prepared as previously described (Genda et al. 2011). Tissue was homogenized in ice cold immunoprecipitation buffer (18.4 ml per gram wet weight), containing 150 mM NaCl, 1 mM ethylene diamine tetraacetic acid (EDTA), 100 mM Tris HCl, pH 7.4, 1% Triton X-100, and 1% sodium deoxycholate plus protease and phosphatase inhibitors (1µg/ml leupeptin, 250 µM phenylmethylsulfonyl fluoride (PMSF), 1 µg/ml aprotinin, 1 mM iodoacetamide, 10 mM NaF, 30 mM sodium pyrophosphate and 1 mM sodium orthovanadate) using a Dounce Teflon/glass homogenizer (7 strokes at 400 RPM). All subsequent steps were performed keeping the tissue at 4º C. Homogenates were rotated on a shaker for 1 hr and then cleared of cellular debris by centrifugation at 13,000 g for 30 min. One ml of lysate was pre-cleared with 80 µl protein-A agarose

beads (Invitrogen, Carlsbad, CA) for 1 hr followed by centrifugation (16,500 g for 15 min). After analyses of protein (bicinchoninic acid protein assay kit; Pierce, Rockford, IL), an aliquot of the supernatant containing 500 µg of protein was mixed overnight with either 15µg antibody or a species-matched IgG (mouse IgG was from Zymed Laboratories/Life Technologies, Grand Island, NY, rabbit IgG was from Invitrogen, Carlsbad, CA). Protein complexes were batch extracted using protein-A agarose beads (30 µl) with gentle mixing for 2 hrs. Agarose beads were washed four times in immunoprecipitation buffer before elution of bound proteins by the addition of 25 µl SDS-PAGE loading buffer followed by incubation at 25°C for 45 min or 95°C for 5 min. Incubation at 25°C for 45 min reduces the formation of GLT-1 aggregates and was used for Figure 1B and C (upper panel) and Figure 4B.

Crude synaptosomal membranes (P2) were prepared as previously described (Robinson et al. 1991) except that the final P2 preparation was resuspended in 4.5 vols. of sucrose (0.32 M). An aliquot (450 µl) of this P2 suspension (containing ~ 1.8 mg of protein) was combined with 50 µl Hexokinase II VDAC binding domain peptide (fused to Antennapedia homeo-domain) (Calbiochem #376816) or control Antennapedia homeo-domain peptide (Calbiochem #287895) that had been resuspended in 0.32 M sucrose (100 µM final concentration) for 30 minutes at 37°C. An aliquot (65 µl) of this material was placed on ice for measurement of uptake (see below). The remainder of the material was centrifuged at 20,000 x g for 20 min. Except for the analyses of HK1 and VDAC interactions, the pellet was resuspended in 1 ml of immunoprecipitation buffer and processed as described above with 200 µl of pre-cleared lysate containing ~240 µg of protein. To test for HK1-VDAC interactions, pre-cleared lysates were incubated

overnight using a Pierce crosslink immunoprecipitation columns (Thermo Scientific, Waltham, MA) prepared using 15 µg HK1 antibody or mouse IgG.

Western Blot Analysis: Proteins were separated using 10% SDS-polyacrylamide gels and transferred to polyvinylidene fluoride membranes (PVDF-FL; Millipore, Billerica, MA), and blocked for 1 hr at 25°C in TBS-T (50 mM Tris, 150 mM NaCl, pH 8.0, 0.1% Tween) containing 5% nonfat dry milk. Membranes were then probed with the appropriate primary antibody: rabbit or mouse anti-GLT-1 (1:5,000; courtesy of Dr. J. Rothstein, Johns Hopkins University, Baltimore, MD USA) (Rothstein et al. 1994); mouse anti-HK1 (1:500; Sigma, St. Louis, MO, #WH0003098M1); mouse anti-ubiquinol-cytochrome-c reductase complex core protein 2 (UQCRC2) (1:5000; Abcam, Cambridge, UK, #AB14745), rabbit anti-VDAC (1:1000; Abcam #AB15895); goat anti-ANT (1:50; Santa Cruz, Santa Cruz, CA, #SC9299). Membranes were incubated with fluorescent dye-conjugated anti-rabbit, anti-mouse, or anti-goat secondary antibodies (1:10,000; LiCor Biosciences, Lincoln, NE). Protein bands were visualized using an Odyssey Infrared Imager (LiCor Biosciences).

Glutamate uptake in P2 membrane fraction. Sodium-dependent transport of L-[^{3}H]-glutamate was measured as previously described (Robinson et al. 1991; Whitelaw and Robinson 2013). HKII or control treated synaptosomes (10 µL, containing ~40 µg of protein) were incubated with 0.5 µM L-[^{3}H]-glutamate (PerkinElmer, Waltham, MA USA) in uptake buffer, containing 5 mM Tris base, 10 mM HEPES, 140 mM NaCl, 2.5 mM KCl, 1.2 mM $CaCl_2$, 1.2 mM $MgCl_2$, 1.2 mM K_2HPO_4, 10 mM glucose (pH=7.2) at 37ºC for 3 min. We have previously determined that ^{3}H-glutamate uptake is linear until at least 5 min in this system (Robinson 1991). Uptake was measured in the absence and presence of sodium by substituting equimolar amounts of choline chloride for NaCl. The assay

was terminated by the addition of 2 ml of ice-cold choline-containing buffer. Following termination, the suspensions were filtered onto glass filter paper (FP-100; Brandel, Gaithersburg, MD USA) using a Brandel cell harvester and rinsed three times with 2 ml of cold choline-containing buffer. Radioactivity was solubilized with 5 ml of Cytoscint ES (MP Biochemicals, Solon, OH USA) and measured using scintillation spectrometry (Beckman-Coulter Instruments LS 6500). Sodium dependent uptake was calculated as the difference between the signal in the sodium-containing buffer from the signal in the choline-containing buffer.

Immunofluorescence. Adult rats (10–12 weeks) were anesthetized with isoflurane and transcardially perfused with ice-cold phosphate buffered saline (PBS) followed by 4% paraformaldehyde in PBS, pH 7.4. Brains were post-fixed overnight (4ºC), equilibrated in 30% sucrose, flash frozen in isopentane (-50ºC), and stored at -80ºC. Sections were cut on a freezing-sliding microtome and processed as free-floating sections. Sections were blocked in PBS containing 5% normal serum and 0.4% Triton X-100 for 1 hr and then incubated with rabbit anti-GLT-1 (Rothstein, 1:100) and/or mouse anti-HK1 (Sigma, St. Louis, MO; 1:100) overnight at 4ºC. After 3 rinses, they were incubated in secondary antibody (either Alexa Fluor 488 or 633; 1:400, Invitrogen) overnight at 4ºC. Sections were mounted on pre-coated slides, cover-slipped with mounting media (VectaShield), and stored at 4ºC until analysis. Controls for each experiment included incubations to confirm the species specificity of secondary antibodies and to confirm that signal was dependent on the presence of primary antibodies. Sections were visualized on a Fluoview 1000 confocal microscope (Olympus, Center Valley, PA) equipped with a PlanApo 60x objective (numerical

aperture = 1.4). All images were collected in sequential scan mode to minimize cross-contamination of fluorophores.

Intensity correlation analysis / intensity co-localization quotient. Single optical sections were background corrected and filtered using a Gaussian filter (r = 1). All image analysis was conducted using NIH ImageJ software (http://rsb.info.nih.gov/ij/). Images were automatically thresholded and the Intensity Co-localization Quotient (ICQ) values calculated using the intensity correlation analysis (ICA) plug-in to the McMaster Biophotonics Facility ImageJ collection. The ICQs were calculated as described by Li et al (2004); results were compared to zero using a one-sample t test. Images representing the product of the differences from the mean (PDM) intensity values were generated using this plugin.

2.3 Results

Interaction between GLT-1, HK1, and VDAC in the cortex

In our earlier study, we identified a number of glycolytic enzymes and mitochondrial proteins in GLT-1 immunoprecipitates from rat brain cortical lysates by mass spectrometry (Genda et al. 2011). Many of these interactions were further validated using conventional immunoprecipitation/western blotting and reverse immunoprecipitation using an antibody against the putative interacting protein. At the time, we were unable to validate the interactions with either HK1 or with VDAC because we could not identify suitable antibodies. For the present study, we found suitable antibodies for this purpose. Using these antibodies, we performed a series of immunoprecipitations followed by western blot analysis to test whether the glial

glutamate transporter GLT-1, the glycolytic enzyme HK1, and the mitochondrial protein VDAC interact in rat cortical tissue. Using an anti-GLT-1 antibody for immunoprecipitation, we observe HK1 (Fig 2.1). In addition, we consistently found ubiquinol-cytochrome-c reductase complex core protein 2 (UQCRC2), as was observed in our earlier study (Genda et al. 2011). In mammals, there are three isoforms of VDAC representing distinct gene products with high homology but different molecular weights due to post-translational modifications (Yamamoto et al. 2006). In the earlier mass spectroscopy analysis, we identified VDAC2 and VDAC3 in GLT-1 immunoprecipitates (Genda et al. 2011). Using an anti-VDAC antibody that recognizes all three isoforms, we observed bands at approximately 29 and 31 kDa in GLT-1 immunoprecipitates. The higher molecular weight band represents the VDAC1 and 2 isoforms, the lower molecular weight band represents VDAC3 **(**Kerner et al. 2012; Shoshan-Barmatz and Golan 2012; Yamamoto et al. 2006). In these same immunoprecipitates, we also verified the presence of GLT-1 (Fig. 2.1A, lower panel) that migrates as a monomer with a molecular weight of approximately 66 kDa and a trimer of approximately 200 kDa (Haugeto et al. 1996). These analyses complement our earlier mass spectroscopic analysis providing evidence that the proteins were appropriately identified, but they do not rule out the possibility that the anti-GLT-1 antibodies directly interact with these proteins.

To address this possibility, we performed a series of 'reverse' immunoprecipitations to determine if GLT-1 co-immunoprecipitates with these targets using antibodies against these putative interacting proteins. Using an anti-HK1 antibody, we find that UQCRC2, VDAC, and GLT-1 all co-immunoprecipitate with HK1 (Figure 2.1B, upper panels). Similarly, using an anti-VDAC antibody, we find that GLT-1, HK1,

and UQCRC2 all co-immunoprecipitate with VDAC (Figure 1C, upper panels). In both of these sets of immunoprecipitations, we confirmed that the intended target was observed in the immunoprecipitates (Figure 2.1B &C, lower panels). Although these results do not formally rule-out the possibility that subsets of these interacting proteins interact separately, the simplest explanation is that these proteins participate in a multi-protein complex that includes GLT-1, HK1, UQCRC2, and VDAC.

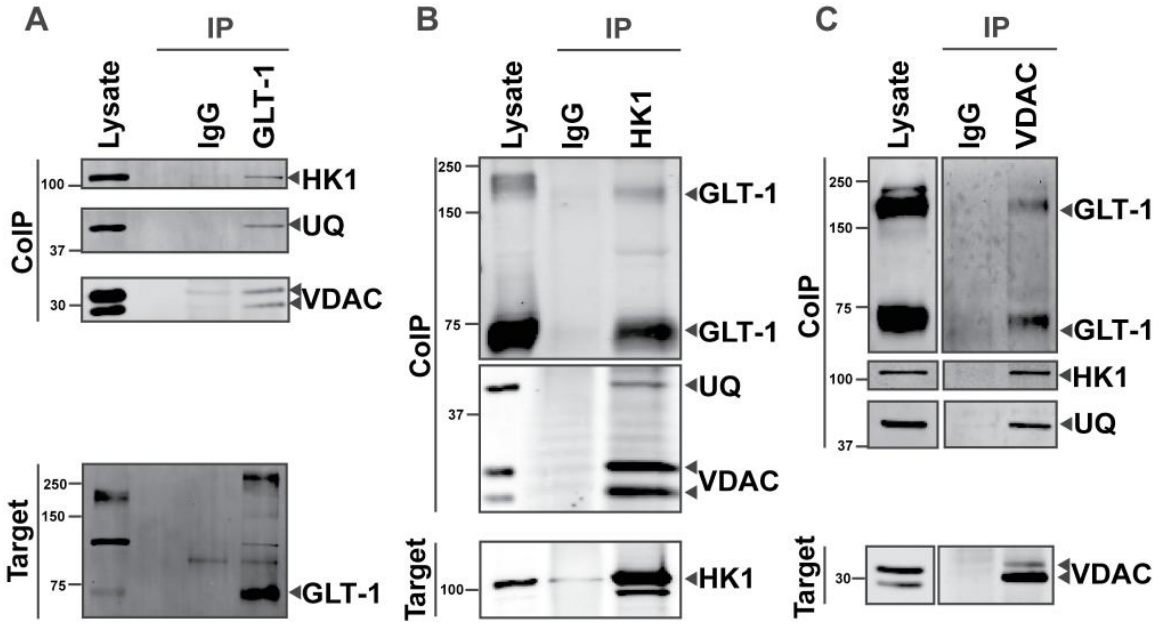

Figure 2.1: GLT-1, HK1, and VDAC form immunoprecipitatable interactions within the cortex. Anti-GLT-1 (A), anti-HK1 (B), anti-VDAC (C) antibodies or IgG were used for immunoprecipitations from rat cortical lysates (500 µg protein). Immunoprecipitation of the target protein was confirmed in every immunoprecipitation. Data are representative of at least 3 independent experiments.

Previously, we examined the extent of co-localization of mRFP-GLT-1 with HK1-EGFP within the processes of transfected astrocytes in hippocampal slice cultures (Genda et al. 2011). We found that virtually all exogenous HK1 localized to mitochondria. Here, we extended this analysis to look at the extent of co-localization of

endogenous HK1 and GLT-1 within rat cortical tissue. We conducted immunofluorescence imaging of HK1 and GLT-1 in sections derived from adult rat cortex (Fig. 2.2) followed by intensity co-localization analysis. This analysis is based on the premise that if HK1 and GLT-1 interact, then their staining intensities should co-vary. Conversely if the proteins are part of different complexes, then their staining patterns should be segregated. We calculated Intensity Co-localization Quotients (ICQs) for HK1 and GLT-1 in the cortex of rat (Genda et al. 2011; Li et al. 2004**)**. This quotient describes the extent of correlation of the staining intensities for two proteins. If two images have staining patterns that are dependent, then their staining intensities will co-vary around their respective means and the product of their differences from the mean (PDM) values will be positive. The ICQ values are equal to the ratio of number of positive PDM values to the total number of pixels and are distributed between -0.5 and +0.5. Positive ICQ values indicate the relative intensities are correlated and consistent with co-localization. An ICQ value of 0 would indicate random staining, while negative values indicate segregated staining. We see a small, but significant co-variance of signal for GLT-1 and HK1 (ICQ=0.06 ± 0.1, p=0.0006, n=8) within rat cortex. This covariance exists despite the fact that the majority of GLT-1 is found in astrocytes *in vivo* (Rothstein et al. 1994), while HK1 is present in high amounts in neurons as well (Cahoy et al. 2008). While the majority of GLT-1 expression in cortex is astrocytic, there is also a small pool of GLT-1 in neurons; therefore we cannot rule out the possibility that the observed co-localization is occurring within the neurons (Chen et al. 2004; Furness et al. 2008).

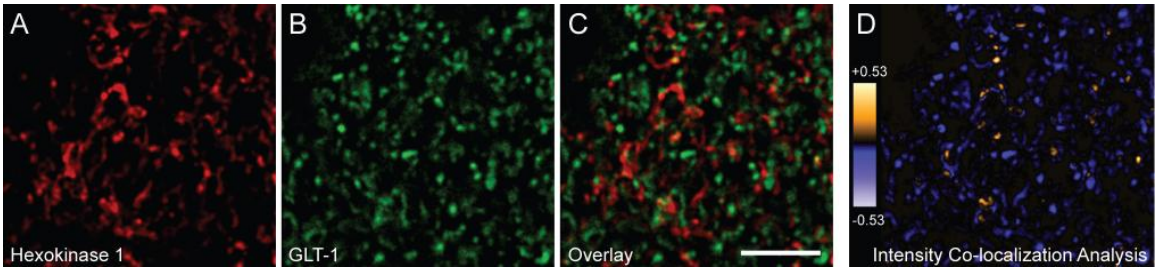

Figure 2.2: GLT-1 and HK1 co-localize in rat brain cortex. (A-C) Representative images from adult rat cortex immunostained with antibodies against HK1 (A), GLT-1 (B), and merged (C). (Scale bar=10 µm). (D) Pseudocolor representation of the product displacement of the mean (PDM) values for the image pair (A, B), where pixel intensity is equal to the PDM at that location. Images with positive PDM (dependent) values are displayed in yellow, while those with negative values (segregated) are displayed in violet.

N-terminal HK peptide disrupts HK1-VDAC binding in synaptosomes

For the next series of experiments, we used crude synaptosomal membranes (P2) from cortex so that we could measure Na^+-dependent L-[^{3}H]-glutamate uptake in parallel. Several lines of evidence indicate that essentially all of the uptake in this preparation is mediated by GLT-1, including the demonstration that the pharmacology of uptake uniquely reflects GLT-1 and genetic deletion of GLT-1 reduces uptake to 5% of control (Arriza et al. 1994; Tanaka et al. 1997, for review see Robinson 1999; Robinson et al. 1991).

We hypothesized that HK1 may act as a cytosolic bridge linking GLT-1 and mitochondria. To test this hypothesis, we used a cell-permeable peptide based on the N-terminal, VDAC-binding domain of HK2 (Pastorino et al. 2002; Sui and Wilson 1997) to disrupt the interaction between HK1 and VDAC (mitochondria), and measured the effect on interactions between GLT-1 and mitochondrial proteins. Several groups have used this peptide to disrupt the interaction between endogenous HK (1 and 2) and VDAC in various cell culture models (Majewski et al. 2004; Pastorino et al. 2002; Sukumaran et al. 2010). The N-terminus of HK2 shares sequence homology (11 of 15

amino acids) and its VDAC binding site with HK1, making the peptide useful for displacing both of these isoforms from VDAC. To confirm that the peptide disrupts the interaction between HK1 and VDAC in the crude synaptosomes, we used an anti-HK1 antibody to immunoprecipitate HK1 and quantified the amount of VDAC immunoreactivity. As anti-VDAC antibodies detected two bands in the VDAC immunoblot, we quantified the bands separately. The total amount of VDAC in the immunoprecipitation was normalized to the targeted HK1 immunoprecipitation (which did not change; Fig 2.3) to yield a VDAC/HK1 ratio for each experiment. We found that a 30 min incubation with 100 µM of the N-terminal HK peptide reduced HK1-VDAC binding by 50.4 ± 5.61% (48.9 ± 6.89% in the upper band, 66.1 ± 4.27% in the lower band) in crude synaptosomes prepared from adult rat cortex (Fig. 2.3). The reduction with peptide treatment compared to control was significant for total VDAC as well as for each individual band. The reductions observed for each band were not significantly different from each other.

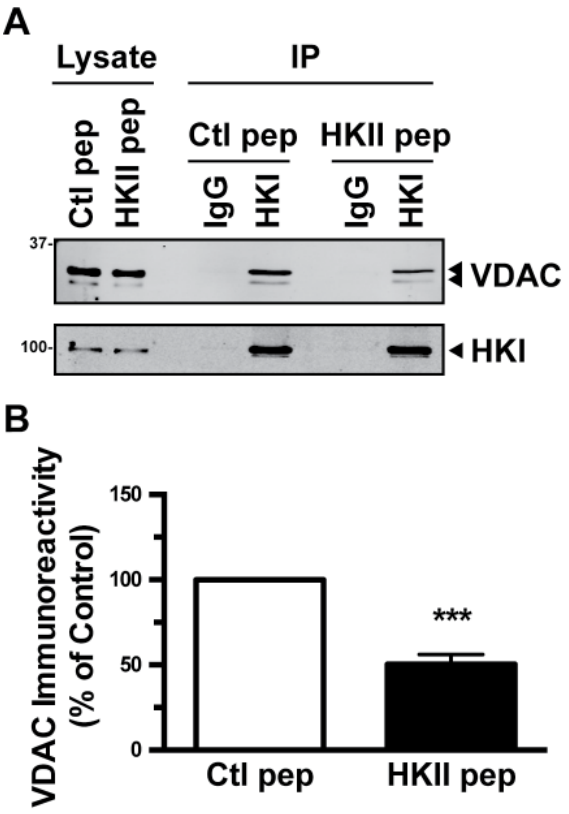

Figure 2.3: An N-terminal HK peptide displaces HK1 from VDAC in synaptosomes prepared from adult rat cortex. Representative western blot of HK1 IPs under control and HK-peptide conditions labeled for HK1 and VDAC (A). The amount of HK1 found in the immunoprecipitates was not significantly affected by the HK peptide (93.6% of control, p=0.781), but normalizing VDAC immunoreactivity to HK1 immunoreactivity (VDAC/HK1 ratio) from each IP slightly reduced the variance. Therefore VDAC/HK1 in each experiment was expressed as percent of control (B). Values are displayed as mean ± SEM; n=4; ***p<0.001.

Effects of disruption of HK1-VDAC interaction on the GLT-1/mitochondria protein complex and GLT-1 function

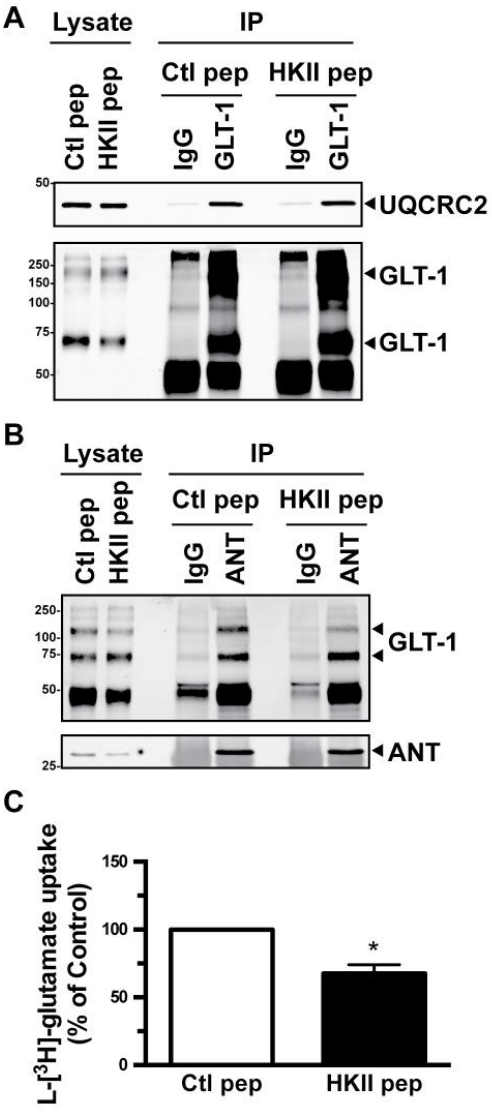

Figure 2.4: HK1-VDAC disruption does not affect the interaction between GLT-1 and mitochondrial proteins, but does reduce sodium-dependent glutamate uptake in crude synaptosomes. Representative western blots of GLT-1 (A) and ANT (B) IPs under control and HK-peptide conditions labeled for GLT-1 and UQCRC2, or ANT and GLT-1, respectively. Uptake of radiolabeled glutamate following treatment with a control or HK-peptide is expressed as percent of control (C). Values are displayed as mean ± SEM; n=3; *p<0.05.

In these same experiments that resulted in a 50% reduction of HK1-VDAC binding, we performed immunoprecipitations targeting GLT-1 and the inner-mitochondrial membrane protein, ANT, to quantify the interaction between GLT-1 and mitochondria. ANT was previously found to co-immunoprecipitate with GLT-1 (Genda et al. 2011), and also interacts with VDAC (Vyssokikh et al. 2001). In GLT-1 immunoprecipitations, co-immunoprecipitation of ANT or the matrix protein UQCRC2 was not affected by incubation with the HK peptide (Fig. 2.4A). Similarly, in immunoprecipitations targeting ANT, co-immunoprecipitation of GLT-1 was unaltered by HK peptide incubation (Fig. 2.4B). These data indicate that displacing 50% of HK1 from VDAC is not sufficient to alter the interaction between GLT-1 and mitochondria.

Glutamate uptake in astrocytes is intimately linked to both glycolytic and oxidative metabolism (Fernandez-Moncada and Barros

2014; Genda et al. 2011; Loaiza et al. 2003; McKenna et al. 1996; Pellerin and Magistretti 1994; Yu et al. 1982), which are in turn supported by HK-VDAC binding (BeltrandelRio and Wilson 1991; Rodrigues-Ferreira et al. 2012). Therefore, we also investigated the effect of disrupting the interaction between HK1 and VDAC on glutamate uptake in the same sets of experiments. We found that disruption of the HK1-VDAC interaction significantly reduced Na^+-dependent L-[^{3}H]-glutamate uptake to approximately 70% of control (Fig. 2.4C).

2.4 Discussion

The assembly of proteins into macromolecular complexes is thought to both increase the specificity of reactions and improve the speed of reactions that are dependent upon multiple proteins by limiting the impact of diffusion (Levitan 2006). Converging lines of evidence provide examples of macromolecular protein complexes coupling plasma membrane transport proteins with metabolic support. In erythrocytes, glycolytic enzymes including phosphoglycerate kinase (Campanella et al. 2005; Mercer and Dunham 1981; Parker and Hoffman 1967), glyceraldehyde phosphate dehydrogenase (GAPDH), and aldolase (Campanella et al. 2005) localize to the plasma membrane and physically interact with membrane proteins such as the anion exchanger 1 (AE1) (Campanella et al. 2005). In this system these proteins contribute to a membrane-associated pool that fuels the Na^+/K^+-ATPase (Mercer and Dunham 1981). The regulation of the glucose transporter GLUT4 by insulin is reciprocally controlled by its interactions with GAPDH or HK2 (Zaid et al. 2009). Previously, we conducted a proteomic analysis of GLT-1 with the purpose of identifying proteins that might be involved in regulating the localization and activity of this astrocytic glutamate transporter.

This analysis revealed the presence of subunits of the Na^+/K^+-ATPase, a number of glycolytic enzymes (HK1, phosphofructokinase, glyceraldehyde dehydrogenase, etc.) and mitochondrial proteins (e.g. UQCRC2, ANT) in GLT-1 immunoprecipitates (Genda et al. 2011). Since then, these results have been extended to the other glial glutamate transporter, GLAST (Bauer et al. 2012), and to human tissue (Shan et al. 2014). These results suggest that the protein interactions observed in astrocytes might serve to fuel glutamate uptake and the concomitant Na^+/K^+-ATPase.

Based on these results, we posited the existence of a macromolecular assembly of proteins that might fuel glutamate transport, as illustrated in Figure 2.5. Several of the proteins identified have previously been shown to interact. Evidence for interaction between GLT-1 and the Na^+/K^+-ATPase in the plasma membrane preceded our own results (Fig. 2.5, arrow #1) (Rose et al. 2009, Genda et al. 2011). Hexokinase is bound to the outer mitochondrial membrane in part by its association with the outer membrane resident protein, VDAC (Fig. 2.5, arrow #2) (Sul and Wilson 1997, Abu-Hamad 2008). VDAC in turn physically interacts with the inner mitochondrial membrane protein ANT (Fig. 2.5, arrow #3) (Beutner 1998, Crompton

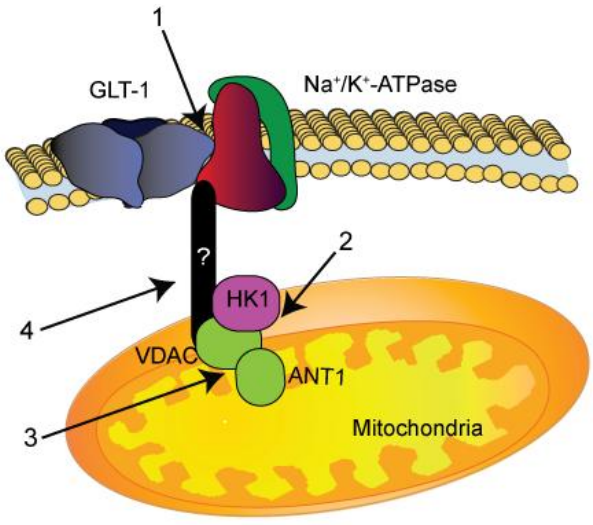

Figure 2.5: Schematic depiction of the interaction between GLT-1, HK1, and mitochondrial proteins. Arrows (#1-3) refer to know protein interactions. A potential model whereby GLT1-1 is linked to mitochondrial proteins is diagramed (arrow #4). Figure is adapted from Genda et al 2011

1998). Based on these known interactions, we proposed that the cytosolic enzyme hexokinase might serve to physically coordinate the interaction of the plasma membrane-bound transporter with the outer mitochondrial membrane protein VDAC and through this to the inner mitochondrial membrane protein, ANT, and the matrix protein, UQCRC2. Here, we have extended this work by validating the interaction between GLT-1, HK1, and VDAC, and we also tested the hypothesis that the interaction between HK1 and VDAC facilitates GLT-1 binding to mitochondrial proteins.

We have considered the possibility that the co-immunoprecipitations between GLT-1, glycolytic enzymes, and mitochondrial proteins could be an artifact due to post-solubilization aggregation. However, as shown in Figure 2.2, HK1 and GLT-1 co-localize within astrocytic processes in cortex. Furthermore, we previously demonstrated that neuronal activity significantly increases the probability that GLT-1 and mitochondria will be apposed in perisynaptic astrocytic processes (Jackson et al. 2014). Similarly, co-culturing astrocytes with neurons increases the overlap of GLT-1 with mitochondria in culture (Ugbode et al. 2014). The close proximity between GLT-1, HK1, and mitochondria, and its regulation by neuronal activity, provide evidence for an *in vivo* interaction between these proteins.

To test whether HK1 serves as a cytosolic link between GLT-1 and mitochondria, we measured the extent of GLT-1 co-immunoprecipitation with mitochondrial proteins while displacing HK1 from the outer mitochondrial membrane protein VDAC. Displacing 50% of HK1 from VDAC did not alter the interaction between GLT-1 and mitochondrial proteins (ANT and UQCRC2; Fig. 2.4A,B). There are two possible explanations for these results: either HK1 does not serve as a cytosolic bridge between GLT-1 and mitochondrial proteins, or the pool of HK1 that serves as the bridge possesses a higher

affinity for VDAC. Displacement of 50% of HK1 from VDAC may not be sufficient to abrogate this interaction. Unfortunately, this possibility could not be tested experimentally, as 100 μM of peptide approaches the solubility limit of the peptide in our buffer. However, we favor the hypothesis that HK1 does not serve as a cytosolic bridge between GLT-1 and mitochondrial proteins. Rather, HK1/GLT-1 interactions are likely indirect through mutual interaction with VDAC. HK1/GLT-1 interactions independent of HK1/VDAC interactions are less likely, as we have previously shown that exogenous HK1 is completely relegated to mitochondria in astrocytes (Genda et al. 2011). GLT-1/VDAC interaction could be direct, or through a connecting cytosolic protein or protein complex (Fig 2.5, arrow #4). Lastly, it is possible that GLT-1 may interact with these proteins through its interaction with the Na^+/K^+-ATPase.

The glutamate transporters couple the inward movement of glutamate to the Na^+ and K^+ electrochemical gradients. Specifically, the inward movement of one molecule of glutamate is accompanied by the inward movement of 3 Na^+ and a H^+ and the counter-transport of a K^+ ion (Zerangue and Kavanaugh 1996). The Na^+ and K^+ gradients that enable this exchange are established, in part, by the actions of the Na^+/K^+-ATPase, which moves 3 Na^+ ions into the cellin exchange for 2 K^+ ions for every ATP hydrolyzed. These molecules function interdependently, as inhibitors of the Na^+/K^+-ATPase inhibit glutamate uptake (Pellerin and Magistretti 1994) and glutamate uptake stimulates Na^+/K^+-ATPase activity (Pellerin and Magistretti 1997). Acute energy depletion results in a reversal of the glutamate transporters, resulting in an increase in extracellular glutamate; an effect attributed to changes in the Na^+ and K^+ electrochemical gradients (Jabaudon et al. 2000; Rossi et al. 2000). This functional interdependence is further supported by the recent demonstration that the glial glutamate transporters physically

interact with members of the Na^+/K^+-ATPase family (Bauer et al. 2012; Genda et al. 2011; Illarionava et al. 2014; Rose et al. 2009).

GLT-1 alone accounts for approximately 1% of brain protein (Lehre and Danbolt 1998). The dependence of GLT-1 upon the Na^+ electrochemical gradient, and its functional and physical coupling to the Na^+/K^+-ATPase, is assumed to impose a metabolic demand upon astrocytes. Both glycolysis and oxidative phosphorylation can fuel gutamate uptake and the Na^+/K^+-ATPase (Fernandez-Moncada and Barros 2014; Genda et al. 2011). Conversely, glutamate uptake and Na^+/K^+-ATPase activity stimulate glucose uptake (Hamai et al. 1999; Loaiza et al. 2003), glycolysis (Pellerin and Magistretti 1994), and oxidative ATP production (Magi et al. 2013). As an alternative to utilizing glucose, glutamate may be converted to alpha-ketoglutarate by glutamate dehydrogenase and subsequently oxidized within the mitochondria (McKenna et al. 1996; Yu et al. 1982). Increasing extracellular glutamate increases the fraction of glutamate that is oxidized in astrocytes (McKenna et al. 1996; Yu et al. 1982), and inhibitors of glutamate dehydrogenase block glutamate uptake (Whitelaw and Robinson 2013). These results indicate that a portion of transported glutamate is oxidized in astrocytes, generating energy that could be used to fuel its own uptake (Dienel 2013; Dienel and McKenna 2014). In astrocytes, it appears that glutamate uptake is deeply integrated with metabolism.

Displacing HK1 from VDAC alters glutamate uptake without affecting protein interactions between GLT-1 and mitochondria. Disrupting HK1/VDAC binding changes ANT to a confirmation that reduces ATP/ADP translocation (for review see Vyssokikh and Brdiczka 2003), which contributes to impairment of both glycolytic and oxidative metabolism (BeltrandelRio and Wilson 1991; Rodrigues-Ferreira et al. 2012). Knockout

or inhibition of ANT reduces glutamate uptake, and increased ANT expression in reactive astrocytes is associated with increased glutamate uptake (Buck et al. 2003). Glutamate uptake can be supported by either glycolytic or oxidative ATP production, but inhibiting both reduces glutamate uptake (Genda et al. 2011(Genda et al., 2011b). Thus, the metabolic consequences of displacing HK1 from VDAC are likely responsible for the impaired glutamate uptake we observed.

Numerous interactions link the uptake and metabolism of glutamate to that of glucose. Glutamate uptake and Na^+/K^+-ATPase activity are fueled by both glycolysis and oxidative phosphorylation (Fernandez-Moncada and Barros 2014; Genda et al. 2011). Glutamate uptake stimulates glutamate oxidation (Sonnewald and McKenna 2002; Yu et al. 1982), glycolysis (Pellerin and Magistretti 1994), glucose uptake (Hamai et al. 1999; Loaiza et al. 2003), and glycogen formation (Hamai et al. 1999; Swanson et al. 1990). L-glutamate itself can be incorporated into glycogen (Schmoll et al. 1995). Since hexokinase catalyzes the first step of glucose metabolism (i.e. glycolysis, oxidative phosphorylation, pentose phosphate pathway, or glycogen formation), physically linking GLT-1 and HK1 may represent a mechanism to coordinate glutamate and glucose metabolism. Perhaps the involvement of HK1 in a GLT-1/mitochondria complex facilitates glutamate oxidation, and thus favors the incorporation of glucose-6-phosphate into glycogen in astrocytes by reducing the demand for glucose-derived pyruvate.

In summary, we provide evidence that HK1 and VDAC interact with GLT-1. The interaction of GLT-1 with mitochondrial proteins does not depend upon the interaction of HK1 with VDAC. However, the interaction of HK1 with VDAC supports glutamate uptake. These results highlight the close integration of glutamate uptake and astrocyte metabolism.

Acknowledgements: We would like to thank members of the Robinson laboratory for their advice and suggestions during the conduct of this research. In particular we would like to thank Meredith Lane for her expert technical assistance.

2.5 References

Abu-Hamad S, Zaid H, Israelson A, Nahon E, Shoshan-Barmatz V (2008) Hexokinase-I protection against apoptotic cell death is mediated via interaction with the voltage-dependent anion channel-1: mapping the site of binding. J Biol Chem 283:13482–13490.

Acin-Perez R, Fernandez-Silva P, Peleato ML, Perez-Martos A, Enriquez JA. 2008. Respiratory active mitochondrial supercomplexes. Molecular cell 32(4):529-539.

Arriza JL, Fairman WA, Wadiche JI, Murdoch GH, Kavanaugh MP, Amara SG. 1994. Functional comparisons of three glutamate transporter subtypes cloned from human motor cortex. Journal of Neuroscience 14(9):5559-5569.

Bauer DE, Jackson JG, Genda EN, Montoya MM, Yudkoff M, Robinson MB. 2012. The glutamate transporter, GLAST, participates in a macromolecular complex that supports glutamate metabolism. Neurochemistry international 61(4):566-574.

BeltrandelRio H, Wilson JE. 1991. Hexokinase of rat brain mitochondria: relative importance of adenylate kinase and oxidative phosphorylation as sources of substrate ATP, and interaction with intramitochondrial compartments of ATP and ADP. Archives of biochemistry and biophysics 286(1):183-194.

Beutner G, Ruck A, Riede B, Brdiczka D. 1998. Complexes between porin, hexokinase, mitochondrial creatine kinase and adenylate translocator display properties of the permeability transition pore. Implication for regulation of permeability transition by the kinases. Biochimica et biophysica acta 1368(1):7-18.

Buck CR, Jurynec MJ, Gupta DK, Law AK, Bilger J, Wallace DC, McKeon RJ. 2003. Increased adenine nucleotide translocator 1 in reactive astrocytes facilitates glutamate transport. Exp Neurol 181(2):149-158.

Cahoy JD, Emery B, Kaushal A, Foo LC, Zamanian JL, Christopherson KS, Xing Y, Lubischer JL, Krieg PA, Krupenko SA, Thompson WJ, Barres BA. 2008. A transcriptome database for astrocytes, neurons, and oligodendrocytes: a new resource for understanding brain development and function. J Neurosci 28(1):264-278.

Campanella ME, Chu H, Low PS. 2005. Assembly and regulation of a glycolytic enzyme complex on the human erythrocyte membrane. Proc Natl Acad Sci U S A 102(7):2402-2407.

Chen W, Mahadomrongkul V, Berger UV, Bassan M, DeSilva T, Tanaka K, Irwin N, Aoki C, Rosenberg PA. 2004. The glutamate transporter GLT1a is expressed in excitatory terminals of mature hippocampal neurons. Journal of Neuroscience 24:1136-1148.

Crompton M, Virji S, Ward JM. 1998. Cyclophilin-D binding proteins. Biochemical Society transactions 26(4):S330.

Danbolt NC. 2001. Glutamate uptake. Progress in neurobiology 65:1-105.

Dienel GA. 2013. Astrocytic energetics during excitatory neurotransmission: What are contributions of glutamate oxidation and glycolysis? Neurochemistry international 63(4):244-258.

Dienel GA, McKenna MC. 2014. A dogma-breaking concept: glutamate oxidation in astrocytes is the source of lactate during aerobic glycolysis in resting subjects. J Neurochem 131(4):395-398.

Fernandez-Moncada I, Barros LF. 2014. Non-preferential fuelling of the Na(+)/K(+)-ATPase pump. The Biochemical journal 460(3):353-361.

Furness DN, Dehnes Y, Akhtar AQ, Rossi DJ, Hamann M, Grutle NJ, Gundersen V, Holmseth S, Lehre KP, Ullensvang K, Wojewodzic M, Zhou Y, Attwell D, Danbolt NC. 2008. A quantitative assessment of glutamate uptake into hippocampal synaptic terminals and astrocytes: new insights into a neuronal role for excitatory amino acid transporter 2 (EAAT2). Neuroscience 157(1):80-94.

Genda EN, Jackson JG, Sheldon AL, Locke SF, Greco TM, O'Donnell JC, Spruce LA, Xiao R, Guo W, Putt M, Seeholzer S, Ischiropoulos H, Robinson MB. 2011. Co-compartmentalization of the astroglial glutamate transporter, GLT-1, with glycolytic enzymes and mitochondria. Journal of Neuroscience 31:18275-18288.

Hamai M, Minokoshi Y, Shimazu T. 1999. L-Glutamate and insulin enhance glycogen synthesis in cultured astrocytes from the rat brain through different intracellular mechanisms. J Neurochem 73(1):400-407.

Haugeto Ø, Ullensveng K, Levy LM, Chaudhry FA, Honore T, Neilsen M, Lehre KP, Danbolt NC. 1996. Brain glutamate transporter proteins form homomultimers. Journal of Biological Chemistry 271(44):27715-27722.

Herman MA, Jahr CE. 2007. Extracellular glutamate concentration in hippocampal slice. J Neurosci 27(36):9736-9741.

Huang Y, Zuo Z. 2005. Isoflurane induces a protein kinase Ca-dependent increase in cell surface protein level and activity of glutamate transporter type 3. Molecular pharmacology 67:1522-1533.

Illarionava NB, Brismar H, Aperia A, Gunnarson E. 2014. Role of Na,K-ATPase alpha1 and alpha2 isoforms in the support of astrocyte glutamate uptake. PLoS One 9(6):e98469.

Jabaudon D, Scanziani M, Gähwiler BH, Gerber U. 2000. Acute decrease in net glutamate upatke during energy failure. Proceedings of the National Academy of Sciences USA 97:5610-5615.

Jackson JG, O'Donnell JC, Takano H, Coulter DA, Robinson MB. 2014. Neuronal activity and glutamate uptake decrease mitochondrial mobility in astrocytes and position mitochondria near glutamate transporters. J Neurosci 34(5):1613-1624.

Kerner J, Lee K, Tandler B, Hoppel CL. 2012. VDAC proteomics: post-translation modifications. Biochimica et biophysica acta 1818(6):1520-1525.

Lehre KP, Danbolt NC. 1998. The number of glutamate transporter subtype molecules at glutamatergic synapses: chemical and stereological quantification in young adult rat brain. Journal of Neuroscience 18:8751-8757.

Levitan IB. 2006. Signaling protein complexes associated with neuronal ion channels. Nat Neurosci 9(3):305-310.

Li Q, Lau A, Morris TJ, Guo L, Fordyce CB, Stanley EF. 2004. A syntaxin 1, Galpha(o), and N-type calcium channel complex at a presynaptic nerve terminal: analysis by quantitative immunocolocalization. J Neurosci 24(16):4070-4081.

Linden M, Gellerfors P, Nelson BD. 1982. Pore protein and the hexokinase-binding protein from the outer membrane of rat liver mitochondria are identical. FEBS letters 141(2):189-192.

Loaiza A, Porras OH, Barros LF. 2003. Glutamate triggers rapid glucose transport stimulation in astrocytes as evidenced by real-time confocal microscopy. J Neurosci 23(19):7337-7342.

Magi S, Arcangeli S, Castaldo P, Nasti AA, Berrino L, Piegari E, Bernardini R, Amoroso S, Lariccia V. 2013. Glutamate-induced ATP synthesis: relationship between plasma membrane Na+/Ca2+ exchanger and excitatory amino acid transporters in brain and heart cell models. Molecular pharmacology 84(4):603-614.

Majewski N, Nogueira V, Bhaskar P, Coy PE, Skeen JE, Gottlob K, Chandel NS, Thompson CB, Robey RB, Hay N. 2004. Hexokinase-mitochondria interaction mediated by Akt is required to inhibit apoptosis in the presence or absence of Bax and Bak. Molecular cell 16(5):819-830.

McKenna MC, Sonnewald U, Huang X, Stevenson J, Zielke HR. 1996. Exogenous glutamate concentration regulates the metabolic fate of glutamate in astrocytes. J Neurochem 66(1):386-393.

Mercer RW, Dunham PB. 1981. Membrane-bound ATP fuels the Na/K pump. Studies on membrane-bound glycolytic enzymes on inside-out vesicles from human red cell membranes. The Journal of general physiology 78(5):547-568.

Nakashima RA, Mangan PS, Colombini M, Pedersen PL. 1986. Hexokinase receptor complex in hepatoma mitochondria: evidence from N,N'-dicyclohexylcarbodiimide-labeling studies for the involvement of the pore-forming protein VDAC. Biochemistry 25(5):1015-1021.

Parker JC, Hoffman JF. 1967. The role of membrane phosphoglycerate kinase in the control of glycolytic rate by active cation transport in human red blood cells. The Journal of general physiology 50(4):893-916.

Pastorino JG, Shulga N, Hoek JB. 2002. Mitochondrial binding of hexokinase II inhibits Bax-induced cytochrome c release and apoptosis. J Biol Chem 277(9):7610-7618.

Pellerin L, Magistretti PJ. 1994. Glutamate uptake into astrocytes stimulates aerobic glycolysis: a mechanism coupling neuronal activity to glucose utilization. Proc Natl Acad Sci U S A 91(22):10625-10629.

Pellerin L, Magistretti PJ. 1997. Glutamate uptake stimulates Na+,K+-ATPase activity in astrocytes via activation of a distinct subunit highly sensitive to ouabain. J Neurochem 69(5):2132-2137.

Robinson MB. 1999. The family of sodium-dependent glutamate transporters: A focus on the GLT-1/EAAT2 subtype. Neurochemistry international 33:479-491.

Robinson MB, Hunter-Ensor M, Sinor J. 1991. Pharmacologically distinct sodium-dependent L-[^{3}H]glutamate transport processes in rat brain. Brain research 544:196-202.

Rodrigues-Ferreira C, da Silva AP, Galina A. 2012. Effect of the antitumoral alkylating agent 3-bromopyruvate on mitochondrial respiration: role of mitochondrially bound hexokinase. Journal of bioenergetics and biomembranes 44(1):39-49.

Rose EM, Koo JC, Antflick JE, Ahmed SM, Angers S, Hampson DR. 2009. Glutamate transporter coupling to Na,K-ATPase. J Neurosci 29(25):8143-8155.

Rossi DJ, Oshima T, Attwell D. 2000. Glutamate release in severe brain ischaemia is mainly by reversed uptake. Nature 403:316-321.

Rothstein JD, Martin L, Levey AI, Dykes-Hoberg M, Jin L, Wu D, Nash N, Kuncl RW. 1994. Localization of neuronal and glial glutamate transporters. Neuron 13(3):713-725.

Schmoll D, Fuhrmann E, Gebhardt R, Hamprecht B. 1995. Significant amounts of glycogen are synthesized from 3-carbon compounds in astroglial primary cultures from mice with participation of the mitochondrial phosphoenolpyruvate carboxykinase isoenzyme. European journal of biochemistry / FEBS 227(1-2):308-315.

Schousboe A. 1981. Transport and metabolism of glutamate and GABA in neurons are glial cells. International review of neurobiology 22:1-45.

Shan D, Mount D, Moore S, Haroutunian V, Meador-Woodruff JH, McCullumsmith RE. 2014. Abnormal partitioning of hexokinase 1 suggests disruption of a glutamate transport protein complex in schizophrenia. Schizophrenia research 154(1-3):1-13.

Shoshan-Barmatz V, Golan M. 2012. Mitochondrial VDAC1: function in cell life and death and a target for cancer therapy. Current medicinal chemistry 19(5):714-735.

Sickmann HM, Walls AB, Schousboe A, Bouman SD, Waagepetersen HS. 2009. Functional significance of brain glycogen in sustaining glutamatergic neurotransmission. J Neurochem 109 Suppl 1:80-86.

Sonnewald U, McKenna M. 2002. Metabolic compartmentation in cortical synaptosomes: influence of glucose and preferential incorporation of endogenous glutamate into GABA. Neurochemical research 27(1-2):43-50.

Sui D, Wilson JE. 1997. Structural determinants for the intracellular localization of the isozymes of mammalian hexokinase: intracellular localization of fusion constructs incorporating structural elements from the hexokinase isozymes and the green fluorescent protein. Archives of biochemistry and biophysics 345(1):111-125.

Sukumaran SK, Fu NY, Tin CB, Wan KF, Lee SS, Yu VC. 2010. A soluble form of the pilus protein FimA targets the VDAC-hexokinase complex at mitochondria to suppress host cell apoptosis. Molecular cell 37(6):768-783.

Swanson RA, Yu AC, Chan PH, Sharp FR. 1990. Glutamate increases glycogen content and reduces glucose utilization in primary astrocyte culture. J Neurochem 54(2):490-496.

Tanaka K, Watase K, Manabe T, Yamada K, Watanabe M, Takahashi K, Iwama H, Nishikawa T, Ichihara N, Kikuchi T, Okuyama S, Kawashima N, Hori S, Takimoto M, Wada K. 1997. Epilepsy and exacerbation of brain injury in mice lacking the glutamate transporter GLT-1. Science 276:1699-1702.

Ugbode CI, Hirst WD, Rattray M. 2014. Neuronal influences are necessary to produce mitochondrial co-localization with glutamate transporters in astrocytes. J Neurochem 130(5):668-677.

Vyssokikh MY, Brdiczka D. 2003. The function of complexes between the outer mitochondrial membrane pore (VDAC) and the adenine nucleotide translocase in regulation of energy metabolism and apoptosis. Acta biochimica Polonica 50(2):389-404.

Vyssokikh MY, Katz A, Rueck A, Wuensch C, Dorner A, Zorov DB, Brdiczka D. 2001. Adenine nucleotide translocator isoforms 1 and 2 are differently distributed in the mitochondrial inner membrane and have distinct affinities to cyclophilin D. The Biochemical journal 358(Pt 2):349-358.

Whitelaw BS, Robinson MB. 2013. Inhibitors of glutamate dehydrogenase block sodium-dependent glutamate uptake in rat brain membranes. Frontiers in endocrinology 4:123.

Yamamoto T, Yamada A, Watanabe M, Yoshimura Y, Yamazaki N, Yoshimura Y, Yamauchi T, Kataoka M, Nagata T, Terada H, Shinohara Y. 2006. VDAC1, having a shorter N-terminus than VDAC2 but showing the same migration in an SDS-polyacrylamide gel, is the predominant form expressed in mitochondria of various tissues. Journal of proteome research 5(12):3336-3344.

Yu AC, Schousboe A, Hertz L. 1982. Metabolic fate of 14C-labeled glutamate in astrocytes in primary cultures. J Neurochem 39(4):954-960.

Zaid H, Talior-Volodarsky I, Antonescu C, Liu Z, Klip A. 2009. GAPDH binds GLUT4 reciprocally to hexokinase-II and regulates glucose transport activity. The Biochemical journal 419(2):475-484.

Zerangue N, Kavanaugh MP. 1996. Flux coupling in a neuronal glutamate transporter. Nature 383(6601):634-637.

CHAPTER 3

Neuronal Activity and Glutamate Uptake Decrease Mitochondrial Mobility in Astrocytes and Position Mitochondria Near Glutamate Transporters

Joshua G. Jackson[1,2], John C. O'Donnell[3], Hajime Takano[1,2], Douglas A. Coulter[1,2,4], Michael B. Robinson[1,2,3].

Children's Hospital of Philadelphia Research Institute[1], and Departments of Pediatrics[2], Pharmacology[3], and Neuroscience[4], University of Pennsylvania, Philadelphia, PA 19104

Address Correspondence to: Michael B. Robinson
Department of Pediatrics, 502N
Abramson Pediatric Research Building
3615 Civic Center Boulevard
Philadelphia, PA 19104-3779
Tel. 215-590-2205; Fax. 215-590-3779
Email: Robinson@mail.med.upenn.edu

Author contributions: J.G.J., J.C.O., H.T., D.A.C., and M.B.R. designed research; J.G.J. and J.C.O. performed research; J.G.J. contributed unpublished reagents/analytic tools; J.G.J., J.C.O., H.T., and D.A.C. analyzed data; J.G.J., J.C.O., and M.B.R. wrote the paper.

Acknowledgments: This work was supported by a grant (RO1 NS077773) to M.B.R. from the National Institute of Neurological Disorders and Stroke. J.C.O. is supported by a predoctoral training grant in pharmacology (T32-GM008076-28). The Institutional Intellectual and Developmental Disabilities Research Center P30 HD26979 Cellular Neuroscience Core also provided valuable support for these studies. The authors would like to thank Dr. Rita Balice-Gordon for the use of equipment. We would also like to thank members of the Robinson and Coulter laboratories for their advice and suggestions during the conduct of this research.

Published in The Journal of Neuroscience, 29 January, 2014. Volume 34, Issue 5, pages 1613-1624.

Abstract

Within neurons, mitochondria are non-uniformly distributed and are retained at sites of high activity and metabolic demand. Glutamate transport and the concomitant activation of the Na^+/K^+-ATPase represent a substantial energetic demand on astrocytes. We hypothesized that mitochondrial mobility within astrocytic processes might be regulated by neuronal activity and glutamate transport. We imaged organotypic hippocampal slice cultures of rat, in which astrocytes maintain their highly branched morphologies and express glutamate transporters. Using time-lapse confocal microscopy, the mobility of mitochondria within individual astrocytic processes and neuronal dendrites was tracked. Within neurons, a greater percentage of mitochondria were mobile than in astrocytes. Furthermore, they moved faster and further than in astrocytes. Inhibiting neuronal activity with tetrodotoxin (TTX) increased the percentage of mobile mitochondria in astrocytes. Mitochondrial movement in astrocytes was inhibited by vinblastine and cytochalasin D, demonstrating that this mobility depends on both the microtubule and actin cytoskeletons. Inhibition of glutamate transport tripled the percentage of mobile mitochondria in astrocytes. Conversely, application of the transporter substrate D-aspartate reversed the TTX-induced increase in the percentage of mobile mitochondria. Inhibition of reversed Na^+-Ca^{2+} exchange also increased the percentage of mitochondria that were mobile. Lastly, we demonstrated that neuronal activity increases the probability that mitochondria appose GLT-1 particles within astrocyte processes, without changing the proximity of GLT-1 particles to VGLUT1. These results imply that neuronal activity and the resulting clearance of glutamate by astrocytes regulates the movement of astrocytic mitochondria and suggests a mechanism by which glutamate transporters might retain mitochondria at sites of glutamate uptake.

3.1 Introduction

Astrocytes express a large cohort of neurotransmitter receptors and transporters that allow them to sense and respond to neuronal stimuli. They possess enormously elaborate processes that contact synapses and the vasculature. A single astrocyte domain can contact tens of thousands of synapses (Halassa et al., 2007b), thus allowing astrocytes to monitor the activity of a large number of synapses (Newman, 2003).

Glutamate is the principle excitatory neurotransmitter in the central nervous system. Synaptic levels of glutamate are kept low (approximately 25 nM), against brain levels that approach 10 mmol/Kg (Herman and Jahr, 2007), to ensure appropriate excitatory signaling and to limit excessive activation of glutamate receptors that can cause excitotoxicity (for review, see Choi, 1992; Conti and Weinberg, 1999). Extracellular glutamate is cleared via a family of Na^+-dependent glutamate transporters (for reviews, see Danbolt, 2001; Sheldon and Robinson, 2007).

These transporters couple the inward movement of glutamate to the inward movement of 3 Na^+ ions and 1 H^+, and the outward movement of a K^+ ion, providing the energy to maintain up to a million-fold concentration gradient of glutamate (Zerangue and Kavanaugh, 1996). Because of this coupling, glutamate uptake results in a significant increase in the Na^+ concentration within the fine astrocytic processes (Rose and Ransom, 1996; Bergles and Jahr, 1997). Glutamate uptake also activates the Na^+/K^+-ATPase in astrocytes; an effect attributed to increased Na^+ concentration (Magistretti and Pellerin, 1999). Not surprisingly, the glial glutamate transporters co-localize and physically interact with Na^+/K^+-ATPase isoforms, glycolytic enzymes, and mitochondria (Rose et al., 2009; Genda et al., 2011; Bauer et al., 2012) and glutamate

uptake is functionally coupled to increases in glucose uptake, glycolysis, and oxidative phosphorylation (Pellerin and Magistretti, 1994; Magistretti, 2006; Loaiza et al., 2003).

While much research has examined the link between glutamate uptake and glycolysis, the role of mitochondria in astrocytes is often overlooked. Astrocytes have a high oxidative metabolism (Hertz et al., 2007) and possess a large number of mitochondria even in the very fine processes (Lovatt et al., 2007; Ito et al., 2009; Lavialle et al., 2011; reviewed in Parpura and Verkhratsky, 2012). In neurons, mitochondria are not uniformly distributed; instead mitochondria are concentrated at sites with heightened demand for ATP or Ca^{2+} buffering, including at axon branches, synapses, nodes of Ranvier, and growth cones. This distribution is established by movement of mitochondria along the microtubule and actin cytoskeleton (Morris and Hollenbeck, 1995; Ligon and Steward, 2000; Hollenbeck, 2005). Little is known about the mechanisms regulating transport of mitochondria in astrocytes.

Here, we present the first description of mobile mitochondria within the processes of astrocytes. We provide evidence that the movement of mitochondria in astrocytic processes is regulated by neuronal activity, astrocytic glutamate uptake, and reversed Na^{+}-Ca^{2+} exchange. Furthermore, we demonstrate that neuronal activity increases the probability that mitochondria appose GLT-1 protein in astrocyte processes. We suggest that regulation of mitochondrial mobility may represent a mechanism to retain mitochondria near sites of glutamate uptake in astrocytes.

3.2 Methods

cDNA contructs. pBluescript-Gfa_{ABC1D} was a gift from Dr. Brenner (University of Alabama-Birmingham). This construct encodes a 681 bp fragment of the glial fibrillary

acidic protein (GFAP) promoter that is sufficient to result in selective expression in astrocytes throughout the CNS (Lee et al., 2008). This 681 bp GFAP promoter fragment was inserted into pTY-CMV-mCherry between Nhe1 and Age1 restriction sites to form pTY-Gfa_{ABC1D}-mcherry and was a gift from Dr. John Wolf (University of Pennsylvania). pTY-Gfa_{ABC1D}-gp43mCherry (referred to as Gfa_{ABC1D}-mCherry) was generated by PCR amplification of the membrane-targeting myristoylation sequence of gap43 into pTY-Gfa_{ABC1D}-mcherry immediately after the initiating methionine of mCherry. pEGFP-mito (a gift from Dr. Stanley Thayer-University of Minnesota, Minneapolis) is a fusion of EGFP with the mitochondrial matrix targeting sequence from CoxVIII and has been shown to result in specific targeting of EGFP into mitochondria (Rizzuto et al., 1993; Wang et al., 2003).

Reagents. Rabbit anti-GLT-1 was a gift from Dr. Jeffrey Rothstein (Johns Hopkins University). Rabbit anti-glial fibrillary acidic protein (GFAP) polyclonal antibody and D-aspartate were purchased from Sigma-Aldrich (St. Louis, MO). Rabbit anti-MAP2 and guinea pig anti-VGLUT1 were purchased from Millipore (Bellerica, MA). Highly cross-adsorbed secondary antibodies conjugated to AlexaFluor dyes were purchased from Invitrogen (Carlsbad, CA). Goat anti-rabbit antibody conjugated to Dylight 405 was purchased from Thermo Fisher Scientific (Rockford IL). Tetrodotoxin (TTX) was purchased from Alamone Labs (Jerusalem, Israel). Vinblastine, cytochalasin D, 6,7-Dinitroquinoxaline-2,3-dione (DNQX), D-(-)-2-amino-5-phosphonopentanoic acid (D-APV), bicuculline, (3*S*)-3-[[3-[[4-(trifluoromethyl)benzoyl]amino]phenyl]methoxy]-L-aspartic acid (TFB-TBOA), (*S*)-3,5-dihydroxyphenylglycine (DHPG), 2-methyl-6-(phenylethynyl)pyridine hydrochloride (MPEP), and 2-[2-[4-(4-Nitrobenzyloxy)phenyl]ethyl] isothiourea mesylate (KB-R7943), *N*-[(3-Aminophenyl)

methyl]-6-[4-[(3-fluorophenyl) methoxy] phenoxy]-3-pyridine carboxamide dihydrochloride (YM 244769) were purchased from Tocris (Minneapolis, MN).

Slice culture and transfection. Organotypic cultures of rat hippocampus were prepared as previously described (Benediktsson et al., 2005; Genda et al., 2011; Kayser et al. 2006). Six to 12 day old rat pups of either sex were decapitated and their brains removed into sucrose-artificial cerebrospinal fluid (aCSF) composed of: sucrose 280, KCl 5, $MgCl_2$ 1, $CaCl_2$ 2, glucose 20, and HEPES 10 (in mM). Hippocampal slices (300 µm) were prepared using a McIlwain tissue chopper (Brinkman Instruments, Westbury, NY) and placed on 0.4 µm Millicell culture inserts (Millipore, Bellerica, MA) in six-well plates. Slices were maintained in a humidified incubator with 5% CO_2 at 37°C with 1 ml of medium containing the following: 50% Neurobasal medium, 25% horse serum, 25% Hank's-buffered saline solution (HBSS), supplemented with 10 mM HEPES, 36 mM glucose, 2 mM glutamine, 10 U/ml penicillin and 100 µg/mL streptomycin, pH 7.2-7.3. Slices were allowed to recover for 2 days prior to transfection with plasmids encoding a mitochondrial-targeted EGFP (mito-EGFP) and Gfa_{ABC1D}-mCherry fluorescent protein using a Helios Gene-Gun (BioRad, Hercules, CA) (McAllister, 2004; Benediktsson et al., 2005). Gene-gun bullets were generated as follows: cDNAs (10 µg total) were combined with 8-10 µg of 1.0 or 1.6 µm gold particles (BioRad) in a solution of 0.02 mg/mL polyvinylpyrrolidone 20 (PVP-20), 0.05 M spermidine, and 1 M $CaCl_2$. This suspension was used to coat Teflon tubing that was subsequently cut and loaded into the Gene-Gun. The cDNA-coated gold particles were shot using high-pressure helium (100-120 psi) into cultured slices in inserts sitting on warmed agarose slabs. We used 1.0 µm gold particles for transfection of astrocytes and 1.6 µm particles for the non-selective transfection of astrocytes and neurons (Benediktsson et al., 2005).

Live Slice Imaging. Two days post transfection, slices were excised from their membrane supports and placed in a closed, flow-through chamber for imaging. Slices were continuously superfused with heated (34°C) ACSF composed of the following: NaCl 130, KCl 3, NaH_2PO_4 1.25, $NaHCO_3$ 26, glucose 10, $MgCl_2$ 1, $CaCl_2$ 2 (mM) and continuously bubbled with 95% O_2/ 5% CO_2. Slices were imaged on an Olympus Fluoview 1000 Laser Scanning Confocal Microscope equipped with a 40x UPlanApo objective (NA=1.4). Slices were allowed to equilibrate in the imaging chamber for 10 minutes prior to imaging. Cells expressing EGFP-mito and/or membrane-targeted mCherry were identified using epifluorescence and were imaged using the 488 and 546 laser lines, respectively (Figure 3.1B-G). To control for possible culture-to-culture variability in the percentage of mobile mitochondria, all experiments included control and experimental slices from the same cultures and were imaged on the same day. Cells were visually selected based on their complex morphology and lack of reactive phenotype. Cells at the surface of the slice or at the slice margins were not imaged. Image stacks (15-25 optical sections, 1 µm z-spacing) were collected from the identified cell to aid in retrospective identification. A subfield of processes was identified and was imaged at 512 x 512 pixels with an additional 4-5x digital zoom. Image stacks (3-8 optical sections; 1 µm z-spacing) were collected every 6 to 10 seconds for 15 minutes from a field containing 3-8 astrocyte processes and at least 10 mitochondria. Under these conditions, we do not observe significant decreases in fluorescence intensity with time (Figure 3.1A). We also did not observe evidence of cell swelling during the imaging epochs as examined with the membrane-targeted mCherry.

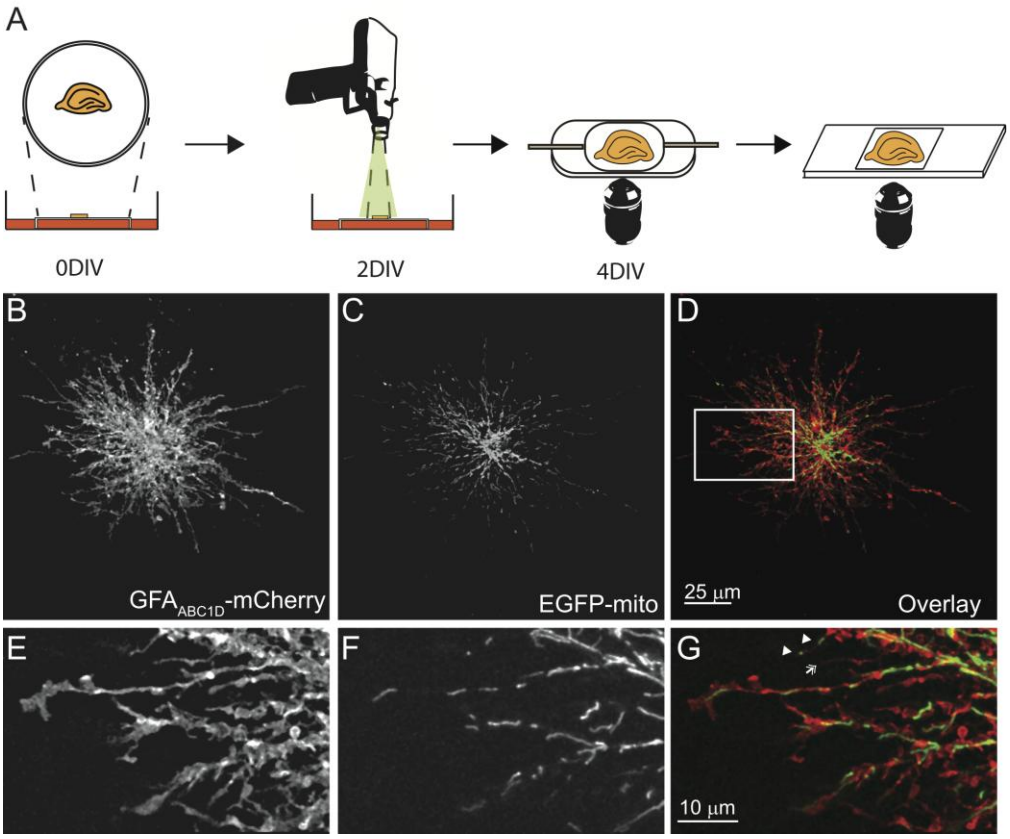

Figure 4.1. Method for imaging of astrocytic mitochondria in hippocampal organotypic cultures. (A) Schematic summary of the experimental approach. Hippocampi from early postnatal rat pups were isolated and plated onto membranes. Two days later slices were transfected via particle based biolistics. Slices were imaged at 4 DIV via confocal. Slices were subsequently fixed for immnofluorescent analysis. (B-D) Representative images of an astrocyte in hippocampal slice culture transfected with a membrane-targeted mCherry fluorescent protein driven by a minimal GFAP promoter (GFAABC1D-mCherry; B and E) and a mitochondrial matrix-targeted enhanced green fluorescent protein (mitoEGFP; C and F) and overlay (D and G). EGFP fluorescence is shown as green and GFAABC1D-mCherry as red. Scale bar is 25 µm. Panels E-G depict magnified views of the astrocyte processes depicted in D (white box). Mitochondria are present in some (G; arrowhead), but not all (chevron) of the small astrocyte processes. Scale bar is 10 µm.

Immediately following the imaging epoch, slices were removed from the chamber and immersed in 4% paraformaldehyde in phosphate buffered saline (0.1 M PBS). Tissues were processed as free-floating sections for subsequent immunostaining. These sections were extracted for 1 hour in a solution of PBS and 1% Triton X-100 at room temperature. Sections were blocked in 5% goat serum for 1 hour at room temperature and incubated with primary antibodies against GFAP (Sigma; 1:100) or MAP2 (Millipore 1:100) for two days at 4°C in a solution containing 1% Triton X-100 and 5% goat serum. Sections were rinsed 3 x 15 min in PBS and incubated overnight with secondary

antibody (goat anti-rabbit or mouse Alexa Fluor 633; Invitrogen). Slices were rinsed 3 x 15 min in PBS before mounting on precoated slides (Superfrost Plus; Fisher Scientific). Sections were imaged on a laser confocal microscope as described above (depicted in Figure 3.1A).

Although there is evidence that the smaller gold particles (1 µm) selectively transduce astrocytes (Benediktsson et al., 2005), a GFAP promoter-driven mCherry was used to ensure selectivity (Lee et al., 2008). To confirm that the combination of 1.0 µm gold particles with this promoter fragment results in selective expression in astrocytes in this system, cells expressing the Gfa_{ABC1D}-driven mCherry fluorescent protein were tested for co-localization with the astrocytic marker, GFAP. In four randomly chosen experiments, all cells expressing Gfa_{ABC1D}-driven mCherry fluorescent protein also expressed GFAP immunoreactivity (data not shown). To confirm neuronal identity, we immunostained every slice previously used to examine mitochondrial mobility in neurons with antibodies against the dendritic marker MAP2. The process that was used for dynamic imaging was re-identified in the fixed and immunostained slices and confirmed to come from a neuronal dendrite (data not shown).

Image Analysis. All data analyses were performed by individuals who were blinded to condition for the particular day. All images were processed using NIH ImageJ software ((http://rsb.info.nih.gov/ij/; Schneider et al., 2012). Images were background corrected and filtered using a Gaussian filter ($\sigma = 1$). Maximal projections of image stacks were generated. Motion artifacts due to slice drift were corrected using the TurboReg plugin of ImageJ to implement rigid registration; aligning all images in a time-lapse series to the original image. The resulting movies were used to examine the mobility of individual mitochondria within the processes of neurons or astrocytes. Individual mitochondria were tracked using the MTrackJ plugin to ImageJ (Meijering et al., 2012). A

mitochondrion was considered mobile if the displacement exceeded 2 µm within the 15 min imaging window. Anterograde and retrograde motion were defined relative to the cell body. Kymographs (displacement vs time) were constructed for individual astrocytic processes for display purposes. Kymographs are displayed such that time is on the y-axis (time increases descending down the page). Mitochondria that are stationary appear as vertical lines, while mitochondria that moved over the imaging period will appear as diagonal lines.

Puncta analysis. **T**he distribution of GLT-1 particles relative to mitochondria and synapses were analyzed in the manner of MacAskill et al. (2000) as detailed below. Hippocampal slice cultures were transfected with EGFP-mito and Gfa_{ABC1D}-mCherry as described above. Slices were immersed in pre-warmed (34°C), oxygenated, ACSF ± TTX (1 µM) for 30 minutes. Slices were immediately immersed in 4% paraformaldehyde (0.1 M PBS) and processed as described earlier in the Methods section. These sections were incubated with primary antibodies against GLT-1 (1:100) or VGLUT1 (Millipore 1:200) and visualized with fluorescent molecule-conjugated secondary antibodies (goat anti-rabbit Dylight 405 (1:400) or goat anti-guinea pig AlexaFluor 633 (1:400)).

Slices were visualized on an Olympus laser scanning confocal microscope equipped with a 40x (1.4 N.A.) objective at an additional 5x optical zoom, using the 405, 488, 546, and 633 laser lines. All images were collected sequentially to avoid contamination of signals from other fluorophores. Sections from each experiment were singly labeled or transfected to verify that the signal measured was specific.

Single optical sections were background corrected and filtered using a Gaussian filter (□=1). mCherry fluorescent images were used to create binary masks that were applied to GLT-1 immunofluorescent images; defining GLT-1 immunoreactivity within

single astrocyte processes. Mitochondria and GLT-1 puncta were identified by thresholding at 3.5 times the standard deviation of the mean image and converted to binary (as per Genda et. al. 2011). VGLUT1 particles were thresholded using an auto-local thresholding plug-in to the FIJI implementation of ImageJ (Gabriel Landini) and converted to binary. The coordinates (centroid) of all particles were recorded and used to calculate the minimum distance between mitochondria:GLT-1 and GLT-1:VGLUT1^{+} pairs. Using this same dataset, we also determined the distance between the edge of each mitochondrion and the edge of the nearest GLT-1 particle using Matlab. These results are displayed as cumulative probabilities.

Statistics. All data are presented as mean ± standard error of the mean (SEM) of separate cells that were acquired from at least 3 independent sets of experiments (separate sets of slices prepared on separate days). Statistical significance was assessed by unpaired Student's t-test or ANOVA with Bonferroni's multiple comparisons test. Statistical significance between cumulative probability distributions was determined using the Kolmogrov-Smirnov test. Statistical analysis was conducted using Graphpad Prism software

3.3 Results

Mitochondrial mobility in astrocyte processes

While numerous groups (for reviews see Cai and Sheng, 2009; MacAskill and Kittler, 2010; Schwarz, 2013) have examined mitochondrial movement in dissociated cultures of neurons, few have looked at mitochondrial movement in neurons in more complex systems (Ohno et al., 2011) and none have examined mitochondrial movement within the processes of astrocytes. Here, we used organotypic cultures of rat

hippocampus to examine the mobility of mitochondria in the processes of astrocytes and neuronal dendrites. Transverse sections of rat hippocampus were cultured on membrane inserts for 2 days. Cultures were transfected via a gene gun with plasmids encoding EGFP-mito and a membrane-targeted mCherry fluorescent protein and visualized 2 days later (Figure 3.1A). Astrocytes in organotypic cultures maintain much of their characteristic three-dimensional morphology (Figure 3.1B-G), with many fine processes radiating from the cell body and the presence of numerous fine branchlets (Benediktsson et al., 2005). Within astrocytes, EGFP-expressing mitochondria were readily identifiable within the astrocyte processes (Figure 3.1C, F). Mitochondria are capable of investing into very small (<0.6 μm diameter) processes, where they occupy a substantial portion of the width of some (Figure 3.1G; white arrowheads) but not all (white chevron) of these processes. Mitochondria within the processes of astrocytes and neurons exist as discrete organelles, whereas those localized to the cell body appear to form a reticular structure, making individual mitochondria more difficult to identify. For our studies of mitochondrial mobility, we confined our analysis to the smaller processes of the astrocyte, where single mitochondria are readily identifiable.

We compared the mobility of mitochondria within individual astrocytes and neuronal dendrites using time-lapse confocal microscopy (Figure 3.2A, B). The majority of mitochondria were stationary for the duration of the 15 min imaging window within both the neurons and astrocytes. However, significantly more mitochondria were mobile within the dendrites of the neurons than in astrocytic processes (Figure 3.2C). The movement of mitochondria within astrocytes and neurons was bidirectional. In astrocytes, 44% of the mitochondria that were mobile moved in the retrograde direction (toward the cell body), while 56% moved in the anterograde direction. In neurons, 61% moved in the retrograde direction, while 39% moved in the anterograde direction. Since

the movement was characterized by brief pauses accompanied by changes in speed and direction, we quantified the maximal instantaneous velocity of each mitochondrion. Neuronal mitochondria moved significantly further (Figure 3.2D) and faster (Figure 3.2E) than did astrocytic mitochondria. The mean maximal velocity of mitochondrial movement in neurons was 0.55 ± 0.05 μm/sec; (n=30) in the anterograde direction and 0.65 ± 0.05 μm/sec (n=47) in the retrograde direction. Within astrocytes, the mean maximal velocity was 0.15 ± 0.01 μm/sec (n=47) in the anterograde direction and 0.2 ± 0.02 μm/sec (n=34) in the retrograde direction (Figure 3.2E inset). These values are similar to those previously observed for the movement of mitochondria along actin filaments in sympathetic ganglia neurons (Morris and Hollenbeck, 1995). The lengths of individual mitochondria in astrocytes and neuronal dendrites, however, were similar (Figure 3.2F).

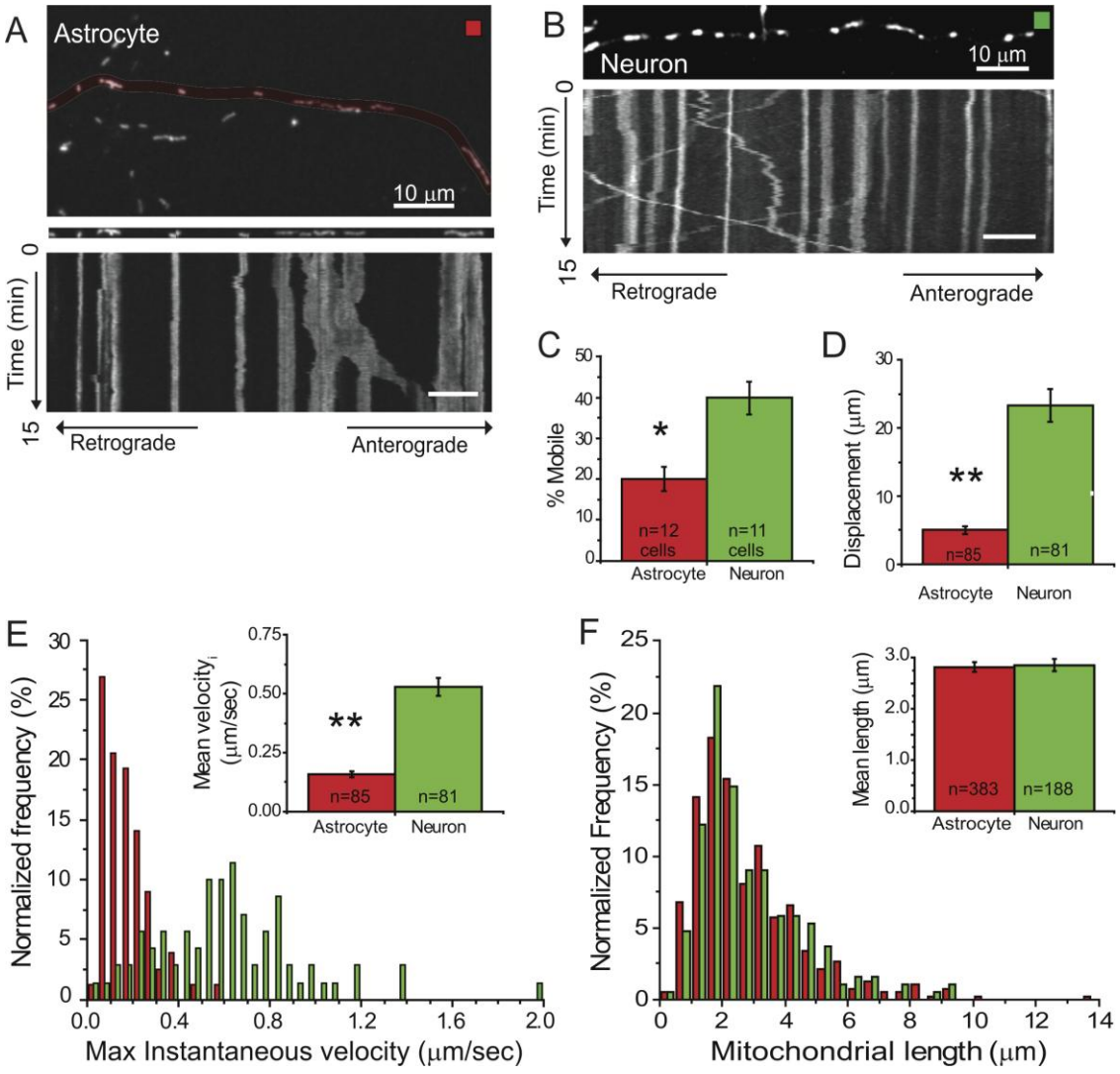

Figure 3.2. Comparison of mitochondrial mobility in astrocytes and neurons in organotypic cultures of hippocampus. Mitochondria in astrocytes and neurons were transfected with plasmids encoding EGFPmito and a membrane-targeted mCherry fluorescent protein. Representative images of astrocytic (A; red box) and neuronal (B: green box) processes are displayed above kymographs that depict the movement of mitochondria in these processes over a 15 min imaging epoch (time increases down page). Stationary mitochondria are seen as straight lines and moving mitochondria as diagonal lines. Scale = 10 μm. (C) Histogram depicts the percentage of mitochondria in astrocytes and neurons that were mobile during the imaging epoch, normalized to the total number of mitochondria that were visualized during that period. Results are mean ± SEM. (D) Histogram displays the average displacement of individual mobile mitochondria. (E) Normalized frequency distribution depicts the maximal instantaneous velocity of individual mitochondria that were mobile within astrocytes (red) and neurons (green). The mean maximal velocity of mobile mitochondria is depicted in inset histogram. (F) Normalized frequency distribution of mitochondrial lengths (mobile and stationary) in astrocytes (red) and neurons (green). The mean length (μm) of mitochondria in astrocytes and neurons is depicted in inset. *p<0.05; **p<0.005 unpaired Student's t-test.

Neuronal activity regulates the percentage of mobile mitochondria in astrocytes

In neurons, mitochondria are retained at sites of high activity and metabolic demand (Li et al., 2004; MacAskill et al., 2010; Ohno et al., 2011). Astrocytic activity and metabolism are highly integrated with neuronal activity. Therefore, we tested whether mitochondrial mobility in astrocytic processes was regulated by neuronal activity within the slice. Slices were pretreated for 15 minutes prior to imaging with TTX (1 μM), a Na^+ channel antagonist commonly used to decrease neuronal activity (Figure 3.3). The percentage of mobile mitochondria in astrocytes increased more than 3-fold in TTX-treated slices compared with untreated controls (Figure 3.3C). The relative ratio of astrocytic mitochondria moving in the anterograde vs retrograde directions changed from 2.6 in controls to 0.9 in TTX-treated slices. Inhibition of neuronal activity did not alter the velocity of mitochondrial movement or mitochondrial length (data not shown). Astrocytes *in vivo* and *in situ* express TTX-sensitive Na^+ channels (Sontheimer et al., 1994). Therefore, as an alternative approach to inhibit neuronal activity, we treated slices

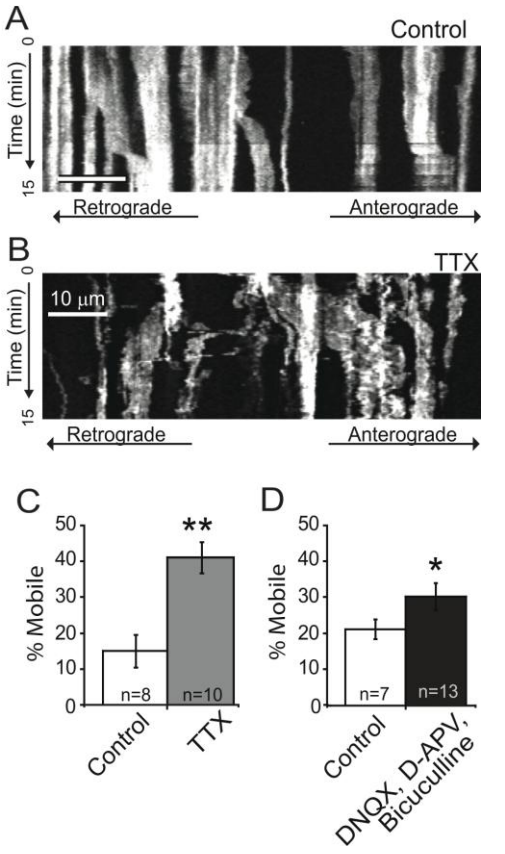

Figure 3.3. Inhibiting neuronal activity increases the percentage of mobile mitochondria in astrocytes. Slice cultures were continuously superfused with ACSF ± TTX (1 μM) for a period of 15 minutes prior to imaging and throughout the imaging period. (A, B) Kymographs show the movement of mitochondria along astrocyte processes in slices treated with control (A; ACSF) or TTX (B) over a 15 minute period (time increases down the page); scale bar is 10 μm. (C) The percentage of mobile mitochondria was calculated and is presented as the mean ± SEM. (D) Histogram depicts the results of inhibiting ionotropic receptors. Slices were treated with APV (50 μM), DNQX (10 μM), and bicuculline (30 μM) for 15 minutes prior to imaging and were continuously superfused with agents for imaging period. Results are mean ± SEM. *p<0.05; **p<0.005 unpaired Student's t-test.

with inhibitors of NMDA (D-APV; 50 μM), AMPA, (DNQX; 10 μM), and GABA (bicuculline; 30 μM) receptors. Bicuculline was included, as GABA may be excitatory during the early post-natal period (Taketo and Yoshioka, 2000), prior to the developmental induction of the chloride pump KCC2 (Rivera C 1999). With this alternative method of blocking neuronal activity, the percentage of mobile mitochondria was again significantly higher in treated slices than in untreated controls (Figure 3.3D). These results suggest that the mobility of mitochondria in astrocytes is influenced by neuronal activity.

Mitochondrial movement depends on both microtubule and actin cytoskeleton

Mitochondrial mobility in neurons depends on both the actin and microtubule cytoskeletons (Morris and Hollenbeck, 1995; Quintero et al., 2009). We examined the dependence of mitochondrial movement in TTX-treated slices in the presence and absence of inhibitors of microtubule (vinblastine) and actin (cytochalasin D) assembly (Figure 3.4). All slices were pretreated with either TTX or ACSF for 15 minutes. Slices were then treated with ACSF or TTX (1 μM), in the presence or absence

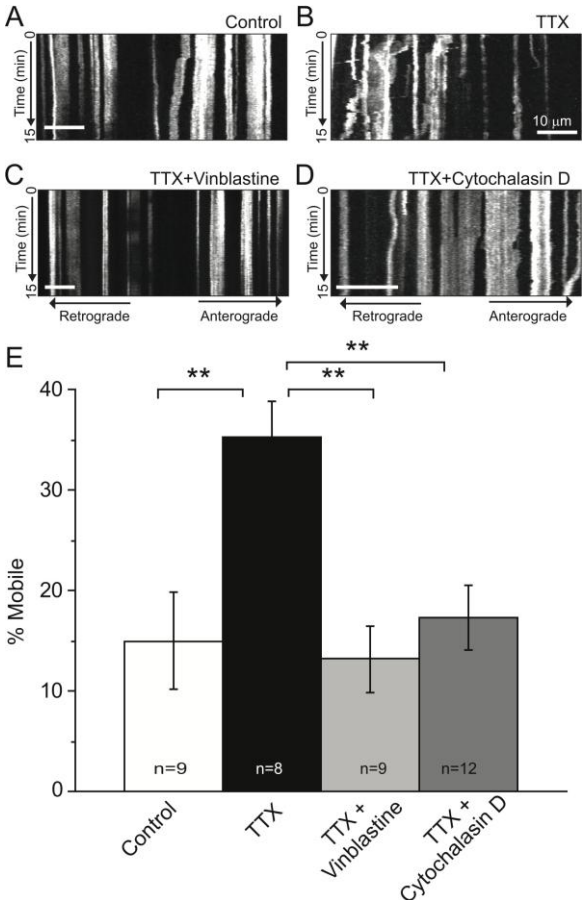

Figure 3.4. Mitochondrial mobility depends on both the actin and microtubule cytoskeletons. (A-D) Kymographs depict the movement of mitochondria along astrocyte processes in slices treated with vehicle (A; ACSF), TTX (B; 1 μM), TTX + vinblastine (C; 1 μg/mL), or TTX + cytochalasin D (D; 20 μM). Slices were continuously superfused with ACSF or TTX for 15 minutes prior to the application of vinblastine (1 μg/mL) or cytochalasin D (20 μM). Slices were continuously superfused with these compounds (in the continued presence of TTX) for an additional 15 minutes prior to the initiation of confocal imaging. Treatments were continued for the entire imaging period. The percentage of mobile mitochondria in astrocytes was determined over a 15 minute imaging epoch. (E) Results are presented as mean ± SEM. **p<0.005 by ANOVA with Bonferonni's multiple comparison test.

of vinblastine (1 µg/ml), or cytochalasin D (20 µM) for an additional 15 minutes prior to imaging. No changes in cell viability or mitochondrial shape were observed following these treatments (data not shown). A greater percentage of mitochondria were mobile in slices treated with TTX than in untreated (ACSF) controls. Application of vinblastine or cytochalasin D decreased the percentage of mobile mitochondria relative to the TTX-treated slices. These results suggest that both the actin and microtubule cytoskeletons contribute to the movement of mitochondria in astrocytic processes.

Mitochondrial mobility in astrocytes is not controlled by mGluR5 activation

Astrocytes express a large complement of neurotransmitter receptors, including metabotropic glutamate receptors and purinergic receptors that allow them to sense and respond to neuronal activity (Newman, 2003). mGluR5 receptors in particular have been linked to increases in astrocytic Ca^{2+} concentration in response to neuronal activity (D'Ascenzo et al., 2007). We hypothesized that the activity-dependent decrease in mitochondrial mobility in astrocytes might be secondary to activation of mGluR5 receptors. Slices were treated with the mGluR5 antagonist (MPEP; 5 µM) for 15 minutes prior to imaging. Inhibition of mGluR5 did not change the percentage of mitochondria that were mobile relative to untreated controls (13 ± 3%, n=12 vs 13 ± 2%, n=9). In another set of experiments, we asked whether activation of mGluR5 receptors is sufficient to decrease mitochondrial mobility. Slices were pre-treated with TTX (1 µM) prior to the addition of DHPG (50 µM). Addition of the mGluR5 agonist did not significantly decrease the TTX-induced increase in mitochondrial mobility (45 ± 7%, n=4 vs. 36 ± 8%, n=6). Together, these results suggest that mitochondrial mobility in astrocytes is not controlled by mGluR5 activation.

Glutamate transport regulates the percentage of mobile mitochondria in astrocytes

Synaptic glutamate concentrations are kept low (approx 25 nM) via the actions of the Na^+-dependent glutamate transporters in astrocytes, particularly GLT-1 and GLAST (Herman and Jahr, 2007). Glutamate transporter activity results in the activation of the Na^+/K^+-ATPase, glycolysis (Pellerin and Magistretti, 1994) and oxidative phosphorylation (Loaiza et al., 2003). We tested whether glutamate uptake influenced mitochondrial mobility in astrocytes by inhibiting glutamate uptake with TFB-TBOA (3 μM) (Shimamoto et al., 2004). Similar to the effects of TTX, inhibition of glutamate uptake resulted in a more than 3-fold increase in the percentage of mitochondria that were mobile relative to untreated controls (Figure 3.5C). Treatment with TFB-TBOA did not alter either the rate of mitochondrial movement (Figure 3.5D) or the proportion of mitochondria moving in the anterograde vs. retrograde directions. We also asked whether activation of the transporters is sufficient to decrease mitochondrial mobility. We inhibited neuronal activity with TTX (1 μM; 15 min) prior to addition of the transporter substrate D-aspartate (1 or 10 mM). Treatment with TTX (Figure 3.5E) increased the percentage of mitochondria that were mobile relative to untreated controls. Application of D-aspartate to TTX-treated slices decreased the percentage of mitochondria that were mobile in a concentration-dependent manner relative to TTX-treated controls (Figure 3.5E). Combined, these results demonstrate that glutamate (aspartate) uptake into astrocytes regulates the mobility of mitochondria in astrocytes.

Glutamate transport results in a significant increase in intracellular $[Na^+]$ (Rose and Ransom, 1996) and stimulates Na^+/K^+-ATPase activity (Pellerin and Magistretti, 1994). It is unsurprising, therefore, that the Na^+/K^+-ATPase physically interacts with both GLT-1 and GLAST (Rose et al., 2009; Genda et al., 2011). Activation of Na^+/K^+-ATPase decreases mitochondrial mobility at the nodes of Ranvier in sciatic nerves (Zhang et al., 2010). Given this, we tested whether an inhibitor of Na^+/K^+-ATPase activity (ouabain)

would influence mitochondrial mobility in astrocytes. Astrocytes possess two isoforms of the Na^+/K^+-ATPase α subunits (α1 and α2) (Juhaszova and Blaustein, 1997). These subunits possess different sensitivities to ouabain; α2 is inhibited at nM concentrations, while the α1 isoform is inhibited at concentrations above 10 μM (Juhaszova and Blaustein, 1997; Pellerin and Magistretti, 1997). We treated slice cultures with either 100 nM or 100 μM ouabain for 15 minutes prior to the start of imaging. Treatment with 100 μM ouabain resulted in a significant increase in the percentage of mitochondria that were mobile in astrocytes (Figure 3.5F).

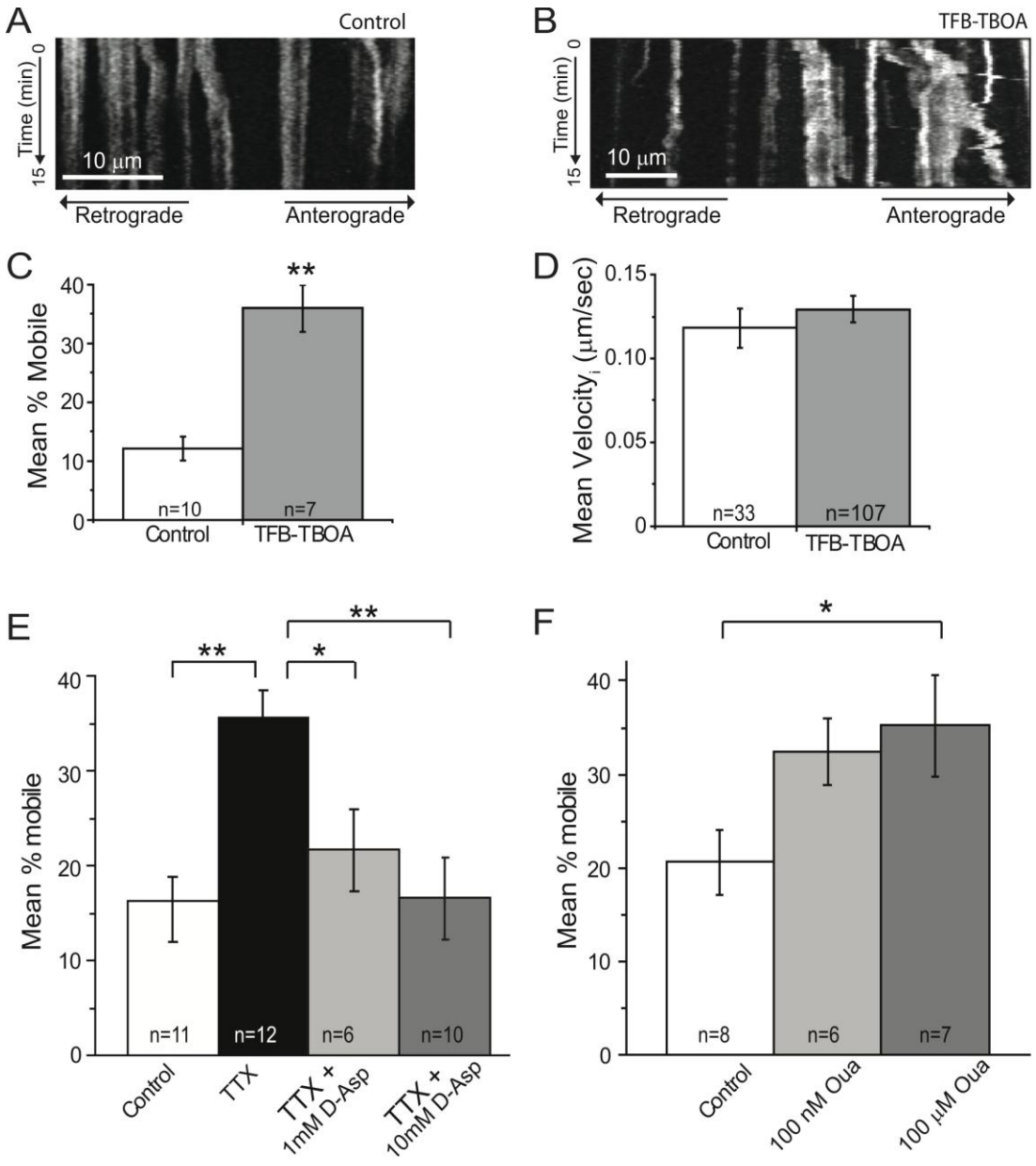

Figure 3.5. Glutamate transport and Na^+K^+-ATPase activation regulate mitochondrial mobility in astrocytes. Astrocytes in slice culture were transfected with mitoEGFP and GFA_{ABC1D}-mcherry at 2 DIV and imaged at 4 DIV. **(A-E)** Slices were continuously superfused with ACSF ± TFB-TBOA (3 μM) for 15 minutes prior to the initiation of imaging and throughout the imaging period. Representative kymographs show the movement of mitochondria in astrocytes in ACSF-treated (**A**) and TFB-TBOA-treated (**B**) slices over a 15 min period (time increases down the page). In these kymographs, stationary mitochondria are seen as straight lines and moving mitochondria as diagonal lines. Scale bar, 10 μm. (**C**). Histogram shows the mean percent of mitochondria that were mobile. **p<0.005 by unpaired Student's t-test. (**D**). Histogram depicts the mean maximal instantaneous velocity of individual astrocytic mitochondria in control (**open**) and TFB-TBOA-treated (**gray**) slices. **(E)** Histogram depicts the effect of treatment with TTX ± D-aspartate on the percentage of mobile mitochondria. Slices were treated with ACSF ± TTX for 15 min at which point D-aspartate (1 or 10 mM) was applied to TTX-treated slices. (**F**) Histogram depicts the effects of ouabain (100 nM or 100 μM) on the percentage of mobile mitochondria in astrocytes. Results are mean ± SEM. *p<0.05; **p<0.005 by ANOVA with Bonferroni's multiple comparisons test.

Reversed Na^+-Ca^{2+} exchange regulates mitochondrial mobility

The bidirectional Na^+/Ca^{2+} exchanger (NCX) normally couples the inward movement of 3 Na^+ ions to the outward movement of one Ca^{2+} ion (Blaustein and Lederer, 1999). In astrocytes, activation of glutamate transport activates the reverse mode of the NCX subsequent to Na^+ entry, resulting in an increase in intracellular [Ca^{2+}] (Rojas et al., 2013; Magi et al., 2013). We tested the hypothesis that reversal of the NCX contributes to immobilization of mitochondria in astrocytes. We treated hippocampal slice cultures with two structurally dissimilar inhibitors of the reverse mode of the NCX (Na^+ efflux/ Ca^{2+} influx) for 15 minutes prior to the start of imaging. At concentrations that selectively block the reversed mode operation of NCX, while minimally affecting normal inward flux of Na^+, KB-R7943 (15 μM) or YM-244769 (1 μM) increased the percentage of

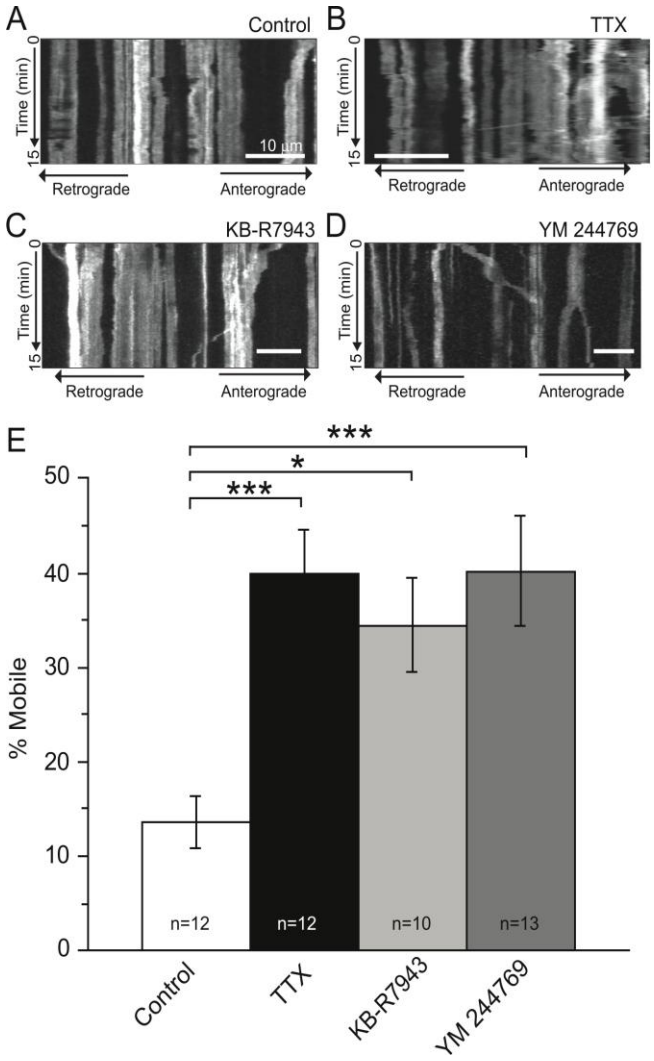

Figure 3.6. Mitochondrial mobility in astrocytes is increased by inhibition of the reverse-mode operation of the Na^+/Ca^{2+} exchanger. (A-D) Slices were continuously superfused with ACSF ± TTX (1 μM), KB-R7943 (15 μM), or YM-244769 (1 μM) for 15 minutes prior to the initiation of imaging and throughout the imaging period. Representative kymographs show the movement of mitochondria in astrocytes treated with ACSF (A), TTX (B), KB-R7943 (C), or YM-244769 (D) over a 15 min period (time increases down the page). In these kymographs, stationary mitochondria are seen as straight lines and moving mitochondria as diagonal lines. Scale bar, 10 μm. (E) Histogram depicts the percentage of mitochondria that were mobile following treatment. Results are mean ± SEM. *p<0.05; **p<0.005 by ANOVA with Bonferroni's multiple comparisons test.

mitochondria that were mobile within the processes of astrocytes to a similar degree to TTX (1 μM; positive control) (Figure 3.6E). While KB-7943 also blocks NMDARs and inhibits complex 1 of the mitochondrial electron transport chain, no such off-target effects have been reported for YM-244769 (Brustovetsky et al., 2011; Clerc and Polster, 2012). Thus, these results suggest that tonic activation of the reverse mode of the NCX is contributing to mitochondrial immobilization in astrocytes.

Association of mitochondria with glutamate transporters

In neurons, the positioning of mitochondria at sites of heightened energy use (presynaptic termini, post-synaptic spines, or nodes of Ranvier) or elevated [Ca^{2+}] is critical to maintain energy and Ca^{2+} homeostasis. We tested whether the neuronal activity-induced decreases in mitochondrial mobility in astrocytes were correlated with the positioning/retention of mitochondria near glutamate transporters (GLT-1), where demand would be predicted to be elevated. GFA_{ABC1D}-mCherry (Figure 3.7A) and EGFP-mito (Figure 3.7B) transfected slices were treated with TTX (1 **μ**M) or vehicle for 30 minutes. Slices were subsequently immunostained for VGLUT1 (Figure 3.7C) and GLT-1 (Figure 3.7D). mCherry fluorescence was used to construct a digital mask allowing for the identification of GLT-1 puncta within individual astrocyte processes. In an earlier study, we examined the overlap between mitochondria and exogenously expressed GLT-1 tagged with a fluorescent epitope using the same system, except that slices were not incubated with artificial CSF for 30 min at 34^{o} C (Genda et al., 2011). As this approach results in over-expression of transporter that could influence the extent of overlap between GLT-1 puncta and mitochondria, we first examined overlap of endogenous GLT-1 with mitochondria. We find that 38 ± 6 % of GLT-1 puncta were overlapped by a mitochondria and 64 ± 7 % of mitochondria were overlapped by GLT-1. These values are somewhat lower than observed in the earlier study, but are indicative

of substantial overlap between GLT-1 and mitochondria under these conditions. These images were also used to compare the anatomic relationship of GLT-1 puncta, mitochondria, and synapses (VGLUT+) in the presence and absence of TTX (Figure 3.7E). The minimum distance between the centers of GLT-1 puncta and VGLUT1 (Figure 3.7F) and between mitochondria and GLT-1 puncta (Figure 3.7G) was measured and expressed as a cumulative probability distribution. Interestingly, reducing neuronal activity (TTX) did not change the relationship between GLT-1+ and VGLUT1+ puncta, suggesting that GLT-1 remains near synapses in the presence of TTX. However, reducing neuronal activity decreased the probability (evident as a rightward shift in the cumulative distribution) that mitochondria approach a GLT-1 puncta (i.e. increased distance), suggesting that neuronal activity regulates the position of mitochondria relative to GLT-1 ($P < 0.0001$). As mitochondria are quite long relative to the distances being measured, we also examined the relationship between the edges of mitochondria and GLT-1 puncta, as any overlap would presumably allow for functional coupling between transporters and mitochondria. As was observed using the centers of the particles, the cumulative probably plot revealed a significant difference in the presence and absence of TTX ($P = 0.02$). In the presence of TTX, there was greater likelihood that mitochondria were further from GLT-1 puncta (data not shown).

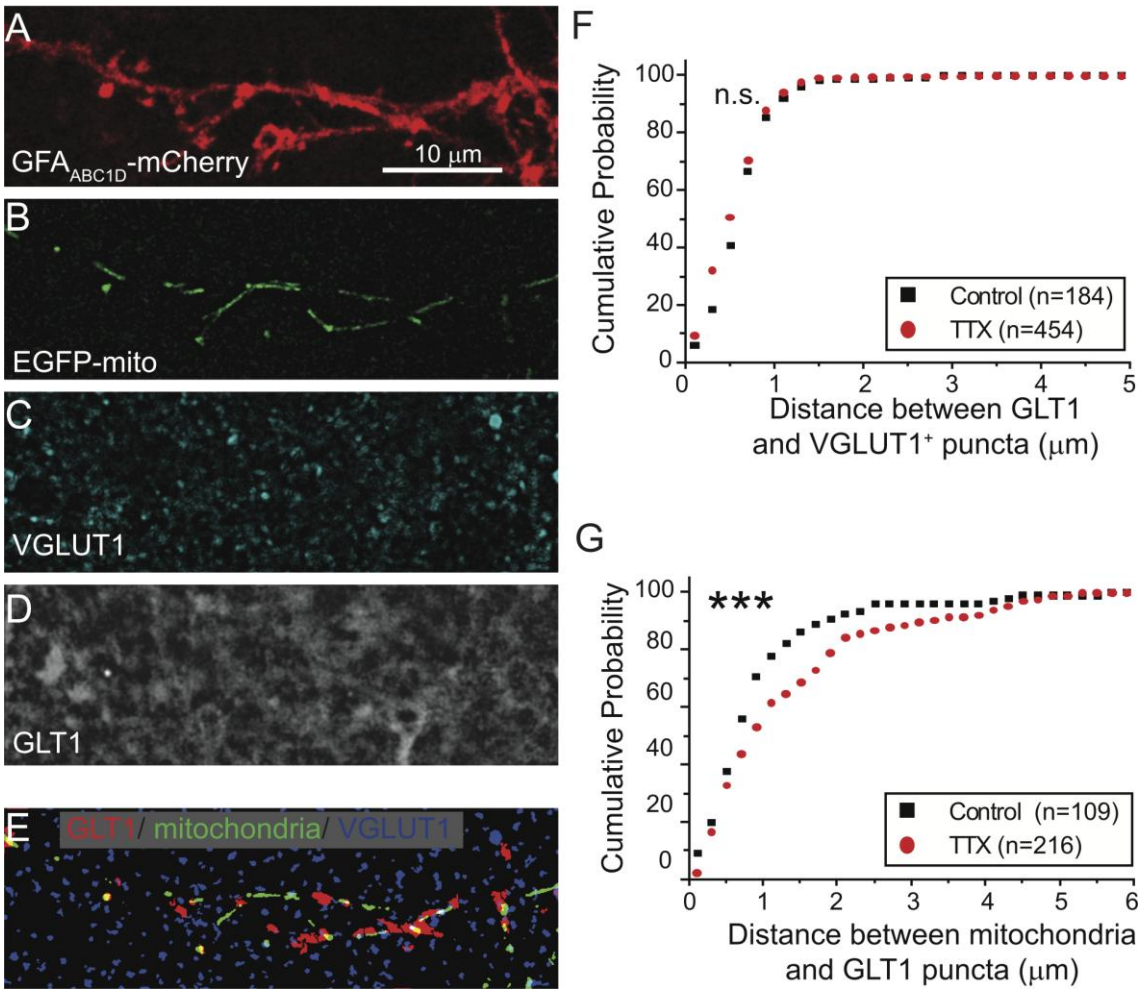

Figure 3.7. Neuronal activity increases the probability that mitochondria appose GLT-1 in astrocytic processes without affecting the relationship of GLT-1 to VGLUT1. Astrocytes were transfected with plasmids encoding EGFPmito and a membrane-targeted mCherry fluorescent protein. Slices were treated in the absence or presence of TTX (1 μM) for 30 minutes. Slices were fixed and subsequently immunostained with antibodies against VGLUT1 and GLT-1. Representative images of an astrocyte process expressing GFA$_{ABC1D}$-mCherry (A), and EGFPmito (B), and immunostained for VGLUT1 (C) and GLT-1 (D). (E) Representative image depicting GLT-1 (red), mitochondria (green) and VGLUT1+ (blue) puncta from the process depicted in (A-D). Cumulative probability distributions depicting the distance between each GLT-1 and the nearest VGLUT1+ (F) puncta and between each mitochondrion and the nearest GLT-1 puncta (G) in the absence (black boxes) and presence (red circles) of TTX. ***p<0.0001 by Kolmogorov-Smirnov test.

3.4 Discussion

In neurons, mitochondria accumulate at sites of high activity and energetic demand, including pre- and post-synaptic terminals (Li et al., 2004; Miller and Sheetz, 2004), growth cones (Morris and Hollenbeck, 1993), and nodes of Ranvier (Ohno et al., 2011), where they provide local energetic support and regulate ionic homeostasis (for review, see Schwarz, 2013). Mitochondria have been localized within the processes of astrocytes (Lovatt et al., 2007; Ito et al., 2009, Lavialle et al., 2011) in close proximity to glutamate transporters (Chaudhry et al., 1995; Genda et al., 2011). Here we describe the mobility of mitochondria within the processes of astrocytes. In addition, we describe a potential mechanism by which glutamate release from neurons is converted to mitochondrial immobilization in astrocytes via glutamate uptake through the astrocytic glutamate transporters, and reversed Na^{+}-Ca^{2+} exchange. Further, we show that neuronal activity is associated with an increased probability that mitochondria approach glutamate transporter clusters in the processes of astrocytes without changing the relationship of GLT-1 puncta to VGLUT1 (synapses). Together, this work suggests a mechanism by which mitochondria may be recruited to, or retained at, areas of high GLT-1 expression that surround synapses.

Mitochondria in astrocyte processes

We used time-lapse imaging of mitochondria to examine mitochondrial movement in neuronal and astrocytic processes. While mitochondria in neurons and astrocytes displayed similar lengths, there were significant differences with regard to rate of movement and the fraction mobile. Our findings in neurons are similar to that which has been observed (fraction mobile, velocity, and size) (see MacAskill et al., 2010, for review). The difference between astrocytic and neuronal mitochondrial movement

suggests that mitochondrial mobility in astrocytes might be regulated by different motor proteins or move along different cytoskeletal elements. Indeed, the rates of movement observed in astrocytes match those observed for short-range mitochondrial transport along actin filaments (Morris and Hollenbeck, 1995).

In neurons, mitochondrial mobility has been linked to both the actin and microtubule cytoskeleton. Long-range mitochondrial movement in neurons depends on transport by kinesins (anterograde) and dynein (retrograde) motors along the microtubule cytoskeleton (reviewed in Schwarz, 2013). Short range-movement along actin fibers has been described (Morris and Hollenbeck, 1995; Ligon and Steward, 2000; Hollenbeck, 2005). We examined the movement of mitochondria in response to treatment with inhibitors of actin and microtubule assembly. Our results suggest that, in astrocytes (as in neurons), mitochondrial movement depends on both the actin and microtubule cytoskeleton. It will be interesting to identify the motor proteins involved. Anterograde transport along microtubules in neurons is mediated primarily by the kinesin isoforms Kif5 and Kif1B (MacAskill and Kittler, 2010). The major kinesin isoforms in astrocytes have yet to be determined, however KIF5A and C are thought to be neuron-specific motor proteins (Kanai et al., 2000).

Retention of mitochondria by neuronal activity.

Why move mitochondria? The coordinated transport of mitochondria along cellular processes likely serves several functions. Firstly, movement of mitochondria appears necessary for the distribution of mitochondria into cellular processes. Mitochondria are primarily generated in the cell body and are transported in an anterograde direction into the processes (reviewed in Schwarz, 2013). Conversely, the observation that depolarized mitochondria move primarily in the retrograde direction has

been used to suggest that dysfunctional mitochondria move toward the cell body for repair/degradation (Frederick and Shaw, 2007). Secondly, movement of mitochondria facilitates the processes of fusion and fission that allow the exchange of proteins and genetic material between discreet mitochondria (Misko et al., 2010). Lastly, mitochondrial transport provides a mechanism for the redistribution of mitochondria to sites of high activity (reviewed in MacAskill and Kittler, 2010; Schwarz, 2013).

In neurons, mitochondria are retained at sites of high activity and metabolic demand (Li et al., 2004; Wang and Schwarz, 2009; Ohno et al., 2011). Neuronal activity and glutamate receptor activation decrease mitochondrial mobility and cause mitochondria to pause at synapses and at nodes of Ranvier in neurons. Astrocytes sense neuronal activity (Halassa et al., 2007a), and much of their activity is devoted to processes such as glutamate uptake that are integrated with neuronal activity (Parpura and Verkhratsky, 2012). We hypothesized that neuronal activity might influence mitochondrial movement within astrocytic processes. Inhibition of neuronal activity with TTX or ionotropic receptor antagonists increased the percentage of mitochondria that were mobile in astrocytes. While, astrocytes *in vitro* and *in situ* express multiple isoforms of the voltage-dependent Na^+ channel family (Sontheimer et al., 1994), the observation that inhibition of ionotropic receptors (NMDARs, AMPARs, and GABARs) also increased mitochondrial mobility suggests that this effect is mediated by neurons. Additionally, our results also indicate that the increased mobility of mitochondria in TTX-treated slices is blocked by application of the transporter substrate D-aspartate (Figure 3.5). Together, these results strongly suggest that mitochondrial mobility in astrocytes is regulated by neuronal activity.

Astrocytes are the primary route of clearance for extracellular glutamate (Danbolt, 2001). Glutamate transport and concomitant activation of the Na^+/K^+-ATPase

represent a substantial energetic demand on astrocytes (Hertz et al., 2007). We hypothesized that glutamate uptake might influence astrocytic mitochondrial mobility. Our results suggest that neuronal activity regulates astrocytic mitochondrial mobility via activation of glutamate transporters. It remains to be determined whether this immobilization is a result of the glutamate transport cycle, or is subsequent to another process, such as activation of the Na^+/K^+-ATPase. Although inhibition of the Na^+/K^+-ATPase decreased the percentage of mitochondria that were mobile in astrocytes (Figure 3.5G), there are at least three possible explanations for this result. First, it is possible the effects of ouabain are related to the spreading depression that ouabain induces via the neuronal Na^+/K^+-ATPase isoforms (Balestrino et al., 1999). Second, ouabain is also known to inhibit glutamate uptake (Li and Stys, 2001; Rose et al., 2009). Finally, it is possible that activation of the Na^+/K^+ ATPase is required for mitochondrial immobilization in astrocytes. Although Zhang et al., 2010, favored this later mechanism to explain docking of mitochondria near nodes of Ranvier, we cannot discriminate between these possibilities in the current study.

Several mechanisms contribute to the immobilization of mitochondria in neurons in response to increased activity. Increases in [ADP] result in decreased mitochondrial transport (Mironov, 2007). Additionally, increases in intracellular $[Ca^{2+}]$ subsequent to NMDAR activation stop mitochondria at the base of dendritic spines (Li et al., 2004; Wang and Schwarz, 2009). As increases in neuronal activity activate mGluR5 receptors in astrocytes (D'Ascenzo et al., 2007), we tested whether activation of mGluR5 contributed to the neuronal activity dependent immobilization of mitochondria in astrocytes. Surprisingly, neither activation nor inhibition of mGluR5 altered mitochondrial mobility. However, selective inhibition of the reverse mode of Na^+-Ca^{2+}

exchange increased the percentage of mobile mitochondria, suggesting that increases in $[Ca^{2+}]_i$ via the NCX might contribute to the immobilization of mitochondria in astrocytes.

Why move mitochondria to sites of glutamate transport? Mitochondria play important roles in a variety of processes, including ATP production, ionic buffering, and glutamate oxidation. Glutamate uptake has been coupled to all three of these processes. For example, glutamate uptake increases astrocytic glycogen utilization (Swanson, 1992), glycolysis (Pellerin and Magistretti, 1994), and oxygen consumption (Eriksson et al., 1995). Glutamate uptake is coupled to an increase in mitochondrial Na^+ concentration (Bernardinelli et al., 2006) and accompanied by rapid mitochondrial acidification (Azarias et al., 2011). These studies imply that mitochondria buffer the ionic changes associated with transporter function. Mitochondria also play a critical role in glutamate metabolism (reviewed in Dienel, 2013). Upon import into astrocytes, glutamate can either be converted to glutamine via glutamine synthetase or oxidized to mitochondrial TCA cycle intermediates (Yudkoff et al., 1988). In brain, most glutamate oxidation is thought to occur in astrocytes (Hertz et al., 1988; Waagepetersen et al., 2002). In fact the fraction of glutamate that is oxidized increases disproportionately with increasing extracellular glutamate (McKenna et al., 1996; Yu et al., 1982). The oxidation of glutamate by mitochondria may fuel glutamate uptake by providing the ATP necessary for Na^+ extrusion (Whitelaw and Robinson, 2013; Peng et al., 2001; reviewed in Dienel, 2013). All of these functions would be supported by the immobilization of mitochondria near sites of glutamate uptake. The development of tools to selectively block the docking of mitochondria in astrocytes will be necessary to test the functional significance of mitochondrial immobilization.

Here, we provide the first description of mitochondrial mobility in the processes of astrocytes. Mitochondrial mobility is regulated by neuronal activity, glutamate transport, and Na^{+}-Ca^{2+} exchange. Further, neuronal activity regulates the retention/accumulation of mitochondria at sites enriched in glutamate transporters that are apposed to synapses. The transport of mitochondria within astrocytes likely influences, and is influenced, by other aspects of astrocyte biology. Future experiments will be necessary to examine whether other processes influence mitochondrial function in astrocytes, to determine which motors are responsible for their movement, and to determine why and how the mitochondria are kept stationary.

3.5 References

Azarias G, Perreten H, Lengacher S, Poburko D, Demaurex N, Magistretti PJ, Chatton JY (2011) Glutamate transport decreases mitochondrial pH and modulates oxidative metabolism in astrocytes. J Neurosci 31:3550-3559.

Balestrino M, Young J, Aitken P (1999) Block of (Na+,K+)ATPase with ouabain induces spreading depression-like depolarization in hippocampal slices. Brain Res 838:37-44.

Bauer DE, Jackson JG, Genda EN, Montoya MM, Yudkoff M, Robinson MB (2012) The glutamate transporter, GLAST, participates in a macromolecular complex that supports glutamate metabolism. Neurochem Int 61:566-574.

Benediktsson AM, Schachtele SJ, Green SH, Dailey ME (2005) Ballistic labeling and dynamic imaging of astrocytes in organotypic hippocampal slice cultures. J Neurosci Methods 141:41-53.

Bergles DE, Jahr CE (1997) Synaptic activation of glutamate transporters in hippocampal astrocytes. Neuron 19:1297-1308.

Bernardinelli Y, Azarias G, Chatton JY (2006) In situ fluorescence imaging of glutamate-evoked mitochondrial Na+ responses in astrocytes. Glia 54:460-470.

Blaustein MP, Lederer WJ (1999) Sodium/calcium exchange: its physiological implications. Physiol Rev 79:763-854.

Brustovetsky T, Brittain MK, Sheets PL, Cummins TR, Pinelis V, Brustovetsky N (2011) KB-R7943, an inhibitor of the reverse Na+ /Ca2+ exchanger, blocks N-methyl-D-aspartate receptor and inhibits mitochondrial complex I. Br J Pharmacol 162:255-270.

Cai Q, Sheng ZH (2009) Mitochondrial transport and docking in axons. Exp Neurol 218:257-267.

Chaudhry FA, Lehre KP, van Lookeren Campagne M, Ottersen OP, Danbolt NC, Storm-Mathisen J (1995) Glutamate transporters in glial plasma membranes: highly differentiated localizations revealed by quantitative ultrastructural immunocytochemistry. Neuron 15:711-720.

Choi DW (1992) Excitotoxic cell death. J Neurobiol 23:1261-1276.

Clerc P, Polster BM (2012) Investigation of mitochondrial dysfunction by sequential microplate-based respiration measurements from intact and permeabilized neurons. PLoS One 7:e34465.

Conti F, Weinberg RJ (1999) Shaping excitation at glutamatergic synapses. Trends Neurosci 22:451-458.

D'Ascenzo M, Fellin T, Terunuma M, Revilla-Sanchez R, Meaney DF, Auberson YP, Moss SJ, Haydon PG (2007) mGluR5 stimulates gliotransmission in the nucleus accumbens. Proc Natl Acad Sci U S A 104:1995-2000.

Danbolt NC (2001) Glutamate uptake. Prog Neurobiol 65:1-105.

Dienel GA (2013) Astrocytic energetics during excitatory neurotransmission: What are contributions of glutamate oxidation and glycolysis? Neurochem Int.

Eriksson G, Peterson A, Iverfeldt K, Walum E (1995) Sodium-dependent glutamate uptake as an activator of oxidative metabolism in primary astrocyte cultures from newborn rat. Glia 15:152-156.

Frederick RL, Shaw JM (2007) Moving mitochondria: establishing distribution of an essential organelle. Traffic 8:1668-1675.

Genda EN, Jackson JG, Sheldon AL, Locke SF, Greco TM, O'Donnell JC, Spruce LA, Xiao R, Guo W, Putt M, Seeholzer S, Ischiropoulos H, Robinson MB (2011) Co-compartmentalization of the astroglial glutamate transporter, GLT-1, with glycolytic enzymes and mitochondria. J Neurosci 31:18275-18288.

Halassa MM, Fellin T, Haydon PG (2007a) The tripartite synapse: roles for gliotransmission in health and disease. Trends Mol Med 13:54-63.

Halassa MM, Fellin T, Takano H, Dong JH, Haydon PG (2007b) Synaptic islands defined by the territory of a single astrocyte. J Neurosci 27:6473-6477.

Herman MA, Jahr CE (2007) Extracellular glutamate concentration in hippocampal slice. J Neurosci 27:9736-9741.

Hertz L, Drejer J, Schousboe A (1988) Energy metabolism in glutamatergic neurons, GABAergic neurons and astrocytes in primary cultures. Neurochem Res 13:605-610.

Hertz L, Peng L, Dienel GA (2007) Energy metabolism in astrocytes: high rate of oxidative metabolism and spatiotemporal dependence on glycolysis/glycogenolysis. J Cereb Blood Flow Metab 27:219-249.

Hollenbeck PJ (2005) Mitochondria and neurotransmission: evacuating the synapse. Neuron 47:331-333.

Ito U, Hakamata Y, Kawakami E, Oyanagi K (2009) Degeneration of astrocytic processes and their mitochondria in cerebral cortical regions peripheral to the cortical infarction: heterogeneity of their disintegration is closely associated with disseminated selective neuronal necrosis and maturation of injury. Stroke 40:2173-2181.

Juhaszova M, Blaustein MP (1997) Na+ pump low and high ouabain affinity alpha subunit isoforms are differently distributed in cells. Proc Natl Acad Sci U S A 94:1800-1805.

Kanai Y, Okada Y, Tanaka Y, Harada A, Terada S, Hirokawa N (2000) KIF5C, a novel neuronal kinesin enriched in motor neurons. J Neurosci 20:6374-6384.

Kayser MS, McClelland A, Hughes EG, Dalva MB (2006) Intracellular and trans-synaptic regulation of glutamatergc synaptogenesis by EphB receptors. J Neurosci 26:12152-12164.

Lavialle M, Aumann G, Anlauf E, Prols F, Arpin M, Derouiche A (2011) Structural plasticity of perisynaptic astrocyte processes involves ezrin and metabotropic glutamate receptors. Proc Natl Acad Sci U S A 108:12915-12919.

Lee Y, Messing A, Su M, Brenner M (2008) GFAP promoter elements required for region-specific and astrocyte-specific expression. Glia 56:481-493.

Li S, Stys PK (2001) Na(+)-K(+)-ATPase inhibition and depolarization induce glutamate release via reverse Na(+)-dependent transport in spinal cord white matter. Neuroscience 107:675-683.

Li Z, Okamoto K, Hayashi Y, Sheng M (2004) The importance of dendritic mitochondria in the morphogenesis and plasticity of spines and synapses. Cell 119:873-887.

Ligon LA, Steward O (2000) Role of microtubules and actin filaments in the movement of mitochondria in the axons and dendrites of cultured hippocampal neurons. J Comp Neurol 427:351-361.

Loaiza A, Porras OH, Barros LF (2003) Glutamate triggers rapid glucose transport stimulation in astrocytes as evidenced by real-time confocal microscopy. J Neurosci 23:7337-7342.

Lovatt D, Sonnewald U, Waagepetersen HS, Schousboe A, He W, Lin JH, Han X, Takano T, Wang S, Sim FJ, Goldman SA, Nedergaard M (2007) The transcriptome and metabolic gene signature of protoplasmic astrocytes in the adult murine cortex. J Neurosci 27:12255-12266.

MacAskill AF, Atkin TA, Kittler JT (2010) Mitochondrial trafficking and the provision of energy and calcium buffering at excitatory synapses. Eur J Neurosci 32:231-240.

MacAskill AF, Kittler JT (2010) Control of mitochondrial transport and localization in neurons. Trends Cell Biol 20:102-112.

Magi S, Arcangeli S, Castaldo P, Nasti AA, Berrino L, Piegari E, Bernardini R, Amoroso S, Lariccia V (2013) Glutamate-induced ATP synthesis: relationship between plasma membrane Na+/Ca2+ exchanger and excitatory amino acid transporters in brain and heart cell models. Mol Pharmacol 84:603-614.

Magistretti PJ (2006) Neuron-glia metabolic coupling and plasticity. J Exp Biol 209:2304-2311.

Magistretti PJ, Pellerin L (1999) Cellular mechanisms of brain energy metabolism and their relevance to functional brain imaging. Philos Trans R Soc Lond B Biol Sci 354:1155-1163.

McAllister AK (2004) Biolistic transfection of cultured organotypic brain slices. Methods Mol Biol 245:197-206.

McKenna MC, Sonnewald U, Huang X, Stevenson J, Zielke HR (1996) Exogenous glutamate concentration regulates the metabolic fate of glutamate in astrocytes. J Neurochem 66:386-393.

Meijering E, Dzyubachyk O, Smal I (2012) Methods for cell and particle tracking. Methods Enzymol 504:183-200.

Miller KE, Sheetz MP (2004) Axonal mitochondrial transport and potential are correlated. J Cell Sci 117:2791-2804.

Mironov SL (2007) ADP regulates movements of mitochondria in neurons. Biophys J 92:2944-2952.

Misko A, Jiang S, Wegorzewska I, Milbrandt J, Baloh RH (2010) Mitofusin 2 is necessary for transport of axonal mitochondria and interacts with the Miro/Milton complex. J Neurosci 30:4232-4240.

Morris RL, Hollenbeck PJ (1993) The regulation of bidirectional mitochondrial transport is coordinated with axonal outgrowth. J Cell Sci 104 (Pt 3):917-927.

Morris RL, Hollenbeck PJ (1995) Axonal transport of mitochondria along microtubules and F-actin in living vertebrate neurons. J Cell Biol 131:1315-1326.

Newman EA (2003) New roles for astrocytes: regulation of synaptic transmission. Trends Neurosci 26:536-542.

Ohno N, Kidd GJ, Mahad D, Kiryu-Seo S, Avishai A, Komuro H, Trapp BD (2011) Myelination and axonal electrical activity modulate the distribution and motility of mitochondria at CNS nodes of Ranvier. J Neurosci 31:7249-7258.

Parpura V, Verkhratsky A (2012) Neuroglia at the crossroads of homoeostasis, metabolism and signalling: evolution of the concept. ASN Neuro 4:201-205.

Pellerin L, Magistretti PJ (1994) Glutamate uptake into astrocytes stimulates aerobic glycolysis: a mechanism coupling neuronal activity to glucose utilization. Proc Natl Acad Sci U S A 91:10625-10629.

Pellerin L, Magistretti PJ (1997) Glutamate uptake stimulates Na+,K+-ATPase activity in astrocytes via activation of a distinct subunit highly sensitive to ouabain. J Neurochem 69:2132-2137.

Peng L, Swanson RA, Hertz L (2001) Effects of L-glutamate, D-aspartate, and monensin on glycolytic and oxidative glucose metabolism in mouse astrocyte cultures: further evidence that glutamate uptake is metabolically driven by oxidative metabolism. Neurochem Int 38:437-443.

Quintero OA, DiVito MM, Adikes RC, Kortan MB, Case LB, Lier AJ, Panaretos NS, Slater SQ, Rengarajan M, Feliu M, Cheney RE (2009) Human Myo19 is a novel myosin that associates with mitochondria. Curr Biol 19:2008-2013.

Rizzuto R, Brini M, Pozzan T (1993) Intracellular targeting of the photoprotein aequorin: A new approach for measuring, in living cells, Ca(2+) concentrations in defined cellular compartments. Cytotechnology 11:S44-46.

Rojas H, Colina C, Ramos M, Benaim G, Jaffe E, Caputo C, Di Polo R (2013) Sodium-calcium exchanger modulates the L-glutamate Ca(i) (2+) signalling in type-1 cerebellar astrocytes. Adv Exp Med Biol 961:267-274.

Rose CR, Ransom BR (1996) Mechanisms of H+ and Na+ changes induced by glutamate, kainate, and D-aspartate in rat hippocampal astrocytes. The Journal of neuroscience : the official journal of the Society for Neuroscience 16:5393-5404.

Rose EM, Koo JC, Antflick JE, Ahmed SM, Angers S, Hampson DR (2009) Glutamate transporter coupling to Na,K-ATPase. J Neurosci 29:8143-8155.

Schneider CA, Rasband WS, Eliceiri KW (2012) NIH Image to ImageJ: 25 years of image analysis. Nature methods 9:671-675.

Schwarz TL (2013) Mitochondrial trafficking in neurons. Cold Spring Harb Perspect Biol 5.

Sheldon AL, Robinson MB (2007) The role of glutamate transporters in neurodegenerative diseases and potential opportunities for intervention. Neurochem Int 51:333-355.

Shimamoto K, Sakai R, Takaoka K, Yumoto N, Nakajima T, Amara SG, Shigeri Y (2004) Characterization of novel L-threo-beta-benzyloxyaspartate derivatives, potent blockers of the glutamate transporters. Mol Pharmacol 65:1008-1015.

Sontheimer H, Fernandez-Marques E, Ullrich N, Pappas CA, Waxman SG (1994) Astrocyte Na+ channels are required for maintenance of Na+/K(+)-ATPase activity. J Neurosci 14:2464-2475.

Swanson RA (1992) Physiologic coupling of glial glycogen metabolism to neuronal activity in brain. Can J Physiol Pharmacol 70 Suppl:S138-144.

Taketo M, Yoshioka T (2000) Developmental change of GABA(A) receptor-mediated current in rat hippocampus. Neuroscience 96:507-514.

Waagepetersen HS, Qu H, Hertz L, Sonnewald U, Schousboe A (2002) Demonstration of pyruvate recycling in primary cultures of neocortical astrocytes but not in neurons. Neurochem Res 27:1431-1437.

Wang GJ, Jackson JG, Thayer SA (2003) Altered distribution of mitochondria impairs calcium homeostasis in rat hippocampal neurons in culture. J Neurochem 87:85-94.

Wang X, Schwarz TL (2009) The mechanism of Ca2+ -dependent regulation of kinesin-mediated mitochondrial motility. Cell 136:163-174.

Whitelaw BS, Robinson MB (2013) Inhibitors of glutamate dehydrogenase block sodium-dependent glutamate uptake in rat brain membranes. Front Endocrinol (Lausanne) 4:123.

Yu AC, Schousboe A, Hertz L (1982) Metabolic fate of 14C-labeled glutamate in astrocytes in primary cultures. J Neurochem 39:954-960.

Yudkoff M, Nissim I, Pleasure D (1988) Astrocyte metabolism of [15N]glutamine: implications for the glutamine-glutamate cycle. J Neurochem 51:843-850.

Zerangue N, Kavanaugh MP (1996) Flux coupling in a neuronal glutamate transporter. Nature 383:634-637.

Zhang CL, Ho PL, Kintner DB, Sun D, Chiu SY (2010) Activity-dependent regulation of mitochondrial motility by calcium and Na/K-ATPase at nodes of Ranvier of myelinated nerves. J Neurosci 30:3555-3566.

CHAPTER 4

Transient Oxygen/Glucose Deprivation Causes a Delayed Loss of Mitochondria and Increases Spontaneous Calcium Signaling in Astrocytic Processes

John C. O'Donnell[1,3], Joshua G. Jackson[1], Michael B. Robinson[1,2,3]

Children's Hospital of Philadelphia Research Institute[1], and Departments of Pediatrics[2], and Systems Pharmacology and Translational Therapeutics[3], University of Pennsylvania, Philadelphia, PA 19104

Address Correspondence to: Michael B. Robinson
Department of Pediatrics, 502N
Abramson Pediatric Research Building
3615 Civic Center Boulevard
Philadelphia, PA 19104-3779
Tel. 215-590-2205; Fax. 215-590-3779
Email: Robinson@mail.med.upenn.edu

Author contributions: J.C.O. and M.B.R. designed research; J.C.O. performed research; J.G.J. contributed unpublished reagents; J.C.O. analyzed data; J.C.O. and M.B.R. wrote the paper.

Acknowledgments: This work was supported by a grant (RO1 NS077773) to M.B.R. from the National Institute of Neurological Disorders and Stroke. Partial support for J.C.O. was provided by a predoctoral training grant in pharmacology (T32 GM008076) followed by an individual NRSA (F31 NS086255). We are grateful for the imaging support of Drs. Douglas Coulter and Hajime Takano (Cellular Neuroscience Core) and statistical support from Dr. Mary Putt (Biostatistics and Bioinformatics Core) of the Institutional Intellectual and Developmental Disabilities Research Center (U54 HD086984). The authors would also like to thank members of the Robinson laboratory for their advice and suggestions during the conduct of this research.

Published in The Journal of Neuroscience, 06 July, 2016. Volume 36, Issue 27, pages 7109-7127.

Abstract

Recently, mitochondria have been localized to astrocytic processes where they shape Ca^{2+} signaling; this relationship has not been examined in models of ischemia/reperfusion. We biolistically transfected astrocytes in rat hippocampal slice cultures to facilitate fluorescent confocal microscopy, and subjected these slices to transient oxygen/glucose deprivation (OGD) that causes delayed excitotoxic death of CA1 pyramidal neurons. This insult caused a delayed loss of mitochondria from astrocytic processes and increased co-localization of mitochondria with the autophagosome marker LC3B. The losses of neurons in CA1 and mitochondria in astrocytic processes were blocked by iGluR antagonists, tetrodotoxin, ziconotide (Ca^{2+} channel blocker), two inhibitors of reversed Na^{+}/Ca^{2+} exchange (KB-R7943, YM-244769), or two inhibitors of calcineurin (cyclosporin-A, FK506). The effects of OGD were mimicked by NMDA. The glutamate uptake inhibitor (3S)-3-[[3-[[4-(trifluoromethyl)benzoyl]amino]phenyl]methoxy]-L-aspartate (TFB-TBOA) increased neuronal loss after OGD or NMDA, and blocked the loss of astrocytic mitochondria. Exogenous glutamate in the presence of iGluR antagonists caused a loss of mitochondria without a decrease in neurons in area CA1. Using the genetic Ca^{2+} indicator Lck-GCaMP-6S, we observed two types of Ca^{2+} signals: 1) in the cytoplasm surrounding mitochondria ('mitochondrially-centered') and 2) traversing the space between mitochondria ('extra-mitochondrial'). The spatial spread, kinetics, and frequency of these events were different. The amplitude of both types was doubled and the spread of both types changed by ~2-fold 24 hrs after OGD. Together, these data suggest that pathologic activation of glutamate transport and increased astrocytic Ca^{2+} through reversed Na^{+}/Ca^{2+} exchange triggers mitochondrial loss and dramatic increases in Ca^{2+} signaling in astrocytic processes.

Significance Statement

Astrocytes, the most abundant cell type in the brain, are vital integrators of signaling and metabolism. Each astrocyte consists of many long, thin branches, called processes, that ensheathe vasculature and thousands of synapses. The majority of each process is occupied by mitochondria. This occupancy is decreased by approximately 50% 24 hrs after an *in vitro* model of ischemia/reperfusion injury, due to delayed fragmentation and mitophagy. The mechanism appears to be independent of neuropathology, instead involving an extended period of high glutamate uptake into astrocytes. Our data suggest that mitochondria serve as spatial buffers, and possibly even a source of calcium signals in astrocytic processes. Loss of mitochondria resulted in drastically altered calcium signaling that could disrupt neurovascular coupling and gliotransmission.

4.1 Introduction

Recent studies have shown that mitochondria are found throughout the fine processes of astrocytes (Lovatt et al., 2007; Genda et al., 2011; Lavialle et al., 2011; Jackson et al., 2014; Derouiche et al., 2015; Jackson and Robinson, 2015; Stephen et al., 2015; for review, see Robinson and Jackson, 2016). As is observed in neurons and other cells, positioning of mitochondria reflects local energy demands and ion buffering (for reviews, see Frederick and Shaw, 2007; Sheng and Cai, 2012; Schwarz, 2013). Neuronal activity and Ca^{2+} influx immobilize mitochondria in astrocytic processes near clusters of the glutamate transporter GLT-1 that appose synapses (Jackson et al., 2014; Stephen et al., 2015). Immobilization is facilitated by Ca^{2+} binding to motor adaptor proteins (Miro1 and Miro2), and mitochondria shape Ca^{2+} signals in astrocytic processes (Jackson and Robinson, 2015; Stephen et al., 2015).

Cerebral ischemia/reperfusion (I/R) injury, as occurs with traumatic brain injury, cardiac arrest, or stroke, is followed by a delayed period of secondary pathology that is self-propagating and progressive. It involves excitotoxic and inflammatory mechanisms and can last for weeks after the initial insult (for reviews, see Choi and Rothman, 1990; Lipton, 1999; Borgens and Liu-Snyder, 2012). This secondary pathology is currently untreatable. Although neuron-targeted approaches (e.g. blocking ionotropic glutamate receptors or their downstream effectors) attenuated damage in preclinical models of I/R injury, they failed in clinical trials (Liebeskind and Kasner, 2001; Muir, 2006). Astrocytes are much more resilient to this type of injury and may play an important role in the damage observed (for reviews, see Chen and Swanson, 2003; Rossi et al., 2007; Barreto et al., 2011). In fact, targeting the SNARE pathway, stimulating purinergic receptors, or manipulating microRNAs in astrocytes all reduce damage in models of stroke (Hines and Haydon, 2013; Zheng et al., 2013; Ouyang et al., 2014).

Although astrocytic mitochondria have been studied in the context of I/R injury, previous work focused mainly on the reticular mitochondria found in cell bodies of dissociated astrocytic cultures (Bambrick et al., 2004; Dugan and Kim-Han, 2004; Ouyang et al., 2011, 2012a). Few studies have focused on mitochondria in the fine astrocytic processes or their role in disease. One such study using electron microscopy in cortical sections after middle cerebral artery occlusion in gerbils reported signs of degenerated astrocytic processes and mitochondria near the infarct, correlating with the progression of neuropathology (Ito et al., 2009). More recently, a study utilizing cortical stab wound in mice revealed transient, inflammation-induced fragmentation of mitochondria in the processes of astrocytes adjacent to the injury site. Recovery of mitochondrial fission/fusion balance required mitophagy (Motori et al., 2013).

Here we present the first evidence that transient oxygen/glucose deprivation (OGD) results in delayed fragmentation and autophagic degradation of mitochondria in astrocytic processes. These effects are blocked by ionotropic glutamate receptor antagonists, by inhibitors of action potential propagation, vesicular neurotransmitter release, glutamate transport, or reversal of Na+/Ca2+ exchangers, and by two different molecules that prevent Ca^{2+}-induced mitochondrial depolarization in astrocytes. The effects of OGD are mimicked by NMDA. The effects on astrocytic mitochondria are also mimicked by exogenous glutamate in the presence of iGluR antagonists that block any glutamate-induced loss of CA1 neurons. We also demonstrate that spontaneous cytosolic Ca^{2+} signaling is dramatically increased 24 hrs after this transient insult. This loss of mitochondria and increase in Ca^{2+} signaling likely alters various astrocytic functions including glutamate metabolism, gliotransmitter release, and neurovascular coupling, all of which are important during recovery after I/R.

4.2 Materials and Methods

cDNA constructs. We have used Mito-EGFP, gfap-gap43-mcherry, gfap-DsRed2-mito, and Lck-GCaMP-6S that are described in previous publications (Jackson et al., 2014; Jackson and Robinson, 2015). Mito-EGFP (also called pEGFP-mito; a gift from Dr. Stanley Thayer, University of Minnesota, Minneapolis) is a fusion of the mitochondrial matrix targeting sequence from CoxVIII with EGFP, and has been shown to result in specific targeting of EGFP into mitochondria (Rizzuto et al., 1993; Wang et al., 2003). gfap-gap43-mcherry (also called pTY-Gfa_{ABC1D}-gap43mCherry) was generated by insertion of the membrane-targeting palmitoylation sequence of gap43 into pTYGfa_{ABC1D}-mCherry (a gift from Dr. John Wolfe, University of Pennsylvania). gfap-DsRed2-mito (also called pGFA_{ABC1D}:DsRed2mito) was generated by replacing the CMV promoter of pDsRed2-mito (Clontech, Cat# 632421) with the minimal GFAP promoter (GFA_{ABC1D}) from gfap-gap43-mcherry. Lck-GCaMP-6S was generated by transferring the Lck-derived membrane-tethering domain from Lck-GCaMP-5G (a gift from Baljit Khakh; Addgene plasmid # 34924; Akerboom et al., 2012) in-frame with GCaMP-6s (a gift from Douglas Kim; Addgene plasmid # 40753; Chen et al., 2013). EGFP-LC3B (also called pEGFP-LC3; human) was obtained from Addgene (plasmid # 24920) and was originally a gift from Toren Finkel (Lee et al., 2008).

Reagents. Bafilomycin A1 (BfA) from *Streptomyces griseus* (Cat# B1793), FK-506 monohydrate (Cat# F4679), ziconotide (ω-conotoxin MVIIA; Cat# C1182), and L-glutamic acid (Cat# G1251) were purchased from Sigma-Aldrich. Tetrodotoxin (TTX) was purchased from Alomone Labs (Cat# T-550). Cyclosporin A (CsA; Cat# 1101), (5S,10R)-(+)-5-Methyl-10,11-dihydro-5H-dibenzo[a,d]cyclohepten-5,10-imine maleate (MK801; Cat# 0924), 2,3-Dioxo-6-nitro-1,2,3,4-tetrahydrobenzo[f]quinoxaline-7-sulfonamide disodium salt (NBQX; Cat# 1044), N-Methyl-D-aspartic acid (NMDA; Cat#

0114), (3S)-3-[[3-[[4-(Trifluoromethyl)benzoyl]amino]phenyl]methoxy]-L-aspartic acid (TFB-TBOA; Cat# 2532), 2-[2-[4-(4-Nitrobenzyloxy)phenyl]ethyl]isothiourea mesylate (KB-R7943; Cat# 1244), and *N*-[(3-Aminophenyl)methyl]-6-[4-[(3-fluorophenyl)methoxy]phenoxy]-3-pyridinecarboxamide dihydrochloride (YM-244769; Cat# 4544) were purchased from Tocris Bioscience.

Hippocampal slice cultures and biolistic transfection. Organotypic hippocampal slices were cultured based on the method of Stoppini et al., 1991, as previously described (Genda et al., 2011a; Jackson et al., 2014). Following decapitation of rat pups (p6-8) of either sex, brains were removed and immediately placed in ice-cold sucrose-supplemented artificial cerebrospinal fluid (ACSF) containing (in mM): 280 sucrose, 5 KCl, 2 $MgCl_2$, 1 $CaCl_2$, 20 glucose, and 10 HEPES, at a pH of 7.3. Hippocampi were dissected on ice and cut into coronal sections 300 µm thick using a Mcilwain tissue chopper. Slices were then transferred onto Millicell membrane inserts (EMD Millipore, Cat# PICM0RG50) in six-well plates atop 1 ml of media consisting of 50% Neurobasal medium (containing 25 mM glucose and 10 mM HEPES; Gibco, Cat# 21103-049), 25% horse serum, 25% HBSS, supplemented with 10 mM HEPES, 36 mM glucose, 2 mM glutamine, 10 U/ml penicillin, 100 µg/ml streptomycin, and Gem21 Neuroplex (1:50 dilution from 50x stock; Gemini, Cat# 400-160), at a pH of 7.3. Slice cultures were maintained in an incubator at 37°C with 5% CO_2.

At 2 DIV, slices were fed (350 µl of media was replaced with 350 µl of fresh media), and biolistically transfected with cDNAs encoding fluorophores relevant to each experiment. Biolistic transfection was performed as described previously (Genda et al., 2011a; Jackson et al., 2014) using the Helios Gene Gun System (Bio-Rad, Cat# 1652431; a generous gift from Dr. Rita Balice-Gordon), in which compressed helium fires cDNA-coated gold particles into slices, resulting in a sparse transfection pattern

ideal for imaging individual cells in a slice culture. Using 1 µm diameter gold particles results in preferential transfection of astrocytes (Benediktsson et al., 2005; Genda et al., 2011a), and additional astrocyte selectivity was achieved by including one construct driven by a minimal gfap promoter in each experiment (de Leeuw et al., 2006). At 4 DIV, inserts were transferred to 1 ml "serum-free" media consisting of Neurobasal-A medium (containing 25 mM glucose and 10 mM HEPES; Gibco, Cat# 10888-022) supplemented with 2 mM GlutaMAX (Gibco, Cat# 35050-061), 10 U/ml penicillin, 100 µg/ml streptomycin, and Gem21 Neuroplex, at a pH of 7.3. Slice cultures were maintained in an incubator at 37°C with 5% CO_2, and fed every other day (350 µl of media replaced). Experiments were performed at 14-18 DIV, when synapse formation and NMDAR subunit expression have reached a developmental stage sufficient to sensitize the slice to excitotoxic injury (Ahlgren et al., 2011), and several weeks before the emergence of spontaneous epileptiform activity (Albus et al., 2013).

Oxygen/glucose deprivation (OGD) injury. Two to four days before each experiment, slice cultures were screened on a Nikon Eclipse TS100 microscope by brightfield transmission for vitality (Trumbeckaite et al., 2013) and epifluorescence for transfection quality. Several criteria were used to exclude slices, including a lack of clear cell body layers containing dentate granule cells or pyramidal cells, darkening of area CA1, discrete areas of cell loss, disconnection between layers of hippocampus, or an insufficient number of transfected astrocytes in stratum radiatum. Variable spreading of slice cultures was observed during the 14-18 DIV, therefore cultures were randomly assigned to different groups. One day before each experiment, serum-free OGD media with no pyruvate and equimolar replacement of glucose with non-metabolizable 2-deoxyglucose (specialty Neurobasal-A medium (no glucose, no pyruvate, 10 mM HEPES; Gibco, Cat# A24775-01) supplemented with 25 mM 2-deoxyglucose, 2 mM

GlutaMAX (Gibco, Cat# 35050-061), 10 U/ml penicillin, 100 µg/ml streptomycin, and Gem21 Neuroplex, at a pH of 7.3) was distributed onto six-well plates (4 ml / well) and placed in a modular hypoxia chamber (Billups-Rothenberg Inc.; Cat# MIC-101). The chamber/media was pre-equilibrated with 95% N_2 / 5% CO_2 at 37°C overnight.

On the day of the experiment, all slices were rinsed and then pre-equilibrated in an incubator at 37^o C and 5% CO_2 for 30 min in fresh serum free media containing glucose ± drugs. Drug treatment concentrations were as follows: BfA (50 nM), MK801 (10 µM), NBQX (20 µM), TFB-TBOA (3 µM), TTX (1 µM), Ziconotide (0.5 µM), KB-R7943 (15 µM), YM-244769 (1 µM), CsA (10 µM), FK506 (10 µM). These slices were then rinsed in either OGD or glucose-containing media ± drug(s). Some slices were moved back to the media used for pre-equilibration (controls). The remainder of the slices were submerged in OGD media (4 mL) ± drug and placed in the hypoxia chamber which was charged with 95% N_2 / 5% CO_2 for 5 min at 2 psi, sealed, and placed at 37°C for 30 min. Slices treated with NMDA were submerged in glucose-containing media with 10 or 100 µM NMDA and returned to the culture incubator for 30 min. Slices were submerged in glucose-containing media with iGluR antagonists (10 µM MK801 + 20 µM NBQX) in the presence or absence of 1 mM L-glutamate for different periods of time in an incubator. After the insult (OGD, NMDA, or glutamate), the slices were rinsed twice in serum free media containing glucose ± drugs and then returned to the media used for pre-equilibration. They were then maintained in an incubator at 37^o C and 5% CO_2 for up to 24 hrs. For experiments involving fixation, slices were rinsed in PBS, submerged in 4% paraformaldehyde in PBS for 10 min, rinsed again in PBS, and then stored in PBS in the dark at 4°C. Slices were cut out and mounted on slides with the transwell membrane against the slide and the slice against coverslip using Vectashield Antifade Mounting Medium with DAPI (Vector Laboratories; Cat# H-1200).

Fixed imaging and analyses. All images were acquired using an Olympus Fluoview 1000 laser scanning confocal microscope equipped with 10x and 40x UPlanApo objectives (numerical aperture 0.4 and 1.3, respectively). All images were processed and analyzed using freely available FIJI/ImageJ software (Schindelin et al., 2012).

DAPI image stacks were acquired from area CA1 using the 10x objective and 405 nm laser for the entire thickness of the stained slice with a 5 µm step size and 512 x 512 pixels/section. Image processing consisted of automated background subtraction (rolling ball algorithm, 50 pixel radius), maximum z-projection, and conversion to binary masks. After processing, images were copied and assigned randomized numeric filenames for blinded analysis. DAPI area in the neuronal cell body layer of CA1, stratum pyramidale, was quantified using a standardized rectangular region of interest (ROI), displayed in Fig. 4.1A and B. All groups were included in at least 3 experiments, with slice cultures prepared from at least 3 separate animals. Each slice was considered an n of 1 (2-4 slices/group/experiment).

Images of mitochondrially-targeted EGFP (mito-EGFP) and minimal-gfap-promoter-driven, plasma-membrane-targeted mcherry (gfap-gap43-mcherry) were acquired from stratum radiatum and pyramidale in area CA1 using the 40x objective with 488 and 546 nm lasers, respectively. Obviously hypertrophic astrocytes were rarely observed during the 24 hrs after insult, and were therefore excluded to avoid confounding the analysis by sampling a heterogeneous population. Image stacks spanned the depth of each astrocyte with a step size of 1 µm, at 800 x 800 pixels/section. Image processing of both channels consisted of automated background subtraction and maximum z-projection, and the mitochondrial channel was converted to a binary mask for cleaner quantification of length and number. After processing, images

were copied and assigned randomized numeric filenames for blinded analysis. Channels from the same image received the same randomized numeric filename along with a channel identifier. Linear ROIs were traced along three separate processes from distal tip, back through tertiary and secondary branches, and through the primary process to the edge of the soma in the plasma membrane channel (gfap-gap43-mcherry). These ROIs were then transferred to the mitochondrial channel (mito-EGFP), where they were used to measure the length of the process, the number of mitochondria, and the lengths of the mitochondria. These values were used to calculate the mean number of mitochondria, length of mitochondria, and % occupancy (% of the process occupied by mitochondria) for each astrocyte. All groups were included in at least 3 experiments, with slice cultures prepared from at least 3 separate animals. Each slice was considered an n of 1 (2-4 slices/group/experiment, 2 astrocytes/slice, 3 processes/astrocyte).

The microtubule-associated protein LC3B is incorporated into autophagosomes during their formation, and as such it is a widely used marker for these structures (Tanida et al., 2008; Maday et al., 2012). Slices were treated with BfA to inhibit lysosomal maturation and allow for detection of cumulative mitophagy in fixed slices 9 and 24 hrs after OGD (for review see Dröse and Altendorf, 1997). Images of EGFP-tagged LC3B (EGFP-LC3B) and minimal-gfap-promoter-driven, mitochondrially-targeted DsRed2 (gfap-DsRed2-mito) were acquired from area CA1 using the 40x objective with 488 and 546 nm lasers, respectively. Hypertrophic reactive astrocytes were avoided. Image stacks spanned the depth of each astrocyte with a step size of 1 µm, at 800 x 800 pixels/section. Exogenous EGFP-LC3B expression appeared as a bimodal signal due to a diffuse, low intensity, cytosolic fluorescence, and the higher intensity, punctate fluorescence from autophagosomes. To filter out the diffuse cytosolic signal, FIJI's

"Minimum" thresholding method was used to generate binary masks for the LC3B channel (EGFP-LC3B). The mitochondrial channel (gfap-DsRed2-mito) was converted to a binary mask using the "default" thresholding method. The "Analyze Particles" function was then used for each channel to filter out particles smaller than 0.1 μm^2. The "AND" function of the Image Calculator was used to create a new z-stack containing only the points in each z plane that were occupied by both mitochondria and LC3B. Analyze Particles was then used to measure the surface area of the particles in each plane of the new colocalization z-stack, as well as the mitochondrial z-stack. By measuring colocalization area in each plane, we avoid false positives from particles that are close in the x/y dimension, but separated by several µm in the z dimension. Colocalization area was normalized to total mitochondrial area in each plane, and mean values from all planes were calculated for each astrocyte. All groups were included in at least 3 experiments, with slice cultures prepared from at least 3 separate animals. Each slice was considered an n of 1 (2-4 slices/group/experiment, 2 astrocytes/slice).

Live calcium imaging. Live recordings of the plasma-membrane-targeted genetic calcium sensor Lck-GCaMP-6S and minimal-gfap-promoter-driven, mitochondrially-targeted DsRed2 (gfap-DsRed2-mito) in distal astrocytic processes were acquired using the 40x objective (and 4-5x digital zoom) with 488 and 546 nm lasers, respectively. Hypertrophic reactive astrocytes were avoided. Twenty-four hours after injury, slices were excised from membrane inserts with a scalpel and placed face-down on a coverslip at the bottom of a flow-through chamber in the microscope stage. The slice was submerged in ACSF (in mM: 130 NaCl, 3 KCl, 1.25 NaH_2PO_4, 26 $NaHCO_3$, 10 glucose, 1 $MgCl_2$, 2 $CaCl_2$; pH 7.3), constantly bubbled with 95%O_2 / 5%CO_2 and heated to 35°C, and continuously flowing at 1-2 ml/min. Ten minute recordings were acquired from a single z-plane at 512 x 512 pixels/frame with a digital zoom (4-5x) sufficient to achieve a

sampling rate of 1 Hz. Recordings were excluded from analysis if the process drifted out of frame or out of the z-plane. In FIJI, automated background and noise (despeckle median filter) subtraction were performed for each channel of the image time-stack, and then the channels were merged to perform rigid alignment (StackReg plugin) to correct for lateral drift during the recording period. After alignment, channels were split again, and copies of the files were assigned randomized numeric filenames for blinded analysis. An ROI was traced along the process using the segmented line tool, and the "Stack Profile Data" plugin (Ver. 1.0, 24-Sep-2010, Michael Schmid) was used to generate an Excel table of intensity values for each pixel along the ROI, with each frame as a column. Each pixel was then converted to ΔF/F0 to generate a new table by first subtracting and then dividing by the mean of all pixels throughout the recording (F0). Conversion to ΔF/F0 helps to isolate signal and allow comparison between separate recordings in which raw fluorescence intensities can vary greatly. Spatial zones of activity, defined as areas in which ΔF/F0 was >0, were identified. Spikes were identified within zones of activity as spans of time in which the ΔF/F0 was greater than the mean ΔF/F0 minus the standard deviation within that zone of activity. In zones of activity containing large-spread extra-mitochondrial spikes overlapping smaller mitochondrially-centered Ca^{2+} events, the extra-mitochondrial spikes were isolated by only including times at which the spread was greater than one standard deviation above the mean.

Mean values for ΔF/F0, spread (μm), duration (sec), and frequency (spikes/min) were calculated for each zone of activity. Zones of activity were classified as either mitochondrially-centered (overlapping and contacting only one mitochondrion) or extra-mitochondrial (traversing extra-mitochondrial space, and contacting two or more mitochondria), and means were calculated for each category for each recording. A single process from each slice was examined and considered an n of 1. Recordings

were acquired on four separate days and from slices prepared from at least four separate animals for each group.

Statistical analyses. Values reported in the Results section are mean ± SEM, unless otherwise noted. All statistical analyses were performed using Graph Pad Prism 6. Means were compared by Student's t-test for two groups, or one-way ANOVA with Bonferroni correction for multiple comparisons when comparing more than two groups. To test for assumptions of normality and equal variance we used the Kolmogorov-Smirnov and Brown-Forsythe tests, respectively. Data from one control slice (Fig. 4.6) were excluded because high mito-EGFP expression masked small spaces between mitochondria, leading to mitochondrial lengths greater than two standard deviations above the mean. To test for differences between the likelihoods of extra-mitochondrial spikes being confined between two mitochondria, contingency tables were constructed and pairs of groups were compared by Fisher's exact test, with Bonferroni correction applied to calculated p values. Fluorescence traces (Fig. 4.8A, B) were constructed in Origin software (Microcal) for display purposes only.

4.3 Results

Astrocytes in organotypic hippocampal slice cultures maintain the highly branched morphologies that are observed *in vivo* (Benediktsson et al., 2005). Using this system, we and others have shown that mitochondria are found throughout processes, ~20 to 40% are mobile, they are immobilized near clusters of GLT1 and synapses, and they shape Ca^{2+} signaling (Jackson et al., 2014; Jackson and Robinson, 2015; Stephen et al., 2015). These slice cultures are also widely used to study secondary pathology after global I/R injury by utilizing transient oxygen/glucose deprivation (OGD) (Bonde et

al., 2005; Noraberg et al., 2005; Ahlgren et al., 2011). To date the effects of OGD on mitochondria and Ca^{2+} signaling in astrocytic processes have not been examined. We biolistically transfected astrocytes with fluorescent markers to achieve sparse labeling that is ideal for imaging individual astrocytes and their processes. In previous studies, we used slices that were maintained in culture for only four days. In the present study, the slices were maintained in culture for two weeks to develop sensitivity to excitotoxic insults (Ahlgren et al., 2011).

Astrocytes were transfected with mitochondrially-targeted EGFP (Rizzuto et al., 1995; for review, see Tsien, 1998) and palmitoylated mcherry under the control of the minimal GFAP promoter. Under these conditions, astrocytes can be easily identified (Jackson et al., 2014). These slices were subjected to 30 min of OGD and fixed at various time points for subsequent imaging analysis. Unlike most assays for cell death, the nuclear stain, DAPI, is compatible with paraformaldehyde fixation and its excitation/emission spectra does not interfere with imaging of the fluorophores that are used throughout this study (e.g. EGFP, mcherry, or DsRed2). It allows for quantification of nuclear condensation and cell number to provide accurate measurement of cell death/loss (Bonde et al., 2002; Lei et al., 2008; Rininger et al., 2012; Zhou et al., 2013; Woeffler-Maucler et al., 2014), and is particularly useful in slice cultures containing phagoctytic microglia that can clear away dead cells. As was previously observed, this insult caused a delayed loss of neurons (Fig. 4.1), and this damage was selective for area CA1 (not shown) (Bonde et al., 2005; Noraberg et al., 2005; Ahlgren et al., 2011). Figures 4.1A & B provide representative examples of the effects of transient OGD on DAPI staining in area CA1. There was a significant reduction in cell density at 12, 18 and 24 hrs after OGD in stratum pyramidale, the neuronal cell body layer of CA1 (Fig. 4.1C; Bonferroni corrected $p=0.0350$ for Baseline (BL) vs. 12 hrs, $p<0.0001$ for BL vs. 18

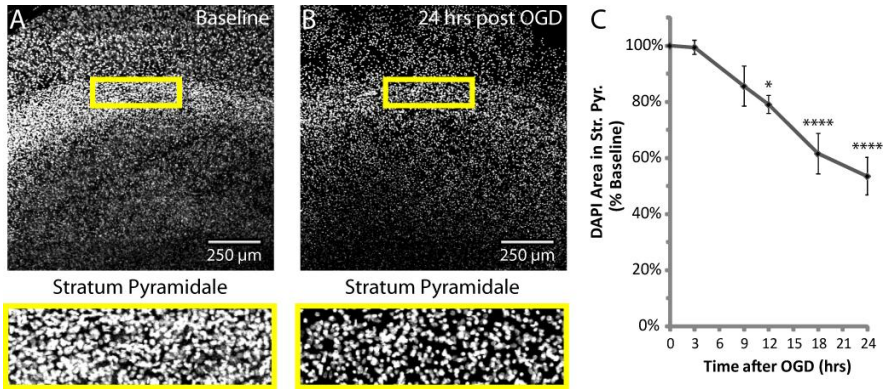

Figure 4.1. 30 min of OGD caused a delayed loss of cells from stratum pyramidale, the neuronal cell body layer of CA1. Hippocampal slice cultures with astrocytes expressing mitochondrially-targeted EGFP and plasma-membrane-targeted mcherry were fixed in 4% paraformaldehyde prior to, as well as 3, 9, 12, 18, and 24 hrs after a 30 min OGD injury, and stained with DAPI in mounting medium. Representative images of DAPI staining in area CA1 at baseline and 24 hrs after OGD, with insets providing magnified views of the neuronal cell body layer, stratum pyramidale (A, B). Mean DAPI area in stratum pyramidale expressed as a percentage of baseline values from each individual experiment (C). All groups were included in at least 3 experiments, with slice cultures prepared from at least 3 separate animals. n=6-12 slices/group (2-4 slices/group/experiment, 2 astrocytes/slice). Error bars indicate SEM. *p<0.05, ****p<0.0001 compared to baseline by one-way ANOVA with Bonferroni correction for multiple comparisons. Mean values for Baseline (no insult / no incubation) and a 24 hr Control group (no insult / 24 hr incubation) were not different (not shown).

or 24 hrs; n=6-12 slices/group). Cell density at 18 hrs was also significantly lower compared to 3 or 9 hrs (Bonferroni corrected p=0.0001 or 0.0281 respectively; n=6-12 slices/group), and at 24 hrs cell density was significantly lower compared to slices fixed 3, 9, or 12 hrs after OGD (Bonferroni corrected p<0.0001, =0.0025, or =0.0396, respectively; n=6-12 slices/group). While optimizing this injury model, we utilized the cell-impermeable nucleic acid dyes propidium iodide or TO-PRO-3 to monitor cell death in CA1, and observed a similar timecourse to that observed with the DAPI method (three independent preliminary experiments; data not shown). These results strongly indicate a delayed, time-dependent loss of CA1 pyramidal cells.

In the DAPI-stained slices, we examined the effects of OGD on mitochondria in the processes of astrocytes in stratum radiatum and pyramidale. As observed by others, we rarely found signs of reactive gliosis within 24 hrs of the insult (Ouyang et al., 2007), and therefore we excluded the few cells that appeared obviously hypertrophic. In control slices (Baseline), there were 5.1 ± 0.3 mitochondria per 50 µm with an average length of 7.2 ± 0.6 µm, occupying 62.7 ± 1.9 % of each astrocytic process (n=7-15 slices/group;

Fig. 4.2A, D, E, F). These values are higher than what we observed previously (average length ~3 µm and occupancy ~45%), perhaps due to the fact that we utilized younger slice cultures and focused only on distal regions of processes in previous studies (Genda et al., 2011a; Jackson et al., 2014). The numbers of mitochondria, the lengths of the mitochondria, and the occupancy of processes by mitochondria were not significantly different in slices 3 hrs after OGD when compared to baseline. By 9 hrs, the number of mitochondria per 50 µm was increased by ~50% (Bonferroni-corrected $p<0.0001$; n=7-15 slices/group), and the length of mitochondria was decreased by ~50% (Bonferroni-corrected $p=0.0010$; n=7-15 slices/group), but the % of the process occupied by mitochondria (% occupancy) remained unchanged relative to baseline (Fig. 4.2B, D, E, F). The transient increase in the number of mitochondria concurrent with a decrease in the size of mitochondria is frequently referred to as fragmentation; this process generally precedes degradation (for reviews, see Itoh et al., 2013; Lemasters, 2014). The mean length of mitochondria continued to decrease to less than half of the baseline value by 24 hrs (Fig 4.2C, E). The number of mitochondria was no longer significantly higher than baseline after 12 hrs, which is consistent with degradation of fragmented mitochondria. Also consistent with degradation, the mean percentage of process length occupied by mitochondria (referred to as % occupancy) was significantly reduced to 46.5 ± 1.7% 12 hrs post OGD (Bonferroni-corrected $p=0.0002$; n=7-15 slices/group), progressing to approximately half of that observed in controls (34.5 ± 2.6% occupancy) by 24 hrs (Fig. 4.2C, F). Scholl analysis of astrocyte morphology revealed mean ramification index values ranging from 1.2 to 1.8, with no significant differences between time points (one-way ANOVA $p=0.80$; n=4-8 cells per time point), indicating that the complex morphology of astrocytic processes was maintained while mitochondria were lost.

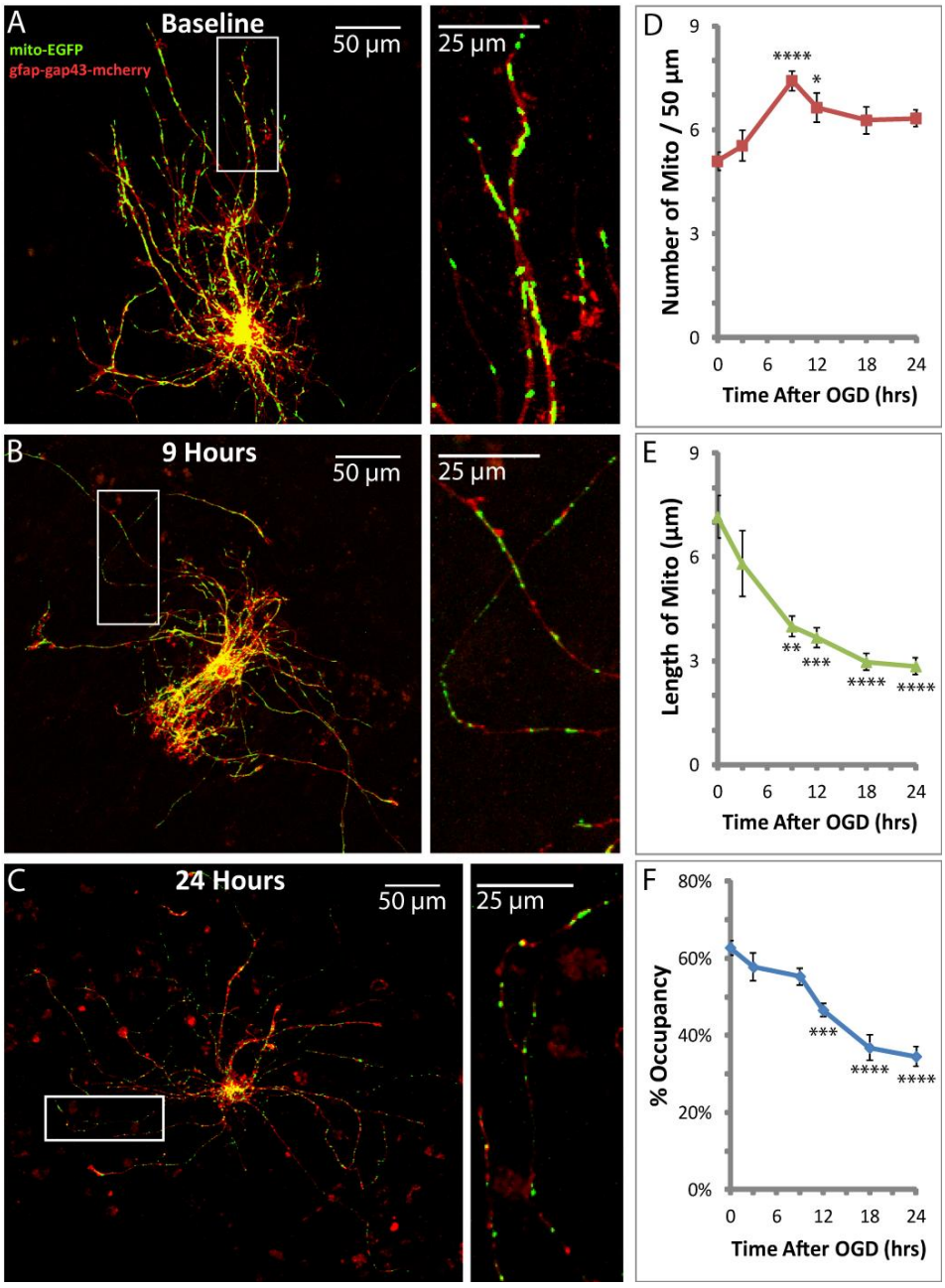

Figure 4.2. 30 min of OGD caused delayed fragmentation and reduced occupancy of mitochondria in astrocytic processes. The same slices used for analyses of DAPI (Fig. 1) were also used to analyze mitochondria in astrocytic processes. Representative images of fluorescently labeled mitochondria (green) and plasma membrane (red) in astrocytes fixed at baseline (A), the onset of mitochondrial fragmentation at 9 hrs (B), and peak mitochondrial loss at 24 hrs after OGD (C). Insets provide magnified views of mitochondria in astrocytic processes. Change in the mean number of mitochondria / 50 µm (D), length of mitochondria in µm (E), and % occupancy of processes by mitochondria (F) during the 24 hr period following 30 min OGD injury. All groups were included in at least 3 experiments, with slice cultures prepared from at least 3 separate animals. n=7-15 slices/group (2-4 slices/group/experiment, 2 astrocytes/slice, 3 processes/astrocyte). Error bars indicate SEM. *p<0.05, **p<0.01, ***p<0.001, ****p<0.0001 compared to baseline by one-way ANOVA with Bonferroni correction for multiple comparisons. Mean values for Baseline (no insult / no incubation) and a 24 hr Control group (no insult / 24 hr incubation) were not different (not shown).

Mitochondria are degraded through a specialized form of autophagy termed mitophagy (Lemasters, 2005). Colocalization of the autophagosome marker LC3B with mitochondria provides a more selective measure of mitophagy compared to assays for overall autophagy (Wong and Holzbaur, 2014). We co-transfected EGFP-tagged LC3B with mitochondrially-targeted DsRed2 to measure colocalization of astrocytic mitochondria and autophagosomes in individual planes of confocal image stacks (40x objective; NA 1.3) (Fig. 4.3). Confocal image stacks of astrocytes containing fluorescently labeled autophagosomes (EGFP-LC3B; green) and mitochondria (gfap-DsRed2-MITO; red) were compressed into two-dimensional images for display purposes (Fig. 4.3A, B). In neurons, autophagosomes form around mitochondria in distal neurite tips, and subsequent lysosomal cargo degradation occurs during retrograde transport to the cell body (Maday et al., 2012). Since mitophagy is a transient process, we used Bafilomycin-A1 (BfA), an inhibitor of the vacuolar H^+-ATPase, to prevent maturation of lysosomes (for review see Dröse and Altendorf, 1997) and allow for accumulation of the mitophagy signal in processes and cell body. In control slices, BfA did not significantly alter astrocytic mitochondria or reduce the density of DAPI-labeled cells for up to 24 hrs. As is observed in neurons (Maday et al., 2012), we observed low levels of LC3B/mitochondria colocalization in astrocytes in control slices, consistent with constitutive low level mitophagy (Figure 4.3C). At 9 hrs post OGD, when there is evidence for mitochondrial fragmentation but preceding a decrease in occupancy (Fig. 4.2D, E, F), there is no evidence for increased co-localization of EGFP-tagged LC3B and mitochondrial DsRed2 (Figure 4.3C). However, at 24 hrs post OGD, when occupancy was decreased to ~50% of control (Fig. 4.2F), we observed a significant accumulation of mitochondria-containing autophagosomes in the cell body and out in processes (Fig. 4.3B, C). This increased signal was not observed in the absence of BfA, providing

evidence that the mitochondria-containing autophagosomes are degraded when lysosomal maturation progresses normally.

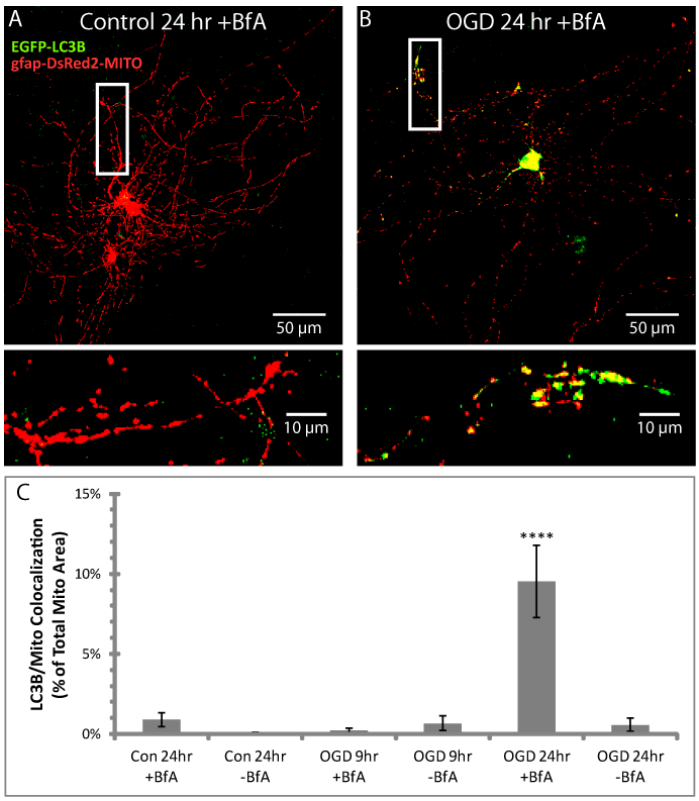

Figure 4.3. 30 min OGD caused delayed degradation of mitochondria by mitophagy. Hippocampal slice cultures with astrocytes expressing autophagosome-targeted EGFP (EGFP-LC3B) and mitochondrially-targeted DsRed2 (gfap-DsRed2-mito) were fixed in 4% paraformaldehyde at 9 or 24 hrs after 30 min OGD or control treatment. Slices were treated 30 min prior to insult, during the 30 min insult, and during the 9 or 24 hr recovery period either with no drug or 50 nM BfA to prevent lysosomal maturation. Representative compressed z-stacks of fluorescently labeled autophagosomes (EGFP-LC3B; green) and mitochondria (gfap-DsRed2-MITO; red) in astrocytes fixed 24 hrs after rinsing with no insult (Control) (A) or OGD (B) in the presence of BfA. Insets provide magnified views of mitochondria in autophagosomes in astrocytic processes. Mean area of autophagosome/mitochondria colocalization normalized to mitochondrial area after OGD or control treatment (C). All groups were included in at least 3 experiments, with slice cultures prepared from at least 3 separate animals. n=6 slices/group (2-4 slices/group/experiment, 2 astrocytes/slice). ****p<0.0001 compared to all other groups by one-way ANOVA with Bonferroni correction for multiple comparisons.

To probe the mechanisms behind this effect on astrocytic mitochondria, we examined the role of ionotropic glutamate receptors (iGluRs; Fig. 4.4). As previously observed, neuronal cell loss was completely blocked by the NMDAR antagonist MK801 (Bonde et al., 2005) (Fig. 4.4A). The protective effect of AMPAR antagonist NBQX was variable, and DAPI staining in stratum pyramidale was not significantly different than in control or OGD groups. Only the combination of both MK801 and NBQX significantly blocked the reduction in mitochondrial length observed after OGD (Fig. 4.4B). Either drug individually attenuated the loss of mitochondria (change in % occupancy), but only the combination of both drugs completely blocked the loss of mitochondria (Fig. 4.4C).

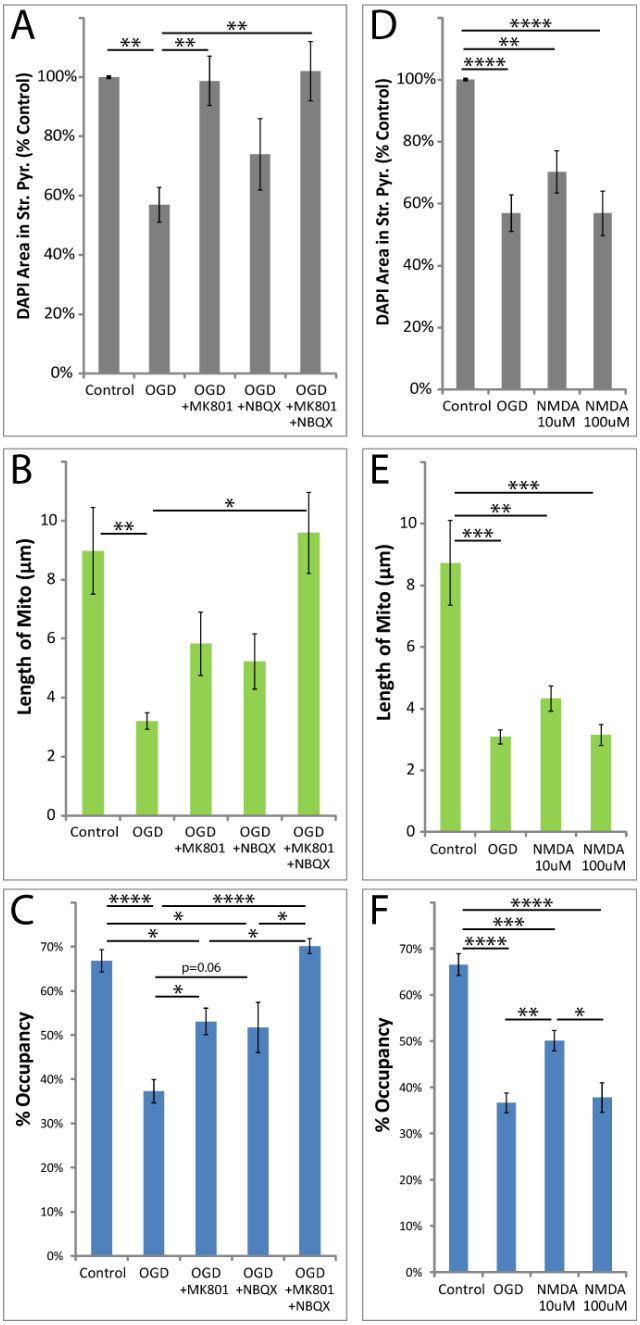

Figure 4.4. MK801 or NBQX blocked, and stimulating NMDARs mimicked the loss of astrocytic mitochondria after OGD. Hippocampal slice cultures with astrocytes expressing mitochondrially-targeted EGFP and plasma-membrane-targeted mcherry were fixed in 4% paraformaldehyde 24 hrs after 30 min OGD, NMDA (10 or 100 µM), or control treatment. OGD slices were treated 30 min prior to insult, during the 30 min insult, and during the 24 hr recovery period either with no drug, 10 µM MK801, 20 µM NBQX, or both MK801 and NBQX. Effects of iGluR antagonists and OGD on mean cell density in stratum pyramidale (A), mitochondrial length in processes (µm; B), and % occupancy of processes by mitochondria (C). Effects of acute NMDA insult on mean cell density in stratum pyramidale (D), mitochondrial length (µm; E), and % occupancy of processes by mitochondria (F). All groups were included in at least 3 experiments, with slice cultures prepared from at least 3 separate animals. n=6-13 slices/group (2-4 slices/group/experiment, 2 astrocytes/slice, 3 processes/astrocyte). Error bars indicate SEM. *p<0.05, **p<0.01, ***p<0.001, ****p<0.0001 compared by one-way ANOVA with Bonferroni correction for multiple comparisons.

Transient NMDA (30 min) caused a loss of DAPI staining comparable to that observed after OGD (Fig. 4.4D). It also mimicked the effects of OGD on astrocytic mitochondria, causing a significant reduction in mitochondrial length and a decrease in mitochondrial occupancy (Fig. 4.4E, F). Together, these studies demonstrate that activation of iGluRs is both necessary and sufficient to induce the delayed loss of astrocytic mitochondria

observed after OGD. These studies suggest that either excessive activation of iGluRs on astrocytes is responsible for the loss of mitochondria or that activation of neuronal iGluRs results in release of one or more substances that subsequently cause a loss of mitochondria in astrocytic processes.

Activation of iGluRs increases glutamate release *in vitro* and *in vivo* (for review, see Mayer and Westbrook, 1987). To further test for the involvement of neuronal glutamate release, we separately blocked action potentials utilizing the voltage-gated Na^+ channel blocker tetrodotoxin (1 µM), or vesicular neurotransmitter release utilizing the N-type Ca^{2+} channel blocker ziconotide (0.5 µM). These drugs block glutamate release and neuronal death after NMDA exposure in similar models of I/R injury, both *in vitro* and *in vivo* (Valentino et al., 1993; Buchan et al., 1994; Dijk et al., 1995; Pringle et al.,

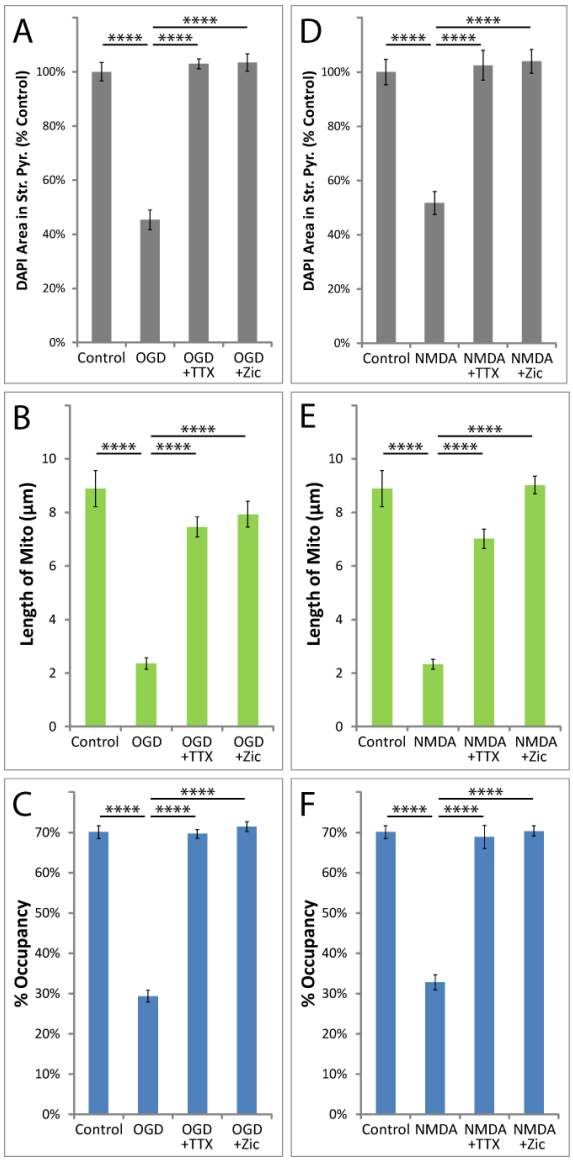

Figure 4.5. TTX or Ziconotide blocked the loss of astrocytic mitochondria after OGD or NMDA injury. Hippocampal slice cultures with astrocytes expressing mitochondrially-targeted EGFP and plasma-membrane-targeted mcherry were fixed in 4% paraformaldehyde 24 hrs after a 30 min OGD, NMDA (100 µM), or control treatment. OGD and NMDA slices were treated 30 min prior to insult, during the 30 min insult, and during the 24 hr recovery period either with no drug, 1 µM TTX, or 0.5 µM Ziconotide. Mean cell density in stratum pyramidale, mitochondrial length in processes (µm), and % occupancy of processes by mitochondria 24 hrs after 30 min OGD (A,B,C) or NMDA (D,E,F) ± TTX or Ziconotide. All groups were included in at least 3 experiments, with slice cultures prepared from at least 3 separate animals. n=8-12 slices/group (2-4 slices/group/experiment, 2 astrocytes/slice, 3 processes/astrocyte). Error bars indicate SEM. ****p<0.0001 compared by one-way ANOVA with Bonferroni correction for multiple comparisons.

1996; Strijbos et al., 1996). We found that they blocked OGD- or NMDA-induced loss of DAPI staining from stratum pyramidale (Fig. 4.5A, D). These drugs also blocked the reduction of mitochondrial size (Fig. 4.5B, E) and occupancy (Fig. 4.5C, F) in astrocytic processes 24 hrs after OGD or exposure to NMDA. These results offer support for the involvement of glutamate-induced glutamate release in the delayed fragmentation and degradation of astrocytic mitochondria observed in this model of I/R injury.

Given that astrocytic glutamate transporter activity regulates mitochondrial mobility in processes (Jackson et al., 2014; Ugbode et al., 2014), we tested the hypothesis that activation of glutamate transport contributes to the loss of mitochondria by blocking transporters with TFB-TBOA. The IC_{50} of TFB-TBOA for iGluRs is >100 µM, and it has no effect on metabotropic glutamate receptors at 100 µM (Shimamoto et al., 2004); at 3 µM it should completely and selectively block glutamate transporter activity. As expected, TFB-TBOA increased the OGD- or NMDA-induced loss of DAPI staining in stratum pyramidale 24 hrs after insult (Fig. 4.6C, F), likely due to increased concentrations of extracellular glutamate. TFB-TBOA also completely blocked the decrease in mitochondrial size and occupancy in astrocytic processes 24 hrs after OGD or NMDA (Fig. 4.6D, E, G, H). These data suggest that OGD induces activation of neuronal iGluRs, triggering neuronal release of glutamate (or other transporter substrates) that is cleared by astroglial glutamate transporters, causing mitochondrial fragmentation and degradation.

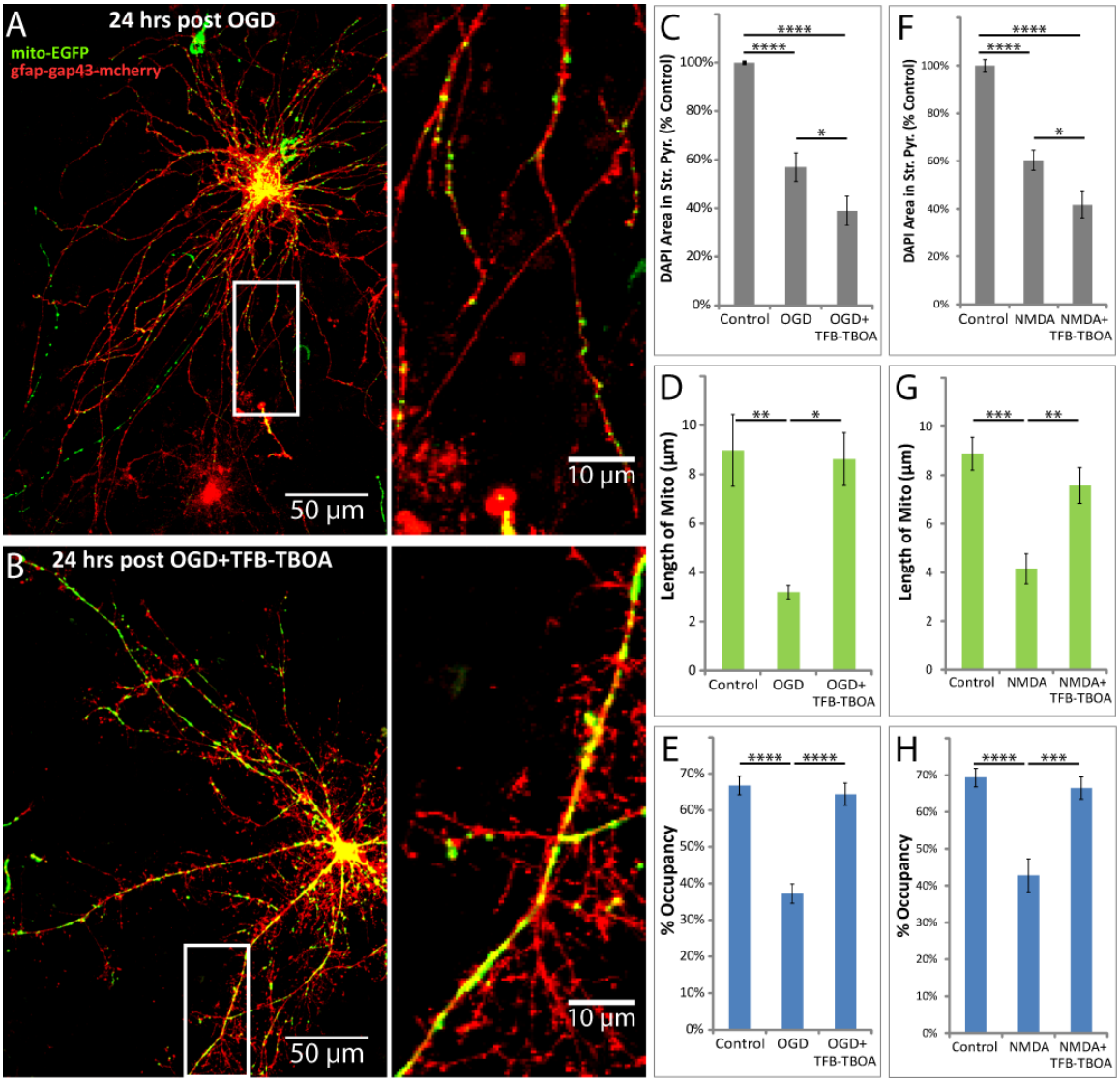

Figure 4.6. TFB-TBOA increased neuronal loss, but blocked the loss of astrocytic mitochondria after OGD or NMDA injury. Hippocampal slice cultures with astrocytes expressing mitochondrially-targeted EGFP (mito-EGFP, green) and plasma-membrane-targeted mcherry (gfap-gap43-mcherry, red) were fixed in 4% paraformaldehyde 24 hrs after a 30 min OGD, NMDA (100 µM), or control treatment. OGD and NMDA slices were treated 30 min prior to insult, during the 30 min insult, and during the 24 hr recovery period either with no drug or 3 µM TFB-TBOA. Representative images of fluorescently labeled mitochondria (green) and plasma membrane (red) in astrocytes fixed 24 hrs after OGD (A) or OGD in the presence of TFB-TBOA (B). Mean cell density in stratum pyramidale, mitochondrial length in processes (µm), and % occupancy of processes by mitochondria 24 hrs after 30 min OGD (C,D,E) or NMDA (F,G,H) insult ± TFB-TBOA. All groups were included in at least 3 experiments, with slice cultures prepared from at least 3 separate animals. n=8-12 slices/group (2-4 slices/group/experiment, 2 astrocytes/slice, 3 processes/astrocyte). Error bars indicate SEM. *p<0.05, **p<0.01, ***p<0.001, ****p<0.0001 compared by one-way ANOVA with Bonferroni correction for multiple comparisons. Insets provide magnified views of mitochondria in astrocytic processes.

To test the hypothesis that increases in extracellular glutamate are sufficient to cause mitochondrial loss in astrocytic processes, we applied glutamate to slices in the presence of MK801 and NBQX to block neuronal death. Although µM glutamate is sufficient to activate iGluRs, robust glutamate uptake prevents glutamate-dependent receptor activation or cell death in slice preparations (Garthwaite, 1985; Vornov et al., 1991). In animal models of I/R injury, extracellular glutamate is elevated for ~2hrs (longer in humans) as measured by microdialysis (Dávalos et al., 1997). Therefore we examined the effects of 1 or 2 hr exposure to 1 mM glutamate in the presence of iGluR antagonists. Control slices were also submerged for 1 or 2 hrs in the presence of MK801 and NBQX. There was no effect of glutamate on DAPI staining in the presence of iGluR antagonists (Fig. 4.7A). In contrast, glutamate caused a significant, time-dependent decrease in mitochondrial length and occupancy 24 hrs after incubation with glutamate (Fig. 4.7B, C). These results demonstrate that exogenous glutamate is sufficient to cause fragmentation and degradation of astrocytic mitochondria in the absence of detectable neuronal pathology.

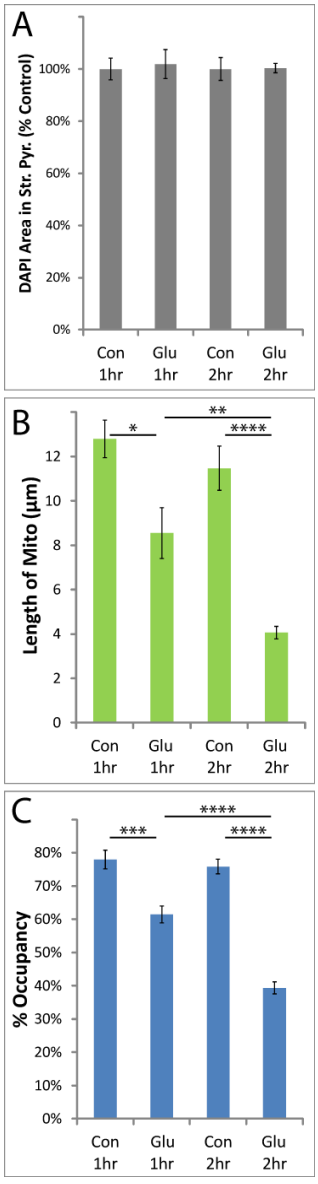

Figure 4.7. Glutamate caused a loss of astrocytic mitochondria in the presence of neuroprotective iGluR antagonists. Hippocampal slice cultures with astrocytes expressing mitochondrially-targeted EGFP and plasma-membrane-targeted mcherry were fixed in 4% paraformaldehyde 24 hrs after a 1 or 2 hr glutamate (1mM) or control treatment. Slices were treated 30 min prior to insult, during the insult, and during the 24 hr recovery period with MK801 (10 µM) + NBQX (20 µM). Mean cell density in stratum pyramidale (A), mitochondrial length in processes (µm; B), and % occupancy of processes (C) by mitochondria 24 hrs after 1 or 2 hr submersion ± glutamate. All groups were included in 4 experiments, with slice cultures prepared from at least 4 separate animals. n=8 slices/group (2-4 slices/group/experiment, 2 astrocytes/slice, 3 processes/astrocyte). Error bars indicate SEM. *p<0.05, **p<0.01, ***p<0.001, ****p<0.0001 compared by one-way ANOVA with Bonferroni correction for multiple comparisons.

Increased glutamate uptake through Na^+-dependent transporters stimulates influx of Ca^{2+} via reversal of the Na^+/Ca^{2+} exchanger (NCX) (Magi et al., 2013b; Rojas et al., 2013; Jackson and Robinson, 2015). High cytosolic Ca^{2+} causes mitochondrial fragmentation, permeability transition, and degradation by mitophagy (for review see Rodriguez-Enriquez et al., 2004). Drugs that selectively inhibit the reverse mode of the NCX (Ca^{2+} influx) are neuroprotective in models of I/R injury *in vitro* and *in vivo* (Schröder et al., 1999; Matsuda et al., 2001; Iwamoto and Kita, 2006). We found that two structurally distinct inhibitors of the reverse-mode of the NCX, KB-R7943 (15 µM) or YM-244769 (1 µM), attenuated the loss of DAPI staining in stratum pyramidale (Fig. 4.8A) as well as the reduction of mitochondrial size (Fig. 4.8B) and occupancy (Fig. 4.8C) in astrocytic processes 24 hrs after OGD. As observed with MK801, these drugs completely blocked the reduction in DAPI staining but only partially blocked the loss of astrocytic mitochondria, suggesting that mitochondrial degradation can occur in the absence of neuronal death.

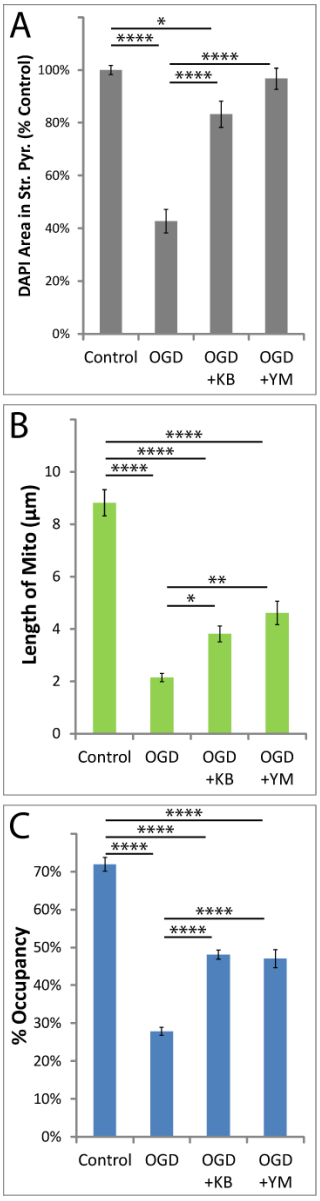

Figure 4.8. KB-R7943 or YM-244769 attenuated the loss of astrocytic mitochondria after OGD or NMDA injury. Hippocampal slice cultures with astrocytes expressing mitochondrially-targeted EGFP and plasma-membrane-targeted mcherry were fixed in 4% paraformaldehyde 24 hrs after a 30 min OGD or control treatment. OGD slices were treated 30 min prior to insult, during the 30 min insult, and during the 24 hr recovery period either with no drug, 15 µM KB-R7943, or 1 µM YM-244769. Mean cell density in stratum pyramidale, mitochondrial length in processes (µm), and % occupancy of processes by mitochondria 24 hrs after 30 min OGD (A,B,C) ± KB-R7943 or YM-244769. All groups were included in at least 3 experiments, with slice cultures prepared from at least 3 separate animals. n=8-12 slices/group (2-4 slices/group/experiment, 2 astrocytes/slice, 3 processes/astrocyte). Error bars indicate SEM. *p<0.05, **p<0.01, ****p<0.0001 compared by one-way ANOVA with Bonferroni correction for multiple comparisons.

Cyclosporin-A (CsA) and FK506 work through different pathways to prevent Ca^{2+}-induced mitochondrial permeability transition and fragmentation, and are neuroprotective in *in vitro* and *in vivo* models of I/R injury (Nakai et al., 1997; Uchino et al., 1998; Li et al., 2000; Yokoyama et al., 2012; Trumbeckaite et al., 2013). Both drugs have been shown to selectively increase Ca^{2+} buffering capacity and prevent Ca^{2+}-induced depolarization of mitochondria in astrocytes, but not in neurons in primary culture (Bambrick et al., 2006; Oliveira and Goncalves, 2008; Kahraman et al., 2011), but at the concentrations used in the present study some effects on neuronal mitochondria could be expected. Each drug blocked the loss of DAPI staining in stratum pyramidale after OGD (Fig. 4.9C). Each of the drugs partially blocked the reduction of mitochondrial size (Fig. 4.9D), and almost entirely blocked loss of mitochondrial occupancy 24 hrs after OGD (Fig. 4.9E). CsA and FK506 exhibit direct neuronal effects, such as inhibition of calcineurin-induced nitric oxide synthase activity, which contribute to their neuroprotective effects in models of I/R injury (Dawson et al., 1993). However, it is unlikely that the neuronal effects of these drugs would reduce astrocytic mitochondrial loss, since inhibition of neuronal calcineurin by CsA has been shown to increase glutamate release (Nichols et al., 1994). Mitochondrial fragmentation precedes degradation, and this process is linked to mitochondrial depolarization (for reviews, see Itoh et al., 2013; Lemasters, 2014). The fact that the loss of mitochondria can be blocked while only attenuating the reduction in size suggests that fragmentation does not necessarily need to progress to degradation.

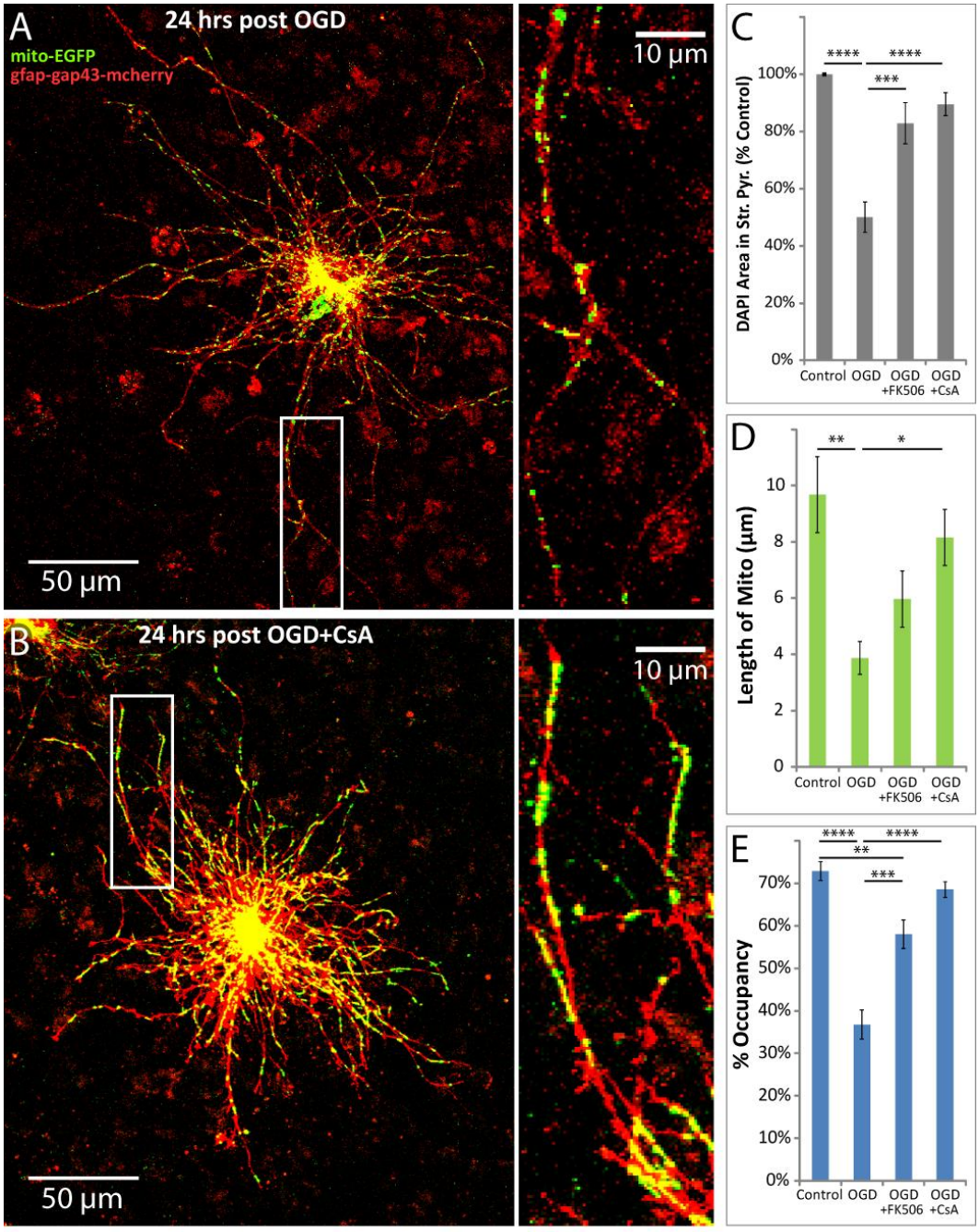

Figure 4.9. CsA or FK506 blocked the loss of astrocytic mitochondria after OGD. Hippocampal slice cultures with astrocytes expressing mitochondrially-targeted EGFP (mito-EGFP, green) and plasma-membrane-targeted mcherry (gfap-gap43-mcherry, red) were fixed in 4% paraformaldehyde 24 hrs after 30 min OGD or control treatmeant. OGD slices were treated 30 min prior to insult, during the 30 min insult, and during the 24 hr recovery period either with no drug, 10 µM CsA, or 10 µM FK506. Representative images of fluorescently labeled mitochondria (green) and plasma membrane (red) in astrocytes fixed 24 hrs after OGD (A) or 24 hrs after OGD in the presence of CsA (B). Insets provide magnified views of mitochondria in astrocytic processes. Effects of CsA or FK506 on mean cell density in stratum pyramidale (C), mitochondrial length in processes (µm; D), and % occupancy of processes by mitochondria (E) 24 hrs after 30 min OGD. All groups were included in at least 3 experiments, with slice cultures prepared from at least 3 separate animals. n=6 slices/group (2 slices/group/experiment, 2 astrocytes/slice, 3 processes/astrocyte). Error bars indicate SEM. *p<0.05, **p<0.01, ***p<0.001, ****p<0.0001 compared by one-way ANOVA with Bonferroni correction for multiple comparisons.

We previously reported that neuronal activity immobilizes astrocytic mitochondria near glutamate transporters and synapses through a mechanism involving glutamate uptake and reversal of the NCX (Jackson et al., 2014). More recently, our lab and others found that this immobilization was dependent on Ca^{2+} binding to motor-adaptor proteins, and that mitochondria shape Ca^{2+} signals in astrocytic processes (Jackson and Robinson, 2015; Stephen et al., 2015). We therefore hypothesized that loss of astrocytic mitochondria would be accompanied by increased Ca^{2+} signaling. For this study, DsRed2-labeled mitochondria were imaged together with spontaneous cytosolic Ca^{2+} signals in astrocytic processes using the high affinity Lck-GCaMP-6s Ca^{2+} sensor (K_d = 144 nM; K_{off} = 1.12 s^{-1}) (Chen et al., 2013).

As was recently reported (Jackson and Robinson, 2015), all of the Ca^{2+} signals observed overlapped with one or more mitochondria. The sensitivity of Lck-GCaMP-6s, along with the presence of a mitochondrial label, revealed a stark anatomical difference between two types of spontaneous Ca^{2+} events that has not been previously described. In addition to the brief, far-reaching Ca^{2+} spikes traversing extra-mitochondrial space that have been previously reported, we also observed a nearly-constant, fluctuating Ca^{2+} signal in the cytosol surrounding individual mitochondria (Fig. 4.10). Mitochondrially-centered events and extra-mitochondrial Ca^{2+} spikes had similar signal amplitudes ($\Delta F/F0$; Fig. 4.10D). However, spread of extra-mitochondrial spikes covered roughly three times the distance of mitochondrially-centered events (Fig. 4.10E). Furthermore, duration and frequency of extra-mitochondrial spikes were much lower than mitochondrially-centered events, at approximately one-third and one-ninth of mitochondrially-centered values, respectively (Fig. 4.10F, G). Duration was used as a measure of kinetics since the dissociation of Ca^{2+} from Lck-GCaMP-6s was too slow for an accurate measurement of decay.

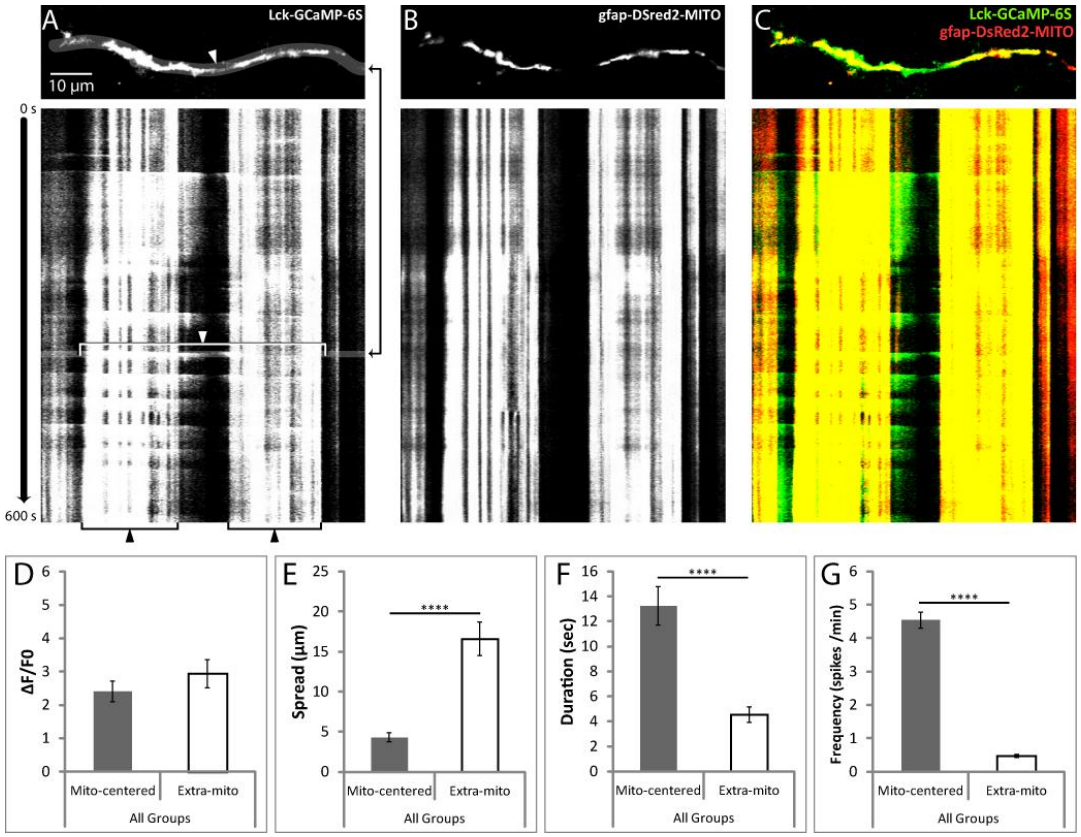

Figure 4.10. Spontaneous cytosolic Ca^{2+} signals were observed surrounding mitochondria or spanning the space between mitochondria with distinct properties. Hippocampal slice cultures with astrocytes expressing a plasma-membrane-targeted Ca^{2+} sensor (Lck-GCaMP-6S, green) and mitochondrially-targeted DsRed2 (gfap-DsRed2-mito, red) were imaged at 1 Hz for 10 min (600 s) in a flow-through chamber 24 hrs after OGD or control treatment to obtain live recordings of Ca^{2+} activity in astrocytic processes. OGD slices were treated 30 min prior to insult, during the 30 min insult, and during the 24 hr recovery period either with no drug or 10 µM CsA, but CsA was not present during live Ca^{2+} imaging. A representative image of a single frame displaying an extra-mitochondrial Ca^{2+} spike (top), and a kymograph displaying both extra-mitochondrial (white arrow and bracket) and mitochondrially-centered (black arrow and bracket) Ca^{2+} signals over time throughout the recording (A). The time at which the representative frame (top) appears in the kymograph is indicated by the black arrows to the right of the image. Corresponding mitochondrial (gfap-DsRed2-MITO) signal (B), and merged Ca^{2+} and mitochondrial signals (C). Comparison of mitochondrially-centered and extra-mitochondrial Ca^{2+} signals by mean intensity (ΔF/F0; D), spread (E), duration (F), and frequency (G). Mitochondrially-centered and extra-mitochondrial Ca^{2+} signals were pooled from Control, OGD, and OGD+CsA groups for this analysis. Means from each recording were considered an n of 1 (mito-centered n=18, extra-mito n=22), and recordings were acquired from 4 separate experiments with slices prepared from at least 4 different animals. Error bars indicate SEM. ****p<0.0001 by one-way ANOVA with Bonferroni correction for multiple comparisons.

We analyzed the effects of OGD on these two types of Ca^{2+} signals. The amplitudes (ΔF/F0) of both signals were more than doubled 24hrs after transient OGD (Fig. 4.11A, B). The frequencies and durations of both events were unchanged (data not shown). The spatial spread of mitochondrially-centered events was decreased to half of that observed in controls 24 hrs after OGD (Fig 4.11C); this correlates with the decrease in mitochondrial length (e.g. Fig 4.2E). The spread of extra-mitochondrial Ca^{2+}

spikes was doubled after OGD (Fig. 4.11D). CsA was used to prevent the loss of astrocytic mitochondria after OGD, but CsA also changes some mitochondria-dependent Ca^{2+} signals (Ichas et al., 1997). To separate the effects of protecting mitochondria from direct effects on Ca^{2+} signaling, CsA was not present during live Ca^{2+} imaging. When we used CsA to prevent the loss of mitochondria in astrocytes after OGD, all effects on ΔF/F0 and spread were completely blocked (Fig. 4.11A-D).

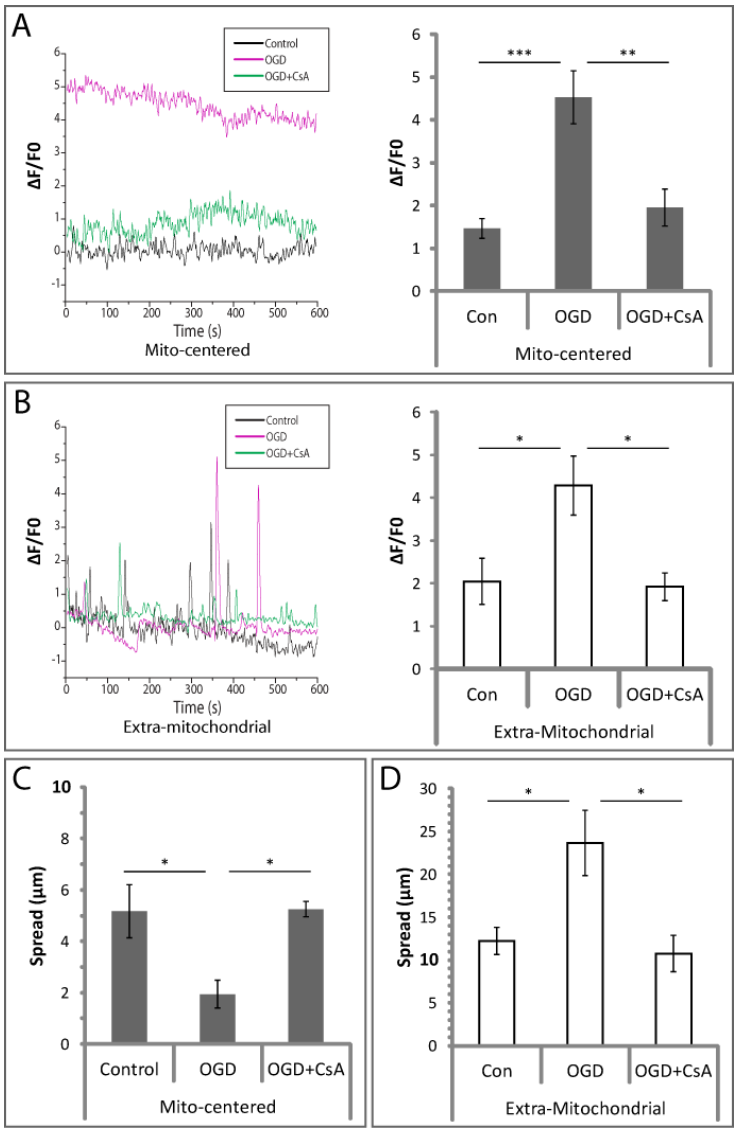

Figure 4.11. Ca^{2+} signal intensity and spread were drastically altered following OGD-induced loss of mitochondria in astrocytic processes. Hippocampal slice cultures with astrocytes expressing a plasma-membrane-targeted Ca^{2+} sensor (Lck-GCaMP-6S) and mitochondrially-targeted DsRed2 (gfap-DsRed2-mito) were imaged at 1 Hz for 10 min (600 s) in a flow-through chamber 24 hrs after OGD or control treatment to obtain live recordings of Ca^{2+} activity in astrocytic processes. OGD slices were treated 30 min prior to insult, during the 30 min insult, and during the 24 hr recovery period either with no drug or 10 μM CsA, but CsA was not present during live Ca^{2+} imaging. Example traces (left) and mean ΔF/F0 values (right), for 24 hr Control, OGD, or OGD+CsA slices, in both mitochondrially-centered (A) and extra-mitochondrial (B) Ca^{2+} signals. Effects of OGD or OGD+CsA on mean spread among mitochondrially-centered fluctuations (C), and extra-mitochondrial spikes (D). Means from each recording were considered an n of 1 (n=5-9 recordings/group), and recordings were acquired from 4 separate experiments with slices prepared from at least 4 different animals. Error bars indicate SEM. *p<0.05, **p<0.01, ***p<0.001 by one-way ANOVA with Bonferroni correction for multiple comparisons.

To further understand the increased spread of extra-mitochondrial Ca^{2+} spikes after OGD, it is helpful to consider Ca^{2+} in the anatomical context of mitochondria (Fig. 4.12). Extra-mitochondrial spikes were observed in 8 of 11 recordings in both control and OGD groups. In control slices, 86% of extra-mitochondrial spikes were contained between two mitochondria (Fig. 4.12A, C). 24 hrs after OGD, none of the extra-mitochondrial spikes were contained between two mitochondria; instead they all traversed multiple mitochondria (Fig. 4.12B, C). Preventing the OGD-induced loss of mitochondria with CsA blocked this effect (Fig. 4.12C).

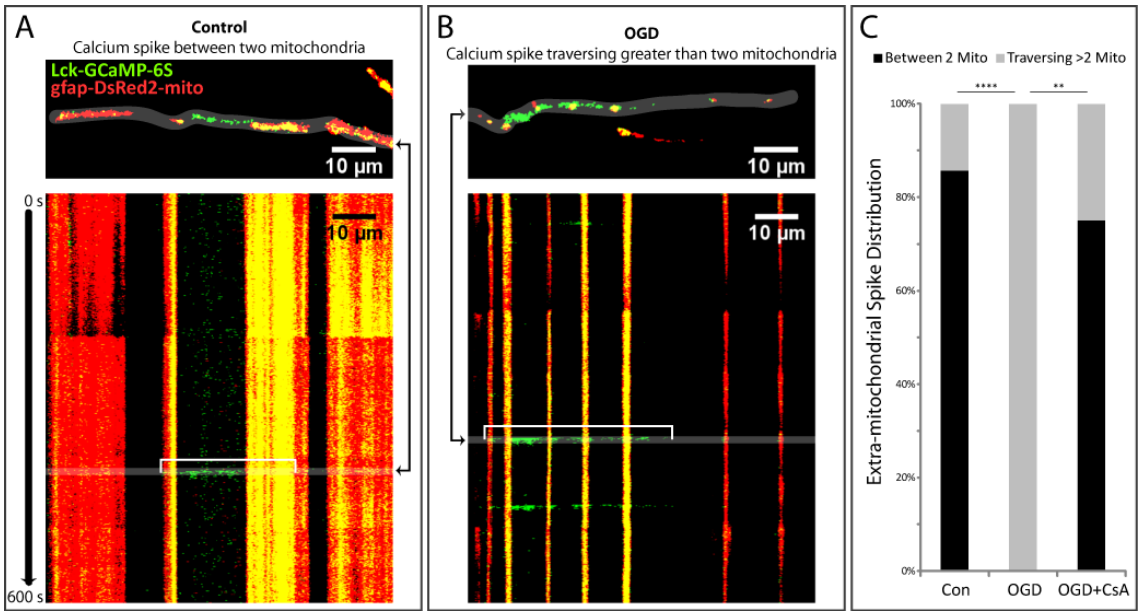

Figure 4.12. Extra-mitochondrial Ca^{2+} spikes were no longer contained between two mitochondria after OGD. Extra-mitochondrial spikes from experiments summarized in Figs. 7 and 8 were analyzed for their anatomic relationship to mitochondria (contained between two mitochondria, or traversing multiple mitochondria). A representative image of a single frame (top) displaying an extra-mitochondrial Ca^{2+} spike (Lck-GCaMP-6S, green) contained between two mitochondria (gfap-DsRed2-mito, red), and a kymograph (bottom) displaying Ca^{2+} and mitochondria over time throughout the recording acquired 24 hrs after control treatment, with the example spike indicated by a white bracket (A). A representative image of a single frame (top) displaying an extra-mitochondrial Ca^{2+} spike (green) traversing greater than two mitochondria (red), and a kymograph (bottom) displaying Ca^{2+} and mitochondria over time throughout the recording acquired 24 hrs after OGD, with the example spike indicated by a white bracket (B). The times at which the representative frames appear in the kymographs are indicated by the black arrows to the side of the image. Distribution of extra-mitochondrial spikes classified into two categories: between two mitochondria or traversing greater than two mitochondria (C). **p<0.01, ****p<0.001 by Fisher's exact test with Bonferroni correction for multiple comparisons.

4.4 Discussion

Mitochondria in astrocytic processes are positioned near glutamate transporters and synapses through a mechanism involving neuronal activity and Ca2+-sensitive motor adaptor proteins. These mitochondria shape Ca2+ signaling (Jackson et al., 2014; Jackson and Robinson, 2015; Stephen et al., 2015). Here we present evidence that the delayed neuronal death observed in area CA1 after transient OGD was accompanied by fragmentation and autophagic degradation of mitochondria in astrocytic processes. The loss of mitochondria was associated with a dramatic increase in spontaneous Ca2+ signals in distal astrocytic processes.

Mechanism of mitochondrial loss

We show that the OGD-induced loss of astrocytic mitochondria is completely blocked by a combination of iGluR antagonists (MK-801 and NBQX), an inhibitor of neuronal action potentials (TTX), an inhibitor of vesicular glutamate release (ziconotide), a glutamate transport inhibitor (TFB-TBOA), or two different inhibitors of calcineurin (CsA or FK506). NMDA or glutamate mimicked the effect of OGD, and the NMDA-induced loss of mitochondria was blocked by TFB-TBOA. The simplest explanation for these data is that OGD triggers an iGluR-dependent increase in extracellular glutamate (or aspartate), activation of astrocytic transporters, and loss of astrocytic mitochondria.

Previous studies have demonstrated that OGD or activation of iGluRs causes an increase in extracellular glutamate (and aspartate) (Bustos et al., 1992; Dijk et al., 1995; Fujimoto et al., 2004; Bonde et al., 2005). During 30 min of OGD, elevated extracellular glutamate is mainly attributed to reversal of neuronal glutamate transporters and some vesicular release (for review, see Rossi et al., 2007). After reperfusion, additional

periods of elevated extracellular glutamate have been observed by *in vivo* microdialysis in CA1, but the source(s) for this glutamate have not been identified (Yang et al., 2001). The fact that inhibitors of neuronal Na^+ channels or the N-type Ca^{2+} channel block the changes in astrocytic mitochondria are consistent with the notion that this glutamate is released from neuronal vesicles.

Glutamate uptake increases intracellular Ca^{2+} through reversed operation of plasma membrane Na^+/Ca^{2+} exchangers, and blocking this reversed mode after OGD attenuated the loss of astrocytic mitochondria (Magi et al., 2013b; Rojas et al., 2013; Jackson and Robinson, 2015). In other systems, coincident increases in Ca^{2+} and reactive oxygen species (ROS) cause mitochondrial swelling, depolarization, fragmentation, opening of the permeability transition pore, and mitophagy (He and Lemasters, 2002; Kim et al., 2012). High mitochondrial Ca^{2+} also activates several TCA cycle dehydrogenases that generate ROS (Denton et al., 1972; for review, see Brookes et al., 2004). Increased oxidation of glutamate itself could contribute to the loss of mitochondria via increased generation of ROS. Glutamate enters the TCA cycle through conversion to α-ketoglutarate (for review, see McKenna, 2013). Conversion of α-ketoglutarate to succinyl CoA by the α-ketoglutarate dehydrogenase complex generates 2- to 3-fold more ROS than the other TCA cycle dehydrogenases (Starkov et al., 2004; Tretter and Adam-Vizi, 2004). However, testing this hypothesis is difficult because inhibiting glutamate dehydrogenase or α-ketoglutarate dehydrogenase inhibits glutamate uptake (Whitelaw and Robinson, 2013, unpublished observations).

Preventing Ca^{2+}-induced mitochondrial depolarization with CsA or FK506 (Bambrick et al., 2006; Oliveira and Goncalves, 2008; Kahraman et al., 2011) likely contributed to the prevention of mitochondrial loss in astrocytes after OGD. However, Ca^{2+}-mediated activation of calcineurin can cause inflammation in astrocytes through

activation of NFAT and NFκB (for review, see Furman and Norris, 2014). The efficacy of CsA and FK506, both calcineurin inhibitors, could imply a role for inflammation in the loss of astrocytic mitochondria after transient OGD, similar to the inflammation-dependent mitophagy observed in astrocytes after cortical stab wound (Motori et al., 2013).

Consequences of mitochondrial loss and insights into Ca^{2+} signaling

We observed two anatomically-distinct, spontaneous Ca^{2+} signals in the cytoplasm of astrocytic processes, one of which has not been previously described. There were constant, fluctuating Ca^{2+} signals surrounding mitochondria, and brief, far-reaching spikes that traversed extra-mitochondrial space. The fact that photo-ablation of individual mitochondria causes a large transient increase in cytoplasmic Ca^{2+} strongly suggests that the mitochondria contain Ca^{2+} (Jackson and Robinson, 2015). Decreased spread of mitochondrially-centered Ca^{2+} signals after OGD correlated with decreased mitochondrial size, implicating mitochondria as the source. With the identification of a localized Ca^{2+} cloud surrounding mitochondria, we suspect that mitochondria may play a role in generating Ca^{2+} spikes in astrocytic processes, as they do in primary culture (Parnis et al., 2013) and other cells (for review, see Rizzuto et al., 2012). While the current study was under review, Jiang et al. described two types of Ca^{2+} signals in astrocytic processes with similar properties to those described in the current study, but without the anatomic relationship to mitochondria (Jiang et al., 2016).

Our lab and others have recently demonstrated that mitochondria shape Ca^{2+} signals in astrocytic processes (Jackson and Robinson, 2015; Stephen et al., 2015). In our recent study, uncoupling oxidative ATP production with FCCP or photo-ablating

mitochondria with KillerRed-mito caused a large increase in cytoplasmic Ca^{2+}. These effects were associated with increased spatial spread, indicating that mitochondria spatially restrict these signals. OGD-induced mitochondrial loss also resulted in increased spread of extra-mitochondrial spikes, and the likelihood of spikes staying confined between two mitochondria went from 86% to zero after OGD. In agreement with observations from recent studies (Jackson and Robinson, 2015; Stephen et al., 2015), this suggests that mitochondria provide spatial restriction for Ca^{2+} signals in astrocytic processes.

A recent study utilizing *in vivo* two-photon imaging in awake mice found that the spread of Ca^{2+} "hotspots" in astrocytic processes increased with sensory stimulation and decreased with tetrodotoxin treatment (Asada et al., 2015). Another study using hippocampal cultures found that activity of local synapses is coordinated by Ca^{2+} signaling in astrocytic processes (Sasaki et al., 2014). Activity-driven positioning of mitochondria at glutamate transporters apposing synapses (Jackson et al., 2014), along with spatial restriction of Ca^{2+} signals by those mitochondria (Jackson and Robinson, 2015; Stephen et al., 2015), could represent a system for coordinating weak signals between neighboring sites of activity, while larger signals are relayed beyond neighboring mitochondria to more distant zones of activity, as was observed in response to sensory stimulation (Asada et al., 2015). Exploring this phenomenon could reveal a new mechanism for integrating local neuronal signaling events via mitochondrially-segmented Ca^{2+} signaling in astrocytic microdomains.

Implications for I/R injury

Following cerebral I/R injury the neurovascular coupling response is depressed in humans, likely impairing recovery (Salinet et al., 2015). Although the mechanisms are not fully understood, astrocytic Ca^{2+} signaling has been implicated in mediating neurovascular coupling (Takano et al., 2006; Dunn et al., 2013; Otsu et al., 2015), which is not surprising given the positioning of astrocytes between synapses and the vasculature, and their reliance on Ca^{2+} for propagating information (for review, see Parpura et al., 2012). In addition to altered neurovascular coupling, Ca^{2+}-induced vesicular glutamate release from astrocytes has been shown to increase excitotoxic damage from seizure and stroke (Ding et al., 2007; Hines and Haydon, 2013; Takemiya and Yamagata, 2013). Increased astrocytic Ca^{2+} signaling with a lower threshold for induction has been observed in *in vitro* and *in vivo* models of I/R (for review, see Ding, 2014), however, none of these studies focused on the period of delayed secondary pathology, or on microdomain Ca^{2+} signaling in the distal astrocytic process. In the current study we provide evidence of dramatically amplified, spatially deregulated Ca^{2+} signaling in astrocytic processes after OGD-induced mitochondrial loss, which could disrupt neurovascular coupling and stimulate vesicular glutamate release from astrocytes during secondary neuronal pathology.

Glutamate metabolism will likely be impaired following the loss of mitochondria. The mitochondrial enzyme glutamate dehydrogenase converts glutamate to α-ketoglutarate for entry into the TCA cycle and generation of ATP (for review, see Dienel, 2013). Glutamate dehydrogenase is enriched (~5 fold) in astrocytes (Zaganas et al., 2001; Zhang et al., 2014), and brain-specific knockouts demonstrate increased glucose deployment from the periphery and utilization in brain to compensate for the loss of glutamate as a fuel source (Karaca et al., 2015). We are currently testing the hypothesis

that the loss of astrocytic mitochondria after OGD will result in a significant reduction of glutamate oxidation, which could impair recovery after I/R injury.

Conclusion

We have presented the first evidence that increased activation of iGluRs, neuronal glutamate release, and glutamate uptake into astrocytes after transient OGD causes a delayed fragmentation and autophagic degradation of mitochondria in astrocytic processes. This effect is associated with a dramatic increase in the amplitude and spread of extra-mitochondrial Ca^{2+} spikes in astrocytic processes. The removal of damaged, dysfunctional mitochondria may be beneficial for astrocyte survival. However, it may also exacerbate neuronal damage, not just through Ca^{2+}-associated effects on neurovascular coupling and glial glutamate release, but also through the loss of astrocytic support of neurons. Astrocytes are more resilient than neurons after I/R injury, so it could be easier to target and correct their less-severe dysfunction, allowing the astrocytes to continue to support and protect neurons (for reviews, see Chen and Swanson, 2003; Rossi et al., 2007; Barreto et al., 2011). Healthy astrocytes providing potassium homeostasis, glutamate clearance, antioxidants, and metabolic support are in a better position to rescue neighboring neurons than any neuronally-targeted therapy.

4.5 References

Ahlgren H, Henjum K, Ottersen OP, Rundén-Pran E (2011) Validation of organotypical hippocampal slice cultures as an ex vivo model of brain ischemia: different roles of NMDA receptors in cell death signalling after exposure to NMDA or oxygen and glucose deprivation. Cell Tissue Res 345:329–341.

Akerboom J et al. (2012) Optimization of a GCaMP calcium indicator for neural activity imaging. J Neurosci 32:13819–13840.

Albus K, Heinemann U, Kovács R (2013) Network activity in hippocampal slice cultures revealed by long-term in vitro recordings. J Neurosci Methods 217:1–8.

Asada A, Ujita S, Nakayama R, Oba S, Ishii S, Matsuki N, Ikegaya Y (2015) Subtle modulation of ongoing calcium dynamics in astrocytic microdomains by sensory inputs. Physiol Rep 3:e12454.

Bambrick L, Kristian T, Fiskum G (2004) Astrocyte Mitochondrial Mechanisms of Ischemic Brain Injury and Neuroprotection. Neurochem Res 29:601–608.

Bambrick LL, Chandrasekaran K, Mehrabian Z, Wright C, Krueger BK, Fiskum G (2006) Cyclosporin a Increases Mitochondrial Calcium Uptake Capacity in Cortical Astrocytes but not Cerebellar Granule Neurons. J Bioenerg Biomembr 38:43–47.

Barreto G, White RE, Ouyang Y, Xu L, Giffard RG (2011) Astrocytes: targets for neuroprotection in stroke. Cent Nerv Syst Agents Med Chem 11:164–173.

Benediktsson AM, Schachtele SJ, Green SH, Dailey ME (2005) Ballistic labeling and dynamic imaging of astrocytes in organotypic hippocampal slice cultures. J Neurosci Methods 141:41–53.

Bonde C, Noraberg J, Noer H, Zimmer J (2005) Ionotropic glutamate receptors and glutamate transporters are involved in necrotic neuronal cell death induced by oxygen-glucose deprivation of hippocampal slice cultures. Neuroscience 136:779–794.

Bonde C, Noraberg J, Zimmer J (2002) Nuclear shrinkage and other markers of neuronal cell death after oxygen-glucose deprivation in rat hippocampal slice cultures. Neurosci Lett 327:49–52.

Borgens RB, Liu-Snyder P (2012) Understanding Secondary Injury. Q Rev Biol 87:89–127.

Brookes PS, Yoon Y, Robotham JL, Anders MW, Sheu S-S (2004) Calcium, ATP, and ROS: a mitochondrial love-hate triangle. Am J Physiol - Cell Physiol 287:C817–C833.

Buchan AM, Gertler SZ, Li H, Xue D, Huang ZG, Chaundy KE, Barnes K, Lesiuk HJ (1994) A selective N-type Ca(2+)-channel blocker prevents CA1 injury 24 h following severe forebrain ischemia and reduces infarction following focal ischemia. J Cereb Blood Flow Metab 14:903–910.

Bustos G, Abarca J, Forray MI, Gysling K, Bradberry CW, Roth RH (1992) Regulation of excitatory amino acid release by N-methyl-d-aspartate receptors in rat striatum: in vivo microdialysis studies. Brain Res 585:105–115.

Chen T-W, Wardill TJ, Sun Y, Pulver SR, Renninger SL, Baohan A, Schreiter ER, Kerr RA, Orger MB, Jayaraman V, Looger LL, Svoboda K, Kim DS (2013)

Ultrasensitive fluorescent proteins for imaging neuronal activity. Nature 499:295–300.

Chen Y, Swanson RA (2003) Astrocytes and Brain Injury. J Cereb Blood Flow Metab 23:137–149.

Choi DW, Rothman SM (1990) The role of glutamate neurotoxicity in hypoxic-ischemic neuronal death. Annu Rev Neurosci 13:171–182.

Dávalos A, Castillo J, Serena J, Noya M (1997) Duration of Glutamate Release After Acute Ischemic Stroke. Stroke 28:708–710.

Dawson TM, Steiner JP, Dawson VL, Dinerman JL, Uhl GR, Snyder SH (1993) Immunosuppressant FK506 enhances phosphorylation of nitric oxide synthase and protects against glutamate neurotoxicity. Proc Natl Acad Sci 90:9808–9812.

de Leeuw B, Su M, Horst M ter, Iwata S, Rodijk M, Hoeben RC, Messing A, Smitt PS, Brenner M (2006) Increased glia-specific transgene expression with glial fibrillary acidic protein promoters containing multiple enhancer elements. J Neurosci Res 83:744–753.

Denton RM, Randle PJ, Martin BR (1972) Stimulation by calcium ions of pyruvate dehydrogenase phosphate phosphatase. Biochem J 128:161–163.

Derouiche A, Haseleu J, Korf H-W (2015) Fine Astrocyte Processes Contain Very Small Mitochondria: Glial Oxidative Capability May Fuel Transmitter Metabolism. Neurochem Res 40:2402–2413.

Dienel GA (2013) Astrocytic energetics during excitatory neurotransmission: What are contributions of glutamate oxidation and glycolysis? Neurochem Int 63:244–258.

Dijk SN, Francis PT, Stratmann GC, Bowen DM (1995) NMDA-induced glutamate and aspartate release from rat cortical pyramidal neurones: evidence for modulation by a 5-HT1A antagonist. Br J Pharmacol 115:1169.

Ding S (2014) Ca2+ Signaling in Astrocytes and its Role in Ischemic Stroke. In: Glutamate and ATP at the Interface of Metabolism and Signaling in the Brain (Parpura V, Schousboe A, Verkhratsky A, eds), pp 189–211. Cham: Springer International Publishing.

Ding S, Fellin T, Zhu Y, Lee S-Y, Auberson YP, Meaney DF, Coulter DA, Carmignoto G, Haydon PG (2007) Enhanced Astrocytic Ca2+ Signals Contribute to Neuronal Excitotoxicity after Status Epilepticus. J Neurosci 27:10674–10684.

Dröse S, Altendorf K (1997) Bafilomycins and concanamycins as inhibitors of V-ATPases and P-ATPases. J Exp Biol 200:1–8.

Dugan LL, Kim-Han J-S (2004) Astrocyte mitochondria in in vitro models of ischemia. J Bioenerg Biomembr 36:317–321.

Dunn KM, Hill-Eubanks DC, Liedtke WB, Nelson MT (2013) TRPV4 channels stimulate Ca2+-induced Ca2+ release in astrocytic endfeet and amplify neurovascular coupling responses. Proc Natl Acad Sci 110:6157–6162.

Frederick RL, Shaw JM (2007) Moving Mitochondria: Establishing Distribution of an Essential Organelle. Traffic 8:1668–1675.

Fujimoto S, Katsuki H, Kume T, Kaneko S, Akaike A (2004) Mechanisms of oxygen glucose deprivation-induced glutamate release from cerebrocortical slice cultures. Neurosci Res 50:179–187.

Furman JL, Norris CM (2014) Calcineurin and glial signaling: neuroinflammation and beyond. J Neuroinflammation 11:158.

Garthwaite J (1985) Cellular uptake disguises action of L-glutamate on N-methyl-D-aspartate receptors. With an appendix: diffusion of transported amino acids into brain slices. Br J Pharmacol 85:297–307.

Genda EN, Jackson JG, Sheldon AL, Locke SF, Greco TM, O'Donnell JC, Spruce LA, Xiao R, Guo W, Putt M, Seeholzer S, Ischiropoulos H, Robinson MB (2011) Co-compartmentalization of the astroglial glutamate transporter, GLT-1, with glycolytic enzymes and mitochondria. J Neurosci 31:18275–18288.

He L, Lemasters JJ (2002) Regulated and unregulated mitochondrial permeability transition pores: a new paradigm of pore structure and function? FEBS Lett 512:1–7.

Hines DJ, Haydon PG (2013) Inhibition of a SNARE-Sensitive Pathway in Astrocytes Attenuates Damage following Stroke. J Neurosci 33:4234–4240.

Ichas F, Jouaville LS, Mazat J-P (1997) Mitochondria Are Excitable Organelles Capable of Generating and Conveying Electrical and Calcium Signals. Cell 89:1145–1153.

Ito U, Hakamata Y, Kawakami E, Oyanagi K (2009) Degeneration of Astrocytic Processes and Their Mitochondria in Cerebral Cortical Regions Peripheral to the Cortical Infarction: Heterogeneity of Their Disintegration Is Closely Associated With Disseminated Selective Neuronal Necrosis and Maturation of Injury. Stroke 40:2173–2181.

Itoh K, Nakamura K, Iijima M, Sesaki H (2013) Mitochondrial dynamics in neurodegeneration. Trends Cell Biol 23:64–71.

Iwamoto T, Kita S (2006) YM-244769, a novel Na+/Ca2+ exchange inhibitor that preferentially inhibits NCX3, efficiently protects against hypoxia/reoxygenation-induced SH-SY5Y neuronal cell damage. Mol Pharmacol 70:2075–2083.

Jackson JG, O'Donnell JC, Takano H, Coulter DA, Robinson MB (2014) Neuronal Activity and Glutamate Uptake Decrease Mitochondrial Mobility in Astrocytes and Position Mitochondria Near Glutamate Transporters. J Neurosci 34:1613–1624.

Jackson JG, Robinson MB (2015) Reciprocal Regulation of Mitochondrial Dynamics and Calcium Signaling in Astrocyte Processes. J Neurosci 35:15199–15213.

Jiang R, Diaz-Castro B, Looger LL, Khakh BS (2016) Dysfunctional Calcium and Glutamate Signaling in Striatal Astrocytes from Huntington's Disease Model Mice. J Neurosci 36:3453–3470.

Kahraman S, Bambrick LL, Fiskum G (2011) Effects of FK506 and cyclosporin a on calcium ionophore-induced mitochondrial depolarization and cytosolic calcium in astrocytes and neurons. J Neurosci Res 89:1973–1978.

Karaca M, Frigerio F, Migrenne S, Martin-Levilain J, Skytt DM, Pajecka K, Martin-del-Rio R, Gruetter R, Tamarit-Rodriguez J, Waagepetersen HS, Magnan C, Maechler P (2015) GDH-Dependent Glutamate Oxidation in the Brain Dictates Peripheral Energy Substrate Distribution. Cell Rep 13:365–375.

Kim J-S, Wang J-H, Lemasters JJ (2012) Mitochondrial permeability transition in rat hepatocytes after anoxia/reoxygenation: role of Ca2+-dependent mitochondrial formation of reactive oxygen species. AJP Gastrointest Liver Physiol 302:G723–G731.

Lavialle M, Aumann G, Anlauf E, Prols F, Arpin M, Derouiche A (2011) Structural plasticity of perisynaptic astrocyte processes involves ezrin and metabotropic glutamate receptors. Proc Natl Acad Sci 108:12915–12919.

Lee IH, Cao L, Mostoslavsky R, Lombard DB, Liu J, Bruns NE, Tsokos M, Alt FW, Finkel T (2008) A role for the NAD-dependent deacetylase Sirt1 in the regulation of autophagy. Proc Natl Acad Sci U S A 105:3374–3379.

Lei Y, Garrahan N, Hermann B, Becker DL, Hernandez MR, Boulton ME, Morgan JE (2008) Quantification of retinal transneuronal degeneration in human glaucoma: a novel multiphoton-DAPI approach. Invest Ophthalmol Vis Sci 49:1940–1945.

Lemasters JJ (2005) Selective Mitochondrial Autophagy, or Mitophagy, as a Targeted Defense Against Oxidative Stress, Mitochondrial Dysfunction, and Aging. Rejuvenation Res 8:3–5.

Lemasters JJ (2014) Variants of mitochondrial autophagy: Types 1 and 2 mitophagy and micromitophagy (Type 3). Redox Biol 2:749–754.

Li PA, Kristián T, He QP, Siesjö BK (2000) Cyclosporin A Enhances Survival, Ameliorates Brain Damage, and Prevents Secondary Mitochondrial Dysfunction after a 30-Minute Period of Transient Cerebral Ischemia. Exp Neurol 165:153–163.

Liebeskind DS, Kasner SE (2001) Neuroprotection for ischaemic stroke: an unattainable goal? CNS Drugs 15:165–174.

Lipton P (1999) Ischemic cell death in brain neurons. Physiol Rev 79:1431–1568.

Lovatt D, Sonnewald U, Waagepetersen HS, Schousboe A, He W, Lin JH-C, Han X, Takano T, Wang S, Sim FJ, Goldman SA, Nedergaard M (2007) The Transcriptome and Metabolic Gene Signature of Protoplasmic Astrocytes in the Adult Murine Cortex. J Neurosci 27:12255–12266.

Maday S, Wallace KE, Holzbaur ELF (2012) Autophagosomes initiate distally and mature during transport toward the cell soma in primary neurons. J Cell Biol 196:407–417.

Magi S, Arcangeli S, Castaldo P, Nasti AA, Berrino L, Piegari E, Bernardini R, Amoroso S, Lariccia V (2013) Glutamate-Induced ATP Synthesis: Relationship between Plasma Membrane Na+/Ca2+ Exchanger and Excitatory Amino Acid Transporters in Brain and Heart Cell Models. Mol Pharmacol 84:603–614.

Matsuda T, Arakawa N, Takuma K, Kishida Y, Kawasaki Y, Sakaue M, Takahashi K, Takahashi T, Suzuki T, Ota T, Hamano-Takahashi A, Onishi M, Tanaka Y, Kameo K, Baba A (2001) SEA0400, a novel and selective inhibitor of the Na+-Ca2+ exchanger, attenuates reperfusion injury in the in vitro and in vivo cerebral ischemic models. J Pharmacol Exp Ther 298:249–256.

Mayer ML, Westbrook GL (1987) The physiology of excitatory amino acids in the vertebrate central nervous system. Prog Neurobiol 28:197–276.

McKenna MC (2013) Glutamate pays its own way in astrocytes. Front Endocrinol 4:191.

Motori E, Puyal J, Toni N, Ghanem A, Angeloni C, Malaguti M, Cantelli-Forti G, Berninger B, Conzelmann K-K, Götz M, Winklhofer KF, Hrelia S, Bergami M (2013) Inflammation-induced alteration of astrocyte mitochondrial dynamics requires autophagy for mitochondrial network maintenance. Cell Metab 18:844–859.

Muir KW (2006) Glutamate-based therapeutic approaches: clinical trials with NMDA antagonists. Curr Opin Pharmacol 6:53–60.

Nakai A, Kuroda S, Kristián T, Siesjö BK (1997) The Immunosuppressant Drug FK506 Ameliorates Secondary Mitochondrial Dysfunction Following Transient Focal Cerebral Ischemia in the Rat. Neurobiol Dis 4:288–300.

Nichols RA, Suplick GR, Brown JM (1994) Calcineurin-mediated protein dephosphorylation in brain nerve terminals regulates the release of glutamate. J Biol Chem 269:23817–23823.

Noraberg J, Poulsen FR, Blaabjerg M, Kristensen BW, Bonde C, Montero M, Meyer M, Gramsbergen JB, Zimmer J (2005) Organotypic hippocampal slice cultures for studies of brain damage, neuroprotection and neurorepair. Curr Drug Targets CNS Neurol Disord 4:435–452.

Oliveira JMA, Goncalves J (2008) In Situ Mitochondrial Ca2+ Buffering Differences of Intact Neurons and Astrocytes from Cortex and Striatum. J Biol Chem 284:5010–5020.

Otsu Y, Couchman K, Lyons DG, Collot M, Agarwal A, Mallet J-M, Pfrieger FW, Bergles DE, Charpak S (2015) Calcium dynamics in astrocyte processes during neurovascular coupling. Nat Neurosci 18:210–218.

Ouyang Y-B, Lu Y, Yue S, Giffard RG (2012) miR-181 targets multiple Bcl-2 family members and influences apoptosis and mitochondrial function in astrocytes. Mitochondrion 12:213–219.

Ouyang Y-B, Voloboueva LA, Xu L-J, Giffard RG (2007) Selective dysfunction of hippocampal CA1 astrocytes contributes to delayed neuronal damage after transient forebrain ischemia. J Neurosci 27:4253–4260.

Ouyang Y-B, Xu L, Liu S, Giffard RG (2014) Role of Astrocytes in Delayed Neuronal Death: GLT-1 and its Novel Regulation by MicroRNAs. In: Glutamate and ATP at the Interface of Metabolism and Signaling in the Brain (Parpura V, Schousboe A, Verkhratsky A, eds), pp 171–188. Cham: Springer International Publishing.

Ouyang Y-B, Xu L-J, Emery JF, Lee AS, Giffard RG (2011) Overexpressing GRP78 influences Ca2+ handling and function of mitochondria in astrocytes after ischemia-like stress. Mitochondrion 11:279–286.

Parnis J, Montana V, Delgado-Martinez I, Matyash V, Parpura V, Kettenmann H, Sekler I, Nolte C (2013) Mitochondrial exchanger NCLX plays a major role in the intracellular Ca2+ signaling, gliotransmission, and proliferation of astrocytes. J Neurosci 33:7206–7219.

Parpura V, Heneka MT, Montana V, Oliet SHR, Schousboe A, Haydon PG, Stout RF Jr, Spray DC, Reichenbach A, Pannicke T, Pekny M, Pekna M, Zorec R, Verkhratsky A (2012) Glial cells in (patho)physiology. J Neurochem 121:4–27.

Pringle AK, Benham CD, Sim L, Kennedy J, Iannotti F, Sundstrom LE (1996) Selective N-Type Calcium Channel Antagonist Omega Conotoxin MVIIA Is Neuroprotective Against Hypoxic Neurodegeneration in Organotypic Hippocampal-Slice Cultures. Stroke 27:2124–2130.

Rininger A, Wayland A, Prifti V, Halterman MW (2012) Assessment of CA1 injury after global ischemia using supervised 2D analyses of nuclear pyknosis. J Neurosci Methods 207:181–188.

Rizzuto R, Brini M, Pizzo P, Murgia M, Pozzan T (1995) Chimeric green fluorescent protein as a tool for visualizing subcellular organelles in living cells. Curr Biol CB 5:635–642.

Rizzuto R, Brini M, Pozzan T (1993) Intracellular targeting of the photoprotein aequorin: A new approach for measuring, in living cells, Ca(2+) concentrations in defined cellular compartments. Cytotechnology 11:S44-46.

Rizzuto R, De Stefani D, Raffaello A, Mammucari C (2012) Mitochondria as sensors and regulators of calcium signalling. Nat Rev Mol Cell Biol 13:566–578.

Robinson MB, Jackson JG (2016) Astroglial Glutamate Transporters Coordinate Excitatory Signaling and Brain Energetics. Neurochem Int.

Rodriguez-Enriquez S, He L, Lemasters JJ (2004) Role of mitochondrial permeability transition pores in mitochondrial autophagy. Int J Biochem Cell Biol 36:2463–2472.

Rojas H, Colina C, Ramos M, Benaim G, Jaffe E, Caputo C, Di Polo R (2013) Sodium-calcium exchanger modulates the L-glutamate Ca(i) (2+) signalling in type-1 cerebellar astrocytes. Adv Exp Med Biol 961:267–274.

Rossi DJ, Brady JD, Mohr C (2007) Astrocyte metabolism and signaling during brain ischemia. Nat Neurosci 10:1377–1386.

Salinet ASM, Robinson TG, Panerai RB (2015) Effects of cerebral ischemia on human neurovascular coupling, CO_2 reactivity, and dynamic cerebral autoregulation. J Appl Physiol 118:170–177.

Sasaki T, Ishikawa T, Abe R, Nakayama R, Asada A, Matsuki N, Ikegaya Y (2014) Astrocyte calcium signalling orchestrates neuronal synchronization in organotypic hippocampal slices. J Physiol 592:2771–2783.

Schindelin J, Arganda-Carreras I, Frise E, Kaynig V, Longair M, Pietzsch T, Preibisch S, Rueden C, Saalfeld S, Schmid B, Tinevez J-Y, White DJ, Hartenstein V, Eliceiri K, Tomancak P, Cardona A (2012) Fiji: an open-source platform for biological-image analysis. Nat Methods 9:676–682.

Schröder UH, Breder J, Sabelhaus CF, Reymann KG (1999) The novel Na+/Ca2+ exchange inhibitor KB-R7943 protects CA1 neurons in rat hippocampal slices against hypoxic/hypoglycemic injury. Neuropharmacology 38:319–321.

Schwarz TL (2013) Mitochondrial trafficking in neurons. Cold Spring Harb Perspect Biol 5:a011304.

Sheng Z-H, Cai Q (2012) Mitochondrial transport in neurons: impact on synaptic homeostasis and neurodegeneration. Nat Rev Neurosci 13:77–93.

Shimamoto K, Sakai R, Takaoka K, Yumoto N, Nakajima T, Amara SG, Shigeri Y (2004) Characterization of novel L-threo-beta-benzyloxyaspartate derivatives, potent blockers of the glutamate transporters. Mol Pharmacol 65:1008–1015.

Starkov AA, Fiskum G, Chinopoulos C, Lorenzo BJ, Browne SE, Patel MS, Beal MF (2004) Mitochondrial α-Ketoglutarate Dehydrogenase Complex Generates Reactive Oxygen Species. J Neurosci 24:7779–7788.

Stephen T-L, Higgs NF, Sheehan DF, Awabdh SA, López-Doménech G, Arancibia-Carcamo IL, Kittler JT (2015) Miro1 Regulates Activity-Driven Positioning of Mitochondria within Astrocytic Processes Apposed to Synapses to Regulate Intracellular Calcium Signaling. J Neurosci 35:15996–16011.

Stoppini L, Buchs P-A, Muller D (1991) A simple method for organotypic cultures of nervous tissue. J Neurosci Methods 37:173–182.

Strijbos PJ, Leach MJ, Garthwaite J (1996) Vicious cycle involving Na+ channels, glutamate release, and NMDA receptors mediates delayed neurodegeneration through nitric oxide formation. J Neurosci 16:5004–5013.

Takano T, Tian G-F, Peng W, Lou N, Libionka W, Han X, Nedergaard M (2006) Astrocyte-mediated control of cerebral blood flow. Nat Neurosci 9:260–267.

Takemiya T, Yamagata K (2013) Intercellular Signaling Pathway among Endothelia, Astrocytes and Neurons in Excitatory Neuronal Damage. Int J Mol Sci 14:8345–8357.

Tanida I, Ueno T, Kominami E (2008) LC3 and Autophagy. In: Autophagosome and Phagosome (Deretic V, ed), pp 77–88. Totowa, NJ: Humana Press.

Tretter L, Adam-Vizi V (2004) Generation of reactive oxygen species in the reaction catalyzed by alpha-ketoglutarate dehydrogenase. J Neurosci 24:7771–7778.

Trumbeckaite S, Gizatullina Z, Arandarcikaite O, Röhnert P, Vielhaber S, Malesevic M, Fischer G, Seppet E, Striggow F, Gellerich FN (2013) Oxygen glucose deprivation causes mitochondrial dysfunction in cultivated rat hippocampal slices: Protective effects of CsA, its immunosuppressive congener [D-Ser]8CsA, the novel non-immunosuppressive cyclosporin derivative Cs9, and the NMDA receptor antagonist MK 801. Mitochondrion 13:539–547.

Tsien RY (1998) The green fluorescent protein. Annu Rev Biochem 67:509–544.

Uchino H, Elmér E, Uchino K, Li P-A, He Q-P, Smith M-L, Siesjö BK (1998) Amelioration by cyclosporin A of brain damage in transient forebrain ischemia in the rat. Brain Res 812:216–226.

Ugbode CI, Hirst WD, Rattray M (2014) Neuronal influences are necessary to produce mitochondrial co-localization with glutamate transporters in astrocytes. J Neurochem 130:668–677.

Valentino K, Newcomb R, Gadbois T, Singh T, Bowersox S, Bitner S, Justice A, Yamashiro D, Hoffman BB, Ciaranello R (1993) A selective N-type calcium

channel antagonist protects against neuronal loss after global cerebral ischemia. Proc Natl Acad Sci U S A 90:7894–7897.

Vornov JJ, Tasker RC, Coyle JT (1991) Direct observation of the agonist-specific regional vulnerability to glutamate, NMDA, and kainate neurotoxicity in organotypic hippocampal cultures. Exp Neurol 114:11–22.

Wang GJ, Jackson JG, Thayer SA (2003) Altered distribution of mitochondria impairs calcium homeostasis in rat hippocampal neurons in culture. J Neurochem 87:85–94.

Whitelaw BS, Robinson MB (2013) Inhibitors of glutamate dehydrogenase block sodium-dependent glutamate uptake in rat brain membranes. Front Endocrinol 4:123.

Woeffler-Maucler C, Beghin A, Ressnikoff D, Bezin L, Marinesco S (2014) Automated immunohistochemical method to quantify neuronal density in brain sections: application to neuronal loss after status epilepticus. J Neurosci Methods 225:32–41.

Wong YC, Holzbaur ELF (2014) Optineurin is an autophagy receptor for damaged mitochondria in parkin-mediated mitophagy that is disrupted by an ALS-linked mutation. Proc Natl Acad Sci 111:E4439–E4448.

Yang Y, Li Q, Miyashita H, Yang T, Shuaib A (2001) Different dynamic patterns of extracellular glutamate release in rat hippocampus after permanent or 30-min transient cerebral ischemia and histological correlation. Neuropathology 21:181–187.

Yokoyama T, Tanoue T, Hasegawa E, Ikeda Y, Ohta S, Omi A, Kudo Y, Uchino H (2012) Evaluation of the Protective Effects of Cyclosporin A and FK506 on Abnormal Cytosolic and Mitochondrial Ca²⁺ Dynamics During Ischemia and Exposure to High Glutamate Concentration in Mouse Brain Slice Preparations. J Pharmacol Sci 120:228–240.

Zaganas I, Waagepetersen HS, Georgopoulos P, Sonnewald U, Plaitakis A, Schousboe A (2001) Differential expression of glutamate dehydrogenase in cultured neurons and astrocytes from mouse cerebellum and cerebral cortex. J Neurosci Res 66:909–913.

Zhang Y, Chen K, Sloan SA, Bennett ML, Scholze AR, O'Keeffe S, Phatnani HP, Guarnieri P, Caneda C, Ruderisch N, Deng S, Liddelow SA, Zhang C, Daneman R, Maniatis T, Barres BA, Wu JQ (2014) An RNA-Sequencing Transcriptome and Splicing Database of Glia, Neurons, and Vascular Cells of the Cerebral Cortex. J Neurosci 34:11929–11947.

Zheng W, Talley Watts L, Holstein DM, Wewer J, Lechleiter JD (2013) P2Y1R-initiated, IP3R-dependent stimulation of astrocyte mitochondrial metabolism reduces and partially reverses ischemic neuronal damage in mouse. J Cereb Blood Flow Metab 33:600–611.

Zhou X, Hollern D, Liao J, Andrechek E, Wang H (2013) NMDA receptor-mediated excitotoxicity depends on the coactivation of synaptic and extrasynaptic receptors. Cell Death Dis 4:e560.

CHAPTER 5

Conclusions and Future Directions

5.1 Summary

Mitochondria in astrocytes have been recognized for some time as the site of brain glutamate synthesis and subsequent oxidation following neurotransmission (for review, see Hertz et al., 2007). Although pervasive electron micrograph images of mitochondria in fine astrocytic processes have existed in the literature for some time (Mugnaini, 1964; Fernandez et al., 1983; Aoki et al., 1987; Xu et al., 2003; Lovatt et al., 2007; Ito et al., 2009; Oberheim et al., 2009; Lavialle et al., 2011; Pardo et al., 2011), their presence in these unique cellular compartments has only recently gained wide acceptance (Genda et al., 2011a; Motori et al., 2013; Jackson et al., 2014; Derouiche et al., 2015; Jackson and Robinson, 2015; Stephen et al., 2015; O'Donnell et al., 2016; for review, see Benjamin Kacerovsky and Murai, 2016). Chapter 2 of this thesis provided evidence for an immunoprecitatible complex between the astrocytic glutamate transporter, GLT-1, and several glycolytic and mitochondrial proteins (Jackson et al., 2015). Chapter 3 described the regulation of astrocytic mitochondrial mobility by glutamate transporter activity and NCX reversal to position mitochondria near transporters and synapses (Jackson et al., 2014). Finally, Chapter 4 detailed a delayed loss of mitochondria from astrocytic processes following transient OGD, due to fragmentation and, at least in part, increased mitophagy (O'Donnell et al., 2016). Surprisingly, the loss of mitochondria occurs independently from the concomitant neuropathology, depending instead on an extended period of high glutamate transporter activity. I also reveal a previously overlooked distinction between two types of spontaneous cytosolic Ca^{2+} signals in astrocytic processes: brief, far-reaching spikes in spaces between mitochondria, and high frequency, long duration Ca^{2+} clouds surrounding mitochondria. Both signals increased in intensity 24 h after OGD. The

extramitochondrial spikes spread farther, no longer contained by mitochondria, while the mitochondrially-centered signals covered less area, corresponding to the decreased size of mitochondria. An expanded discussion of these results, their broader implications, and future directions is provided below.

5.2 Transporter-Mitochondria Interactions in Astrocytic Processes

Chapter 2 provides evidence that the mitochondrial matrix protein UQCRC2, inner mitochondrial membrane protein ANT, outer mitochondrial membrane protein VDAC, and the glycolytic enzyme HK1 coimmunoprecipitate with each other, and with the plasma membrane protein GLT-1, an astrocytic glutamate transporter (Jackson et al., 2015). We hypothesized that HK1 may act as a cytoplasmic bridge between the transporter and mitochondria, since it binds VDAC on the surface of mitochondria (Lindén et al., 1982; Nakashima et al., 1986; Sui and Wilson, 1997) and its isoform HK2 also interacts with the plasma membrane glucose transporter, GLUT4 (Zaid et al., 2009). Using a peptide to displace 50% of HK1 from VDAC did not affect the interaction between GLT-1 and mitochondrial proteins, and therefore HK1 does not serve as a cytoplasmic link between the transporter and mitochondria. While displacing HK1 from VDAC did not affect GLT-1 interactions with mitochondria, it did reduce its glutamate uptake activity by ~30%. When HK1 is bound to VDAC, it favors interactions with ANT in a manner that provides nucleotide transfer (ATP out, ADP in) facilitating glycolysis and oxidative phosphorylation. Therefore, the metabolic consequences of disrupting this interaction likely lead to the reduced transport activity of GLT-1.

This study raises some obvious follow up questions. For one, if HK1 isn't a cytoplasmic bridge, how is GLT-1 interacting with mitochondria? Protein interactions between mitochondria and ER facilitate efficient Ca^{2+} signaling between the organelles that is important for regulating energy production and apoptosis (Rizzuto et al., 1998; Csordás et al., 2010). These junctions are formed between VDAC on mitochondria and IP3R on ER via linkage by the chaperone protein Grp75 (Szabadkai et al., 2006). Grp75, also called Hsp70-9, is a member of the 70kD heat-shock protein family, and another member of that protein family, Hsp70-12A, was identified in previous proteomic analysis of GLT-1 (Genda et al., 2011a). Synapsin 1, synapsin 2, and Syntaxin-binding protein 1 (also known as MUNC18-1) were also identified in the proteome, and are known to be involved in Ca^{2+}-regulated docking of synaptic vesicles at the plasma membrane (Hilfiker et al., 1999; Voets et al., 2001; Gulyás-Kovács et al., 2007; Coleman et al., 2008). These proteins represent some of the most appealing bridge candidates from the proteome, and future investigations will provide more details on the organizational structure of these interactions.

The protein complex between mitochondria and ER served as a model for envisioning the structure of the interactions between mitochondria and GLT-1 in the plasma membrane, but mitochondria/ER junctions are also likely to play an important role in astrocytic processes in their own right. Astrocytic ER is perinuclear in primary culture, but has been observed in processes *in situ* (Pivneva et al., 2008; Patrushev et al., 2013). Previous studies have shown that IP3R-induced Ca^{2+} release is not relevant to neurovascular coupling (Schulz et al., 2012; Nizar et al., 2013), and IP3R-independent Ca^{2+} signaling is prevalent in processes (Lind et al., 2013; Otsu et al., 2015; Srinivasan et al., 2015; Tang et al., 2015; for review see Bazargani and Attwell, 2016).

However, mitochondrial fission, which we have frequently observed in astrocytic processes, typically involves interaction with ER (for review, see Phillips and Voeltz, 2016). Furthermore, overexpression of the ER protein Grp78 (Hsp70-5), another member of the 70kD heat-shock protein family, prevented the loss of mitochondrial membrane potential and respiration under hypoglycemic conditions in primary astrocyte cultures (Ouyang et al., 2011). In truth, little is known about the role of ER in astrocytic processes, let alone the interactions between ER and mitochondria, and further investigation is needed.

5.3 Mitochondrial Mobility and Ca^{2+} Signaling in Astrocytic Processes

As detailed in Chapter 3, mitochondria in astrocytic processes are immobilized near glutamate transporters and synapses by a mechanism involving neuronal activity, astrocytic glutamate uptake, and Ca^{2+}influx through reversal of the NCX (Jackson et al., 2014). This positions mitochondria in processes at sites of high energy and ion-buffering demand, similar to immobilization of neuronal mitochondria near nodes of Ranvier, growth cones, and pre and post synaptic terminals (for reviews, see Sheng and Cai, 2012; Schwarz, 2013). Since this paper was published, additional studies have replicated these results and found that Ca^{2+} binding to MIRO motor adaptor proteins causes mitochondrial immobilization in astrocytes (Jackson and Robinson, 2015; Stephen et al., 2015), again resembling neuronal mechanisms (for review, see Schwarz, 2013). Mitochondria were also found to buffer and shape Ca^{2+} signals in astrocytic processes (Jackson and Robinson, 2015; Stephen et al., 2015), and I found that 86% of extramitochondrial Ca^{2+} spikes are contained between two mitochondria under control conditions, as described in Chapter 4 (O'Donnell et al., 2016). I also found that the long

duration, high frequency Ca^{2+} signals in astrocytic processes reported by another lab while our paper was under review (Jiang et al., 2016), are in fact Ca^{2+} clouds surrounding mitochondria (O'Donnell et al., 2016).

Astrocytic mitochondria move more slowly, and don't travel as far as their neuronal counterparts (Jackson et al., 2014). This may indicate that isoforms of the kinesin and dynein motor proteins are different in astrocytes compared to neurons. While these motors have been studied in some detail in neurons, which appear to rely primarily on the KIF5 motors of the kinesin 1 family along with dynein (for reviews, see Hirokawa et al., 2009; Schwarz, 2013; Sheng, 2014), they have yet to be identified in astrocytes. Motor proteins use microtubules and actin filaments as tracks to transport cargo, and in Chapter 3 we demonstrated that mitochondrial mobility in astrocytic processes is impaired when microtubules or actin filaments are destabilized (Jackson et al., 2014). Microtubules of the neuronal cytoskeleton are unipolar and aligned so that the plus ends extend into the periphery; this means that the plus-end-directed KIF5 is responsible for anterograde mitochondrial mobility away from the cell body, and dynein provides retrograde transport (for reviews, see Hirokawa et al., 2009; Schwarz, 2013; Sheng, 2014). The tortuous, highly ramified morphology of astrocytic processes suggests that their cytoskeletons may be organized very differently from neurons. Remodeling of the actin cytoskeleton in astrocytes is essential for stellation during development, and remodeling at the synapse to facilitate structural plasticity involved in learning and memory (Oliet et al., 2001; Haber et al., 2006; Schweinhuber et al., 2015; for reviews, see Bernardinelli et al., 2014; Heller and Rusakov, 2015;). However, the organization of the cytoskeleton in astrocytic processes largely remains a mystery. For example, future investigations can reveal whether the astrocytic microtubules are

unipolar and aligned like their neuronal counterparts, as well as the role that positioning and activity of mitochondria play in the motility of astrocytic processes.

As has been observed in neurons, most mitochondria in astrocytes are in a more permanent stationary phase. My unpublished preliminary observations indicate that the stationary population of mitochondria may increase with development, as the morphology of primary and secondary astrocytic processes becomes more static. It has been suggested that in neurons this stationary phase arises after an extended period of pausing without reestablishing mobility, and may be facilitated by disengaging motors from the cytoskeleton or mitochondria, or by engaging anchoring proteins like syntaphilin (for reviews, see Schwarz, 2013; Sheng, 2014). Syntaphilin is also expressed in astrocytes, but no data are available on its function in these cells (Miki et al., 2014; Zhang et al., 2014). The mechanisms maintaining the stationary pool of mitochondria in neurons have yet to be defined, and even less is known in astrocytes. This field is wide open for future studies.

Mitochondria positioned at glutamate transporters and synapses spatially restrict Ca^{2+} signals, integrating sites of activity into the information coded in the signal. Thus, the positioning of mitochondria in astrocytic processes may provide another level of signaling plasticity in the brain. Although IP3R-induced Ca^{2+} signaling in astrocytes is not necessary for neurovascular coupling (Schulz et al., 2012; Nizar et al., 2013), the ER is not the only intracellular Ca^{2+} store. Mitochondrial Ca^{2+} signaling has been observed in primary astrocyte cultures (Parnis et al., 2013) and in many other cell types (for review, see Rizzuto et al., 2012). Future studies are necessary to explore the mechanisms and relevance of mitochondrial Ca^{2+} release in astrocytic processes. However, cytosolic Ca^{2+} signals may not even reveal half of the story. For many

astrocytic processes, most of their volume is occupied by mitochondria. The possibility that mitochondria form close junctions with ER as well as plasma membrane glutamate transporters and NCX suggests that by focusing on cytoplasmic Ca^{2+} we may be missing the majority of Ca^{2+} signaling events in astrocytic processes. Therefore, future studies should include Ca^{2+} sensors targeted to mitochondria and ER in addition to the cytoplasm in order to obtain a more complete picture.

5.4 Loss of Astrocytic Mitochondria after Transient OGD

In Chapter 4 I described the delayed fragmentation and loss of mitochondria from astrocytic processes that correlates with, but is not dependent on delayed neuronal pathology following transient OGD or treatment with NMDA. I also observed increased mitophagy in astrocytes between 9 and 24 h after OGD, indicating that at least some of the mitochondrial loss is due to autophagic degradation. While the NMDAR antagonist MK801 was completely neuroprotective, completely blocking the loss of astrocytic mitochondria required combination of MK801 with the AMPAR antagonist NBQX. This was our first indication that the mitochondrial effect may be independent of neuronal pathology. Given that iGluR activation increases glutamate release (for review, see Mayer and Westbrook, 1987), and that glutamate elevations in area CA1 have been observed by *in vivo* microdialysis after reperfusion from ischemia (Yang et al., 2001), I hypothesized that the loss of mitochondria was dependent on glutamate release, and not neuropathology. Blocking action potentials or the neuronal Ca^{2+} channels involved in vesicular neurotransmitter release during and after OGD or NMDA also blocked the loss of mitochondria, but since they were neuroprotective the contribution of glutamate per se was not clear. When 1 mM glutamate was applied for 1 – 2 h in the presence of iGluR

antagonists, there was no measurable neuropathology, but there was clear fragmentation and degradation of astrocytic mitochondria that was greater with longer exposure to glutamate. This was compelling evidence that glutamate was involved independent of neuropathology, and since we knew that astrocytic glutamate transporter activity regulates mitochondrial distribution, I hypothesized that glutamate was driving mitochondrial loss through a mechanism involving transporter activity. Incredibly, blocking glutamate transporters with TFB-TBOA completely blocked the loss of mitochondria even though it increased neuronal pathology after OGD or NMDA. Na^+-dependent glutamate transporter activity causes cytosolic Ca^{2+} elevation due to localized reversal of NCX, which immobilizes mitochondria (Magi et al., 2013a; Rojas et al., 2013; Jackson et al., 2014; Jackson and Robinson, 2015). High Ca^{2+} concentrations can drive mitochondrial fragmentation and autophagic degradation (He and Lemasters, 2002; Kim et al., 2012), but blocking NCX reversal only attenuated the loss of mitochondria after OGD, suggesting that additional mechanisms are involved. Blocking mitochondrial depolarization with CsA or FK506 blocked the loss of astrocytic mitochondria. These results suggest that after transient OGD, an extended period of high glutamate transporter activity causes delayed fragmentation and loss of mitochondria from astrocytic processes that is due at least in part to increased mitophagy.

In neurons, PINK1/Parkin-mediated ubiquitination of dysfunctional mitochondria facilitates engulfment by autophagosomes and degradation via mitophagy (Matsuda et al., 2010 p.1; Chan et al., 2011; Wang et al., 2011; Yoshii et al., 2011; Wong and Holzbaur, 2014, 2015). Parkin is also present in astrocytes, where it maintains a healthy pool of mitochondria (Ledesma et al., 2002; Schmidt et al., 2011). Parkin knockdown increases anterograde transport of mitochondria and prevents degradation of

dysfunctional mitochondria (Wang et al., 2011; Cai et al., 2012). Transfection with a dominant-negative Parkin mutant lacking E3 ligase activity also inhibits mitophagy (Lazarou et al., 2013). Utilizing the tools available for genetic Parkin inhibition, future studies can determine its contribution to loss of astrocytic mitochondria after transient OGD. This could potentially provide a tool for direct and selective prevention of mitochondrial loss in astrocytes, allowing for studies that more directly evaluate the effects of astrocytic mitochondrial loss after OGD.

In a recent study utilizing a mouse model of focal I/R injury, Ca^{2+}-dependent release of astrocytic mitochondria and transfer into neurons was observed, and blocking this phenomenon exacerbated neuropathology (Hayakawa et al., 2016). Therefore, in addition to the increased mitophagy I observed, some of the mitochondrial loss after OGD could be due to extracellular release. The transfer of mitochondria from astrocytes to neurons was prevented by using shRNA to knock down expression of the glycoprotein CD38, which is involved in synthesis of cyclic ADP ribose along with other molecules and influences Ca^{2+} signaling in many cell types, including astrocytes (for review, see Malavasi et al., 2008). Interestingly, astrocytic expression of CD38 is increased in response to glutamate (Bruzzone et al., 2004). Future studies will determine if this mitochondrial transfer occurs in our injury model, and if increased CD38 expression and/or mitochondrial transfer can be prevented by blocking glutamate transporters. Astrocytic glutamate transporters GLAST and GLT-1 have been found on neurons in hippocampal slices after transient OGD (Bonde et al., 2005). Future work is needed to determine if mitochondria are encapsulated within astrocytic plasma membrane containing glutamate transporters for transfer to neurons.

Application of FCCP causes loss of mitochondrial membrane potential, efflux of Ca^{2+} from mitochondria into the cytoplasm, eliminates mitochondrial Ca^{2+} uptake, prolongs cytoplasmic Ca^{2+} elevations, and increases speed of propagation for Ca^{2+} waves in primary astrocyte cultures (Boitier et al., 1999). Similar results are found in astrocytic processes, with the additional observation that cytoplasmic Ca^{2+} signals spread farther after FCCP treatment (Jackson and Robinson, 2015). The higher intensity and farther spread of extramitochondrial Ca^{2+} signals I observed after OGD are consistent with loss of membrane potential, which has been observed in primary astrocyte cultures after similar insults (Dugan and Kim-Han, 2004; Ouyang et al., 2011, 2012b). However, the increased intensity of mitochondrially centered Ca^{2+} signals after OGD indicates that while efflux is increased, mitochondria still contain and replenish Ca^{2+}, otherwise the Ca^{2+} clouds surrounding mitochondria would dissipate as observed after FCCP treatment. However, if mitochondria/ER junctions are present in astrocytic processes and maintained after injury, depolarized mitochondria could potentially leak Ca^{2+} into the cytosol without rapid depletion of their stores. Multiple sources, including glutamate transporters, impose a constant influx of extracellular Na^{+} into astrocytes (for review, see Chatton et al., 2016); loss of mitochondria means loss of a major intracellular Na^{+} buffer, and could also reduce ATP available for Na^{+} extrusion via the Na^{+}/K^{+}ATPase. It is possible that mitochondrial membrane potential recovers to some extent 24 h after OGD, allowing for some Ca^{2+} retention, but high cytoplasmic Na^{+} concentrations could simultaneously increase Ca^{2+} efflux through the mitochondrial NCX. Further investigation into mitochondria/ER interaction, changes in Na^{+} concentrations, and mitochondrial membrane potential in astrocytic processes after OGD will be necessary to understand the observed dysregulation of Ca^{2+} signaling. Developing genetic fluorescent sensors for measuring mitochondrial membrane potential

will greatly enhance the specificity of signal as compared to available dyes, and provide precision in studies examining mitochondrial membrane potential in fine astrocytic and neuronal processes in slice cultures and *in vivo*.

Additional studies are needed to determine whether preventing the loss of astrocytic mitochondria is a viable therapeutic goal, or if the loss—and possible neuronal transfer—of astrocytic mitochondria is neuroprotective in its own right. CsA and FK506 may be selective for astrocytic mitochondria but they also have neuronal and general anti-inflammatory effects, so their neuroprotective effects can't be attributed to preventing mitochondrial loss in astrocytes. We need to develop more specific tools in order to evaluate the effects of preventing mitochondrial loss. Furthermore, we need to study the effect in vivo to understand how the dysregulation of Ca^{2+} signaling after mitochondrial loss effects neurovascular coupling, metabolic cycles, and greater brain function. During my doctoral career we've been fortunate enough to make a few surprising discoveries, and generate many new and exciting avenues for continuing research.

5.5 References

Aoki C, Milner TA, Berger SB, Sheu KF, Blass JP, Pickel VM (1987) Glial glutamate dehydrogenase: ultrastructural localization and regional distribution in relation to the mitochondrial enzyme, cytochrome oxidase. J Neurosci Res 18:305–318.

Bazargani N, Attwell D (2016) Astrocyte calcium signaling: the third wave. Nat Neurosci 19:182–189.

Benjamin Kacerovsky J, Murai KK (2016) Stargazing: Monitoring subcellular dynamics of brain astrocytes. Neuroscience 323:84–95.

Bernardinelli Y, Muller D, Nikonenko I (2014) Astrocyte-synapse structural plasticity. Neural Plast 2014:232105.

Boitier E, Rea R, Duchen MR (1999) Mitochondria Exert a Negative Feedback on the Propagation of Intracellular Ca2+ Waves in Rat Cortical Astrocytes. J Cell Biol 145:795–808.

Bonde C, Noraberg J, Noer H, Zimmer J (2005) Ionotropic glutamate receptors and glutamate transporters are involved in necrotic neuronal cell death induced by oxygen-glucose deprivation of hippocampal slice cultures. Neuroscience 136:779–794.

Bruzzone S, Verderio C, Schenk U, Fedele E, Zocchi E, Matteoli M, De Flora A (2004) Glutamate-mediated overexpression of CD38 in astrocytes cultured with neurones. J Neurochem 89:264–272.

Cai Q, Zakaria HM, Simone A, Sheng Z-H (2012) Spatial Parkin Translocation and Degradation of Damaged Mitochondria via Mitophagy in Live Cortical Neurons. Curr Biol 22:545–552.

Chan NC, Salazar AM, Pham AH, Sweredoski MJ, Kolawa NJ, Graham RLJ, Hess S, Chan DC (2011) Broad activation of the ubiquitin-proteasome system by Parkin is critical for mitophagy. Hum Mol Genet 20:1726–1737.

Chatton J-Y, Magistretti PJ, Barros LF (2016) Sodium signaling and astrocyte energy metabolism. Glia 64:1667–1676.

Coleman WL, Bill CA, Simsek-Duran F, Lonart G, Samigullin D, Bykhovskaia M (2008) Synapsin II and calcium regulate vesicle docking and the cross-talk between vesicle pools at the mouse motor terminals. J Physiol 586:4649–4673.

Csordás G, Várnai P, Golenár T, Roy S, Purkins G, Schneider TG, Balla T, Hajnóczky G (2010) Imaging interorganelle contacts and local calcium dynamics at the ER-mitochondrial interface. Mol Cell 39:121–132.

Derouiche A, Haseleu J, Korf H-W (2015) Fine Astrocyte Processes Contain Very Small Mitochondria: Glial Oxidative Capability May Fuel Transmitter Metabolism. Neurochem Res 40:2402–2413.

Dugan LL, Kim-Han J-S (2004) Astrocyte mitochondria in in vitro models of ischemia. J Bioenerg Biomembr 36:317–321.

Fernandez B, Suarez I, Gianonatti C (1983) Fine structure of astrocytic mitochondria in the hypothalamus of the hamster. J Anat 137 (Pt 3):483–488.

Genda EN, Jackson JG, Sheldon AL, Locke SF, Greco TM, O'Donnell JC, Spruce LA, Xiao R, Guo W, Putt M, Seeholzer S, Ischiropoulos H, Robinson MB (2011) Co-compartmentalization of the astroglial glutamate transporter, GLT-1, with glycolytic enzymes and mitochondria. J Neurosci 31:18275–18288.

Gulyás-Kovács A, de Wit H, Milosevic I, Kochubey O, Toonen R, Klingauf J, Verhage M, Sørensen JB (2007) Munc18-1: sequential interactions with the fusion machinery

stimulate vesicle docking and priming. J Neurosci Off J Soc Neurosci 27:8676–8686.

Haber M, Zhou L, Murai KK (2006) Cooperative astrocyte and dendritic spine dynamics at hippocampal excitatory synapses. J Neurosci Off J Soc Neurosci 26:8881–8891.

Hayakawa K, Esposito E, Wang X, Terasaki Y, Liu Y, Xing C, Ji X, Lo EH (2016) Transfer of mitochondria from astrocytes to neurons after stroke. Nature 535:551–555.

He L, Lemasters JJ (2002) Regulated and unregulated mitochondrial permeability transition pores: a new paradigm of pore structure and function? FEBS Lett 512:1–7.

Heller JP, Rusakov DA (2015) Morphological plasticity of astroglia: Understanding synaptic microenvironment. Glia 63:2133–2151.

Hertz L, Peng L, Dienel GA (2007) Energy metabolism in astrocytes: high rate of oxidative metabolism and spatiotemporal dependence on glycolysis/glycogenolysis. J Cereb Blood Flow Metab Off J Int Soc Cereb Blood Flow Metab 27:219–249.

Hilfiker S, Pieribone VA, Czernik AJ, Kao HT, Augustine GJ, Greengard P (1999) Synapsins as regulators of neurotransmitter release. Philos Trans R Soc Lond B Biol Sci 354:269–279.

Hirokawa N, Noda Y, Tanaka Y, Niwa S (2009) Kinesin superfamily motor proteins and intracellular transport. Nat Rev Mol Cell Biol 10:682–696.

Ito U, Hakamata Y, Kawakami E, Oyanagi K (2009) Degeneration of Astrocytic Processes and Their Mitochondria in Cerebral Cortical Regions Peripheral to the Cortical Infarction: Heterogeneity of Their Disintegration Is Closely Associated With Disseminated Selective Neuronal Necrosis and Maturation of Injury. Stroke 40:2173–2181.

Jackson JG, O'Donnell JC, Krizman E, Robinson MB (2015) Displacing hexokinase from mitochondrial voltage-dependent anion channel impairs GLT-1-mediated glutamate uptake but does not disrupt interactions between GLT-1 and mitochondrial proteins: HK1 Supports GLT-1 Function. J Neurosci Res 93:999–1008.

Jackson JG, O'Donnell JC, Takano H, Coulter DA, Robinson MB (2014) Neuronal Activity and Glutamate Uptake Decrease Mitochondrial Mobility in Astrocytes and Position Mitochondria Near Glutamate Transporters. J Neurosci 34:1613–1624.

Jackson JG, Robinson MB (2015) Reciprocal Regulation of Mitochondrial Dynamics and Calcium Signaling in Astrocyte Processes. J Neurosci 35:15199–15213.

Jiang R, Diaz-Castro B, Looger LL, Khakh BS (2016) Dysfunctional Calcium and Glutamate Signaling in Striatal Astrocytes from Huntington's Disease Model Mice. J Neurosci 36:3453–3470.

Kim J-S, Wang J-H, Lemasters JJ (2012) Mitochondrial permeability transition in rat hepatocytes after anoxia/reoxygenation: role of Ca2+-dependent mitochondrial formation of reactive oxygen species. AJP Gastrointest Liver Physiol 302:G723–G731.

Lavialle M, Aumann G, Anlauf E, Prols F, Arpin M, Derouiche A (2011) Structural plasticity of perisynaptic astrocyte processes involves ezrin and metabotropic glutamate receptors. Proc Natl Acad Sci 108:12915–12919.

Lazarou M, Narendra DP, Jin SM, Tekle E, Banerjee S, Youle RJ (2013) PINK1 drives Parkin self-association and HECT-like E3 activity upstream of mitochondrial binding. J Cell Biol 200:163–172.

Ledesma MD, Galvan C, Hellias B, Dotti C, Jensen PH (2002) Astrocytic but not neuronal increased expression and redistribution of parkin during unfolded protein stress. J Neurochem 83:1431–1440.

Lind BL, Brazhe AR, Jessen SB, Tan FCC, Lauritzen MJ (2013) Rapid stimulus-evoked astrocyte Ca2+ elevations and hemodynamic responses in mouse somatosensory cortex in vivo. Proc Natl Acad Sci U S A 110:E4678-4687.

Lindén M, Gellerfors P, Nelson BD (1982) Pore protein and the hexokinase-binding protein from the outer membrane of rat liver mitochondria are identical. FEBS Lett 141:189–192.

Lovatt D, Sonnewald U, Waagepetersen HS, Schousboe A, He W, Lin JH-C, Han X, Takano T, Wang S, Sim FJ, Goldman SA, Nedergaard M (2007) The Transcriptome and Metabolic Gene Signature of Protoplasmic Astrocytes in the Adult Murine Cortex. J Neurosci 27:12255–12266.

Magi S, Arcangeli S, Castaldo P, Nasti AA, Berrino L, Piegari E, Bernardini R, Amoroso S, Lariccia V (2013) Glutamate-induced ATP synthesis: relationship between plasma membrane Na+/Ca2+ exchanger and excitatory amino acid transporters in brain and heart cell models. Mol Pharmacol 84:603–614.

Malavasi F, Deaglio S, Funaro A, Ferrero E, Horenstein AL, Ortolan E, Vaisitti T, Aydin S (2008) Evolution and function of the ADP ribosyl cyclase/CD38 gene family in physiology and pathology. Physiol Rev 88:841–886.

Matsuda N, Sato S, Shiba K, Okatsu K, Saisho K, Gautier CA, Sou Y-S, Saiki S, Kawajiri S, Sato F, Kimura M, Komatsu M, Hattori N, Tanaka K (2010) PINK1 stabilized by mitochondrial depolarization recruits Parkin to damaged mitochondria and activates latent Parkin for mitophagy. J Cell Biol 189:211–221.

Mayer ML, Westbrook GL (1987) The physiology of excitatory amino acids in the vertebrate central nervous system. Prog Neurobiol 28:197–276.

Miki A, Kanamori A, Nakamura M, Matsumoto Y, Mizokami J, Negi A (2014) The expression of syntaphilin is down-regulated in the optic nerve after axonal injury. Exp Eye Res 129:38–47.

Motori E, Puyal J, Toni N, Ghanem A, Angeloni C, Malaguti M, Cantelli-Forti G, Berninger B, Conzelmann K-K, Götz M, Winklhofer KF, Hrelia S, Bergami M (2013) Inflammation-induced alteration of astrocyte mitochondrial dynamics requires autophagy for mitochondrial network maintenance. Cell Metab 18:844–859.

Mugnaini E (1964) HELICAL FILAMENTS IN ASTROCYTIC MITOCHONDRIA OF THE CORPUS STRIATUM IN THE RAT. J Cell Biol 23:173–182.

Nakashima RA, Mangan PS, Colombini M, Pedersen PL (1986) Hexokinase receptor complex in hepatoma mitochondria: evidence from N,N'-dicyclohexylcarbodiimide-labeling studies for the involvement of the pore-forming protein VDAC. Biochemistry (Mosc) 25:1015–1021.

Nizar K et al. (2013) In vivo stimulus-induced vasodilation occurs without IP3 receptor activation and may precede astrocytic calcium increase. J Neurosci Off J Soc Neurosci 33:8411–8422.

Oberheim NA, Takano T, Han X, He W, Lin JHC, Wang F, Xu Q, Wyatt JD, Pilcher W, Ojemann JG, Ransom BR, Goldman SA, Nedergaard M (2009) Uniquely Hominid Features of Adult Human Astrocytes. J Neurosci 29:3276–3287.

O'Donnell JC, Jackson JG, Robinson MB (2016) Transient Oxygen/Glucose Deprivation Causes a Delayed Loss of Mitochondria and Increases Spontaneous Calcium Signaling in Astrocytic Processes. J Neurosci Off J Soc Neurosci 36:7109–7127.

Oliet SH, Piet R, Poulain DA (2001) Control of glutamate clearance and synaptic efficacy by glial coverage of neurons. Science 292:923–926.

Otsu Y, Couchman K, Lyons DG, Collot M, Agarwal A, Mallet J-M, Pfrieger FW, Bergles DE, Charpak S (2015) Calcium dynamics in astrocyte processes during neurovascular coupling. Nat Neurosci 18:210–218.

Ouyang Y-B, Lu Y, Yue S, Xu L-J, Xiong X-X, White RE, Sun X, Giffard RG (2012) miR-181 regulates GRP78 and influences outcome from cerebral ischemia in vitro and in vivo. Neurobiol Dis 45:555–563.

Ouyang Y-B, Xu L-J, Emery JF, Lee AS, Giffard RG (2011) Overexpressing GRP78 influences Ca2+ handling and function of mitochondria in astrocytes after ischemia-like stress. Mitochondrion 11:279–286.

Pardo B, Rodrigues TB, Contreras L, Garzón M, Llorente-Folch I, Kobayashi K, Saheki T, Cerdan S, Satrústegui J (2011) Brain glutamine synthesis requires neuronal-born aspartate as amino donor for glial glutamate formation. J Cereb Blood Flow Metab Off J Int Soc Cereb Blood Flow Metab 31:90–101.

Parnis J, Montana V, Delgado-Martinez I, Matyash V, Parpura V, Kettenmann H, Sekler I, Nolte C (2013) Mitochondrial exchanger NCLX plays a major role in the intracellular Ca2+ signaling, gliotransmission, and proliferation of astrocytes. J Neurosci 33:7206–7219.

Patrushev I, Gavrilov N, Turlapov V, Semyanov A (2013) Subcellular location of astrocytic calcium stores favors extrasynaptic neuron–astrocyte communication. Cell Calcium 54:343–349.

Phillips MJ, Voeltz GK (2016) Structure and function of ER membrane contact sites with other organelles. Nat Rev Mol Cell Biol 17:69–82.

Pivneva T, Haas B, Reyes-Haro D, Laube G, Veh RW, Nolte C, Skibo G, Kettenmann H (2008) Store-operated Ca2+ entry in astrocytes: Different spatial arrangement of endoplasmic reticulum explains functional diversity in vitro and in situ. Cell Calcium 43:591–601.

Rizzuto R, De Stefani D, Raffaello A, Mammucari C (2012) Mitochondria as sensors and regulators of calcium signalling. Nat Rev Mol Cell Biol 13:566–578.

Rizzuto R, Pinton P, Carrington W, Fay FS, Fogarty KE, Lifshitz LM, Tuft RA, Pozzan T (1998) Close contacts with the endoplasmic reticulum as determinants of mitochondrial Ca2+ responses. Science 280:1763–1766.

Rojas H, Colina C, Ramos M, Benaim G, Jaffe E, Caputo C, Di Polo R (2013) Sodium-calcium exchanger modulates the L-glutamate Ca(i) (2+) signalling in type-1 cerebellar astrocytes. Adv Exp Med Biol 961:267–274.

Schmidt S, Linnartz B, Mendritzki S, Sczepan T, Lübbert M, Stichel CC, Lübbert H (2011) Genetic mouse models for Parkinson's disease display severe pathology in glial cell mitochondria. Hum Mol Genet 20:1197–1211.

Schulz K, Sydekum E, Krueppel R, Engelbrecht CJ, Schlegel F, Schröter A, Rudin M, Helmchen F (2012) Simultaneous BOLD fMRI and fiber-optic calcium recording in rat neocortex. Nat Methods 9:597–602.

Schwarz TL (2013) Mitochondrial trafficking in neurons. Cold Spring Harb Perspect Biol 5:a011304.

Schweinhuber SK, Meßerschmidt T, Hänsch R, Korte M, Rothkegel M (2015) Profilin Isoforms Modulate Astrocytic Morphology and the Motility of Astrocytic Processes. PLoS ONE 10 Available at: http://www.ncbi.nlm.nih.gov/pmc/articles/PMC4309604/ [Accessed August 17, 2016].

Sheng Z-H (2014) Mitochondrial trafficking and anchoring in neurons: New insight and implications. J Cell Biol 204:1087–1098.

Sheng Z-H, Cai Q (2012) Mitochondrial transport in neurons: impact on synaptic homeostasis and neurodegeneration. Nat Rev Neurosci 13:77–93.

Srinivasan R, Huang BS, Venugopal S, Johnston AD, Chai H, Zeng H, Golshani P, Khakh BS (2015) Ca(2+) signaling in astrocytes from Ip3r2(-/-) mice in brain slices and during startle responses in vivo. Nat Neurosci 18:708–717.

Stephen T-L, Higgs NF, Sheehan DF, Awabdh SA, López-Doménech G, Arancibia-Carcamo IL, Kittler JT (2015) Miro1 Regulates Activity-Driven Positioning of Mitochondria within Astrocytic Processes Apposed to Synapses to Regulate Intracellular Calcium Signaling. J Neurosci 35:15996–16011.

Sui D, Wilson JE (1997) Structural determinants for the intracellular localization of the isozymes of mammalian hexokinase: intracellular localization of fusion constructs incorporating structural elements from the hexokinase isozymes and the green fluorescent protein. Arch Biochem Biophys 345:111–125.

Szabadkai G, Bianchi K, Várnai P, De Stefani D, Wieckowski MR, Cavagna D, Nagy AI, Balla T, Rizzuto R (2006) Chaperone-mediated coupling of endoplasmic reticulum and mitochondrial Ca2+ channels. J Cell Biol 175:901–911.

Tang W, Szokol K, Jensen V, Enger R, Trivedi CA, Hvalby Ø, Helm PJ, Looger LL, Sprengel R, Nagelhus EA (2015) Stimulation-Evoked Ca2+ Signals in Astrocytic Processes at Hippocampal CA3–CA1 Synapses of Adult Mice Are Modulated by Glutamate and ATP. J Neurosci 35:3016–3021.

Voets T, Toonen RF, Brian EC, de Wit H, Moser T, Rettig J, Südhof TC, Neher E, Verhage M (2001) Munc18-1 promotes large dense-core vesicle docking. Neuron 31:581–591.

Wang X, Winter D, Ashrafi G, Schlehe J, Wong YL, Selkoe D, Rice S, Steen J, LaVoie MJ, Schwarz TL (2011) PINK1 and Parkin Target Miro for Phosphorylation and Degradation to Arrest Mitochondrial Motility. Cell 147:893–906.

Wong YC, Holzbaur ELF (2014) Optineurin is an autophagy receptor for damaged mitochondria in parkin-mediated mitophagy that is disrupted by an ALS-linked mutation. Proc Natl Acad Sci 111:E4439–E4448.

Wong YC, Holzbaur ELF (2015) Temporal dynamics of PARK2/parkin and OPTN/optineurin recruitment during the mitophagy of damaged mitochondria. Autophagy 11:422–424.

Xu N-J, Bao L, Fan H-P, Bao G-B, Pu L, Lu Y-J, Wu C-F, Zhang X, Pei G (2003) Morphine withdrawal increases glutamate uptake and surface expression of glutamate transporter GLT1 at hippocampal synapses. J Neurosci Off J Soc Neurosci 23:4775–4784.

Yang Y, Li Q, Miyashita H, Yang T, Shuaib A (2001) Different dynamic patterns of extracellular glutamate release in rat hippocampus after permanent or 30-min transient cerebral ischemia and histological correlation. Neuropathology 21:181–187.

Yoshii SR, Kishi C, Ishihara N, Mizushima N (2011) Parkin Mediates Proteasome-dependent Protein Degradation and Rupture of the Outer Mitochondrial Membrane. J Biol Chem 286:19630–19640.

Zaid H, Talior-Volodarsky I, Antonescu C, Liu Z, Klip A (2009) GAPDH binds GLUT4 reciprocally to hexokinase-II and regulates glucose transport activity. Biochem J 419:475–484.

Zhang Y, Chen K, Sloan SA, Bennett ML, Scholze AR, O'Keeffe S, Phatnani HP, Guarnieri P, Caneda C, Ruderisch N, Deng S, Liddelow SA, Zhang C, Daneman R, Maniatis T, Barres BA, Wu JQ (2014) An RNA-Sequencing Transcriptome and Splicing Database of Glia, Neurons, and Vascular Cells of the Cerebral Cortex. J Neurosci 34:11929–11947.